AD-A115 887 ANALYTIC INFORMATION PROCESSING INC DANVILLE CA F/G 20/6
RESEARCH AND DEVELOPMENT IN SPECKLE IMAGING.(U)
NOV 81 J W SHERMAN F49620-80-C-0032
UNCLASSIFIED AFOSR-TR-82-0361 NL

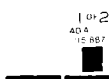

AFOSR-TR- 82-0361

(5)

FINAL TECHNICAL REPORT

RESEARCH AND DEVELOPMENT IN SPECKLE IMAGING

James W. Sherman

Analytic Information Processing, Inc.
P.O. Box 966
Danville, CA 94526

November 30, 1981

Unclassified

SECURITY CLASSIFICATION OF THIS PAGE (When Data Entered)

REPORT DOCUMENTATION PAGE	READ INSTRUCTIONS BEFORE COMPLETING FORM
1 REPORT NUMBER: AFOSR-TR- 82-0361	2 GOVT ACCESSION NO.: AD A115 887 — 3 RECIPIENT'S CATALOG NUMBER:
4 TITLE (and Subtitle): RESEARCH AND DEVELOPMENT IN SPECKLE IMAGING	5 TYPE OF REPORT & PERIOD COVERED: FINAL TECHNICAL REPORT 1/1/80 to 9/30/81
	6 PERFORMING ORG. REPORT NUMBER:
7 AUTHOR(s): James W. Sherman	8 CONTRACT OR GRANT NUMBER(s): F49620-80-C-0032
9 PERFORMING ORGANIZATION NAME AND ADDRESS: Analytic Information Processing, Inc. P.O. Box 966 Danville, CA 94526	10 PROGRAM ELEMENT PROJECT, TASK AREA & WORK UNIT NUMBERS: 61102F 2311/A1
11 CONTROLLING OFFICE NAME AND ADDRESS: Air Force Office of Scientific Research (NP) Building 410 Bolling AFB, D.C. 20332	12 REPORT DATE: November 30, 1981
	13 NUMBER OF PAGES: 170
14 MONITORING AGENCY NAME & ADDRESS (if different from Controlling Office): [redacted]	15 SECURITY CLASS (of this report): Unclassified
	15a DECLASSIFICATION DOWNGRADING SCHEDULE:

16 DISTRIBUTION STATEMENT (of this Report)

Approved for public release; distribution unlimited.

17 DISTRIBUTION STATEMENT (of the abstract entered in Block 20, if different from Report)

18 SUPPLEMENTARY NOTES

19 KEY WORDS (Continue on reverse side if necessary and identify by block number)

Speckle, Image Reconstruction, Imaging Models, Recursive Estimation

20 ABSTRACT (Continue on reverse side if necessary and identify by block number)

The progress made under AFOSR Contract F49620-80-C-0032 for research and development in Speckle Imaging is reviewed. The efforts were concentrated on modelling non-isoplanatic speckle images , developing restoration algorithms for non-isoplanatic conditions, and developing recursive algorithms for image reconstruction.

DD FORM 1 JAN 73 1473

Unclassified

SECURITY CLASSIFICATION OF THIS PAGE (When Data Entered)

INTRODUCTION

This report summarizes the research progress made under contract number F49620-80-C-0032 entitled "Research and Development in Speckle Imaging". Analytic Information Processing, Inc. pursued this effort for the Air Force Office of Scientific Research (AFSC), United States Air Force. The AFOSR programs manager is Dr. H. Radoski and the principal investigator is Dr. J. W. Sherman.

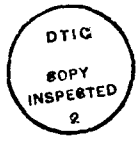

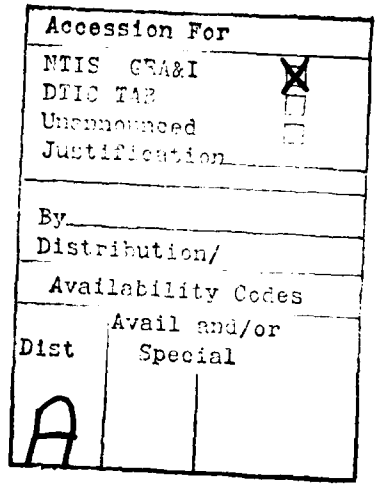

RESEARCH OBJECTIVES

The objectives of the effort were to:

1. Develop a better understanding of the random processes which degrade the coherence of light propagating through the atmosphere.

2. Develop a first cut capability to process atmospherically degraded images to obtain diffraction limited resolution.

To accomplish these research objects, the statment of work for this effort delineated six tasks.

1. Develop mathematical models for the random speckle image produced by atmospheric turbulence and by recording effects.

2. Develop equations for the second order statistics of a set of speckle images.

3. Evaluate reconstruction performance in terms of algorithm complexity and reconstruction accuracy.

4. Develop computational techniques from the reconstruction equations with constraints describing the object's characteristics.

5. Publish the results of analyses in relevant scientific journals and at technical conferences.

6. Coordinate the speckle imaging techniques developed with those of other researchers.

Although the feasibility of Speckle Imaging had been shown previously, the models and algorithms used were the simplest possible. The development of improved models and associated algorithms was necessary as a basis for improved Speckle Imaging and for analysis of the accuracy of the reconstructed images. These improved models were developed by analytic and experimental means. These tasks emphasized the development of models which allow for the natural variation of the degradation and the development of speckle imaging algorithms which estimate not only the underlying image but also the model parameters or degradation conditions.

STATUS OF RESEARCH TASKS

The status of the research tasks will be discussed in terms of two areas:

1. Non-isoplanatic Modeling

2. Recursive Algorithms

We have chosen to concentrate our research in these two areas because they appear to have the greatest potential for improving the range of applications for Speckle Imaging. The treatment of the non-isoplanatic case will allow Speckle Imaging to be used over wider fields-of-view in order to image extended objects. The development of recursive algorithms will allow the use of generally available mini-computers to process Speckle Images because they reduce the large I/O requirements of non-recursive algorithms.

Non-Isoplanatic Modeling

Our modeling efforts for Speckle Imaging under non-isoplanatic conditions were designed to determine the nature of the degradation of Speckle Images and the extent to which the underlying image can be recovered. The two-point source wave-structure function and the altitude dependence of the index-of-refraction structure constant were used as the basis of the modeling. The first and second order statistics of speckle images were derived. An analysis of the information recoverable from these statistics has shown that diffraction limited resolution can be obtained. Two important assumptions, which are usually satisfied, were made:

1. The isoplanatic patch encompasses the average spread function.

2. The greatest contribution to the atmospheric distortion comes from turbulence at low altitudes.

Under these conditions, the aberrations of the telescope do not affect the second-order statistics. Also, the integral equation relating the object and measured second-order statistics is well conditioned. These results were presented at the SPIE annual symposium and published in the SPIE Proceedings, Volume 243.

This modeling effort was continued. The parameters of the mathematical model for the non-isoplanatic degradation are determined from the index-of-refraction structure constant profile. A random process model of the index-of-refraction structure constant profile was used to derive the dependence on this profile of the function which smooths the second-order statistics under non-isoplanatic conditions. We found that for the purposes of this model the atmospheric structure function was reasonably approximated by a 5/3-law model for all values of its argument. Simple useful models were obtained for the smoothing function which describes the non-isoplanatic conditions. These models were verified numerically. We plan to submit these results to the Journal of the Optical Society of America for publication.

The results of this modelling effort were used to develop a restoration algorithm for non-isoplanatic Speckle Imaging. The tradeoffs in computational complexity were examined. The Speckle Imaging equations were formulated in a general framework based on linear algebra to allow an examination of the many alternatives. We plan to submit these results to the Journal of the Optical Society of America and/or the IEEE Transaction on ASSP for publication.

Recursive Algorithms

The recursive algorithm development effort was pursued because it

allows Speckle Imaging to be used for a wider range of applications. Extended Kalman filter formulations were developed so that subject image models can be introduced easily. For example, time evolutionary models for solar features or restrictive models like limited spatial extent can be used easily. The recursive nature of the algorithm will allow the use of mini-computers for data reduction, because of the removal of the requirement for storing the second-order statistics. These second-order statistics require millions of words of intermediate storage which must be accessed many times for non-recursive algorithms, producing an I/O burden too great for most mini-computer systems.

Recursive algorithms based on an extended Kalman filter approach have been derived. A detailed analysis of the decomposition of the Speckle Imaging equations into manageable subsets has been performed. The decomposition has a "natural" format that results in very reasonable computation requirements.

The evaluation of a one-dimensional example was started. An oversimplication in the models led to singularity problems. In finding the problem, we also found simpler forms for the Kalman gain equations. These simplified Kalman equations were compared to a recursive form of the least square algorithm previously developed.

We plan to submit these results to the Journal of the Optical Society of America and/or the IEEE transaction on Acoustics, Speech, and Signal Processing.

LIST OF PUBLICATIONS

PUBLISHED DURING 1980

J. W. Sherman, Speckle Imaging Under Non-Isoplanatic Conditions, SPIE Proceedings, Volume 243.

IN PREPARATION (WITH PROBABLE TITLES AND JOURNALS)

D. O. Anderton, C. K. Rushforth, and J. W. Sherman, Non-Isoplanatic Model for the Statistics of Speckle Images, to be submitted to JOSA.

D. Sauquet and J. W. Sherman, Isoplanatic Recursive Speckle Imaging, to be submitted to JOSA and/or IEEE Trans. on ASSP.

J. W. Sherman and H. Ur, Restoration Algorithms for Speckle Imaging Under Non-Isoplanatic Conditions, to be submitted to JOSA.

LIST OF PERSONNEL

NAME AND POSITION	RESEARCH EFFORT
J. W. Sherman Principal Investigator	Development of Models, speckle imaging equations and restoration algorithm for non-isoplanatic conditions; Recursive formulation development.
D. Sauquet Engineer	Recursive (Kalman Filter) formulation development.
S. P. DeMarta Programmer	Development of recursive speckle imaging programs.
T. P. Liu Engineer	Library research on turbulence models.
H. Ur Engineer	Non-isoplanatic restoration algorithm development.
C. K. Rushforth Consultant	Non-isoplanatic modeling.
D. O. Anderton Consultant	Non-isoplanatic modeling.

KALMAN FILTERING FOR SPECKLE IMAGING

Dominique Sauquet
James W. Sherman

Analytic Information Processing, Inc.

November 30, 1981

TABLE OF CONTENTS

Section 1 Introduction and Definition of the Problem

1-1 Definition of the Problem

A solution to the problem of reconstructing telescopic images whose resolution has been degraded by passage through the turbulent atmosphere has already been proposed with the process called "Speckle Imaging". Speckle Imaging is the reconstruction of diffraction limited images from atmospherically degraded, multi-frame imagery.

The process of recording the images viewed through the telescope introduces noise effects making the treatment of the turbulence effects difficult. A model has been developed for both the turbulence effects and the noise effects. With these two models and a data set composed of images of the object, a speckle imaging algorithm provides an estimate of the object. The algorithm previously reported [1] is based on a least-squares method.

The goal of this effort was to develop a new algorithm in speckle imaging in order to increase the range of applications. The new algorithm should meet the three following requirements:

1) To be a real-time algorithm, treating each image when it arrives,
2) To allow the treatment of time evolutionary models for both the object and the atmospheric statistical characteristics,
3) To allow the use of a mini-computer.

One of our main concerns for the use of a mini-computer will be the reduction of data storage. The recursive nature of a real time algorithm will aid in this reduction.

1-2 - Speckle Image Model

In the effort to demonstrate the feasability of the least-squares algorithm, several simplifying assumptions on the speckle image model

were used and the new algorithm will be developed under the same set of assumptions.

- The imaging is assumed to be isoplanatic which means the speckle image from a point source is constant over the field of view. This allows for the use of Fourier techniques to convert convolutions into algebraic equations,
- very simplified mathematical models for the statistics of the point spread response are assumed,
- to avoid any analysis or question of degrading effects, the imaging conditions are restricted to narrowband exposures of a constant, bright object.

Models for the two principal sources of image distortion that occur when using a ground-based telescope can be developed under the previous assumptions. The first source is the turbulence of the intervening atmosphere. The second source is the error or noise associated with the physical measurement of the image and we shall refer to it as the noise of measurement. This latter affects the quality of the imaging less than the former, but it is its presence which has previously made the correction for the turbulence difficult.

Model for the Turbulence Effects:

For simplicity, consider incoherent imaging over an isoplanatic patch. The image can be expressed as a convolution of the object and a point spread response function.

$$i_f(\underline{x},t) = \iint_{-\infty}^{\infty} o(\underline{\lambda})\, s(\underline{x}-\underline{\lambda},t)\, d\underline{\lambda} \qquad (1)$$

where $i_f(\underline{x},t)$ is the formed image, $o(\underline{\lambda})$ is the object, and $s(\underline{x},t)$ is the point spread response. The point spread response depends on the optical system and the phase delay and amplitude disturbance processes caused by turbulence. Let $S(\underline{z},t)$ be the optical transfer function

corresponding to $s(\underline{x},t)$, that is,

$$S(\underline{z},t) = F_{\underline{x}}\{s(\underline{x},t)\} = \int_{-\infty}^{\infty} a(\underline{\beta}+\underline{z})\,a(\underline{\beta})\exp\left(j\theta(\underline{\beta}+\underline{z}) - j\theta(\underline{\beta})\right) \quad (2)$$
$$\exp\left[\chi(\underline{\beta}+\underline{z},t) + j\phi(\underline{\beta}+\underline{z},t) + \chi(\underline{\beta},t) - j\phi(\underline{\beta},t)\right] d\underline{\beta}$$

where

$a(\cdot)$ is the aperture function of the telescope,

$\theta(\cdot)$ is the phase aberration function of the telescope

$\chi(\cdot,\cdot)$ is the log-amplitude disturbance at the aperture caused by turbulence,

$\phi(\cdot,\cdot)$ is the phase delay disturbance at the aperture caused by turbulence,

and $F_{\underline{x}}\{\cdot\}$ indicates Fourier transform with respect to $\underline{x}$.

The random properties of the function $S(\underline{z},t)$ will be characterized by its mean $\overline{S(\underline{z})}$ and covariance $S_S(\underline{z}_1,\underline{z}_2)$.

Assuming the usual Gaussian distribution for χ and ϕ allows the mean and covariance of $S(\underline{z},t)$ to be written in terms of the wave structure function $D(\cdot)$. Using the results of Fante [2], the mean and covariance of $S(\underline{z},t)$ are well approximated by

$$\overline{S(\underline{z})} = \exp\left[-\frac{D(\underline{z})}{2}\right] \int_{-\infty}^{\infty} a(\underline{\beta}+\underline{z})\,a(\underline{\beta})\exp\left[j\theta(\underline{\beta}+\underline{z}) - j\theta(\underline{\beta}+\underline{z})\right] d\underline{\beta} \quad (3)$$

and

$$S_S(\underline{z}_1,\underline{z}_2) = \int_{-\infty}^{\infty}\int_{-\infty}^{\infty} a(\underline{\beta}_1+\underline{z}_1)\,a(\underline{\beta}_1)\,a(\underline{\beta}_2+\underline{z}_2)\,a(\underline{\beta}_2) \quad (4)$$
$$\exp\left[j\theta(\underline{\beta}_1+\underline{z}_1) - j\theta(\underline{\beta}_1) + j\theta(\underline{\beta}_2+\underline{z}_2) - j\theta(\underline{\beta}_2)\right] \exp\left[-\frac{D(\underline{z}_1)+D(\underline{z}_2)}{2}\right]$$
$$\left(\exp\left[-\frac{D(\underline{\beta}_1-\underline{\beta}_2+\underline{z}_1)+D(\underline{\beta}_1-\underline{\beta}_2-\underline{z}_2)-D(\underline{\beta}_1-\underline{\beta}_2)-D(\underline{\beta}_1-\underline{\beta}_2+\underline{z}_1-\underline{z}_2)}{2}\right] - 1\right) d\underline{\beta}_1\,d\underline{\beta}_2$$

For the mean $\overline{S(\underline{z})}$, the effects of the atmosphere and of the telescope separate into a product form. $\overline{S(\underline{z})}$ is dominated by the exponential factor and decays to zero rapidly as the spatial frequency increases in magnitude. For the covariance $S_S(\underline{z}_1,\underline{z}_2)$, the expression (4) is quite complex.

However, the Fourier transforms of astronomical data were studied and the analysis of their first and second order moments have shown that the characteristics of the statistics of the point spread response are reasonably simple in spite of the complex nature of (3) and (4). Therefore, ad hoc approximations to (3) and (4) were developed; these approximations have the same general characteristics as the data.

The mean $\overline{S(\underline{z})}$ was approximated by a gaussian function,

$$\overline{S(\underline{z})} \approx \exp\left[-\left(\frac{|\underline{z}|}{r_o}\right)^2\right] \qquad (5)$$

whose width was proportional to the correlation distance, r_o, of the complex disturbance in the aperture plane resulting from the turbulence. r_o is small compared to the diameter of the aperture D.

The approximation of the covariance was proportional to the product of two factors.

- one that models the narrowband dimensions of the covariance and the effects of decorrelation across the aperture:

$$\overline{S\left(\frac{\underline{z}_1-\underline{z}_2}{2}\right)}$$

This term exponentially decreases with increasing distance from the plane $\underline{z}_1-\underline{z}_2=0$.

- another one that models the broadband dimension of the covariance:

$$\left(1-\frac{|\underline{z}_1+\underline{z}_2|}{2D}-\overline{S\left(\frac{\underline{z}_1+\underline{z}_2}{2}\right)}\right)$$

The $\overline{S\left(\frac{\underline{z}_1+\underline{z}_2}{2}\right)}$ term models the effect of removing the mean in the covariance. The remainder of this second factor approximates the ideal diffraction limited optical transfer function.

Let the covariance of the optical transfer function be denoted by

$$\Gamma_S(\underline{z}_1,\underline{z}_2) = E\left\{\left(S(\underline{z}_1,t)-\overline{S(\underline{z}_1)}\right)\left(S(\underline{z}_2,t)-\overline{S(\underline{z}_2)}\right)\right\} \quad (6)$$

Because of the symmetry properties of the Fourier transforms of real functions, it is also true that:

$$\Gamma_S(\underline{z}_1,\underline{z}_2) = E\left\{\left(S(\underline{z}_1,t)-\overline{S(\underline{z}_1)}\right)\left(S(-\underline{z}_2,t)-\overline{S(-\underline{z}_2)}\right)\right\} \quad (7)$$

Model for the Noise Effects

Although the formed images $i_f(\underline{x},t)$ of (1) are instantaneous functions of time, there is some finite exposure (i.e., averaging) time involved in their measurement. We assume that these times ΔT are short enough to "freeze" the turbulence effects and this will allow us to apply (1) for these time-average images:

$$i(\underline{x},T_j) = \frac{1}{\Delta T}\int_{T_j-\frac{\Delta T}{2}}^{T_j+\frac{\Delta T}{2}} i_f(\underline{x},t)\,dt \quad (8)$$

and to obtain:

$$i(\underline{x},T_j) = \iint_{-\infty}^{\infty} o(\underline{\lambda})\, s(\underline{x}-\underline{\lambda},T_j)\,d\underline{\lambda} \quad (9)$$

Telescopic images are generally recorded using either photographic film or electronic cameras, often at limited photon flux levels. For both systems and under various hypotheses, the effect of these noises of measurement can be modeled using combinations of Poisson, additive, and multiplicative noise terms.

Each type of noise models physical random processes that occur in the measurement process. In the recording of speckle images a particular order is useful; additive noise modeling scatted and background light occurs first, then Poisson noise modeling photon reception, and finally multiplicative noise modeling sensor non-linearities.

Then, if $i_d(\underline{x}, T_j)$ denotes the measured image, the following diagram and equations will represent the measurement noise process.

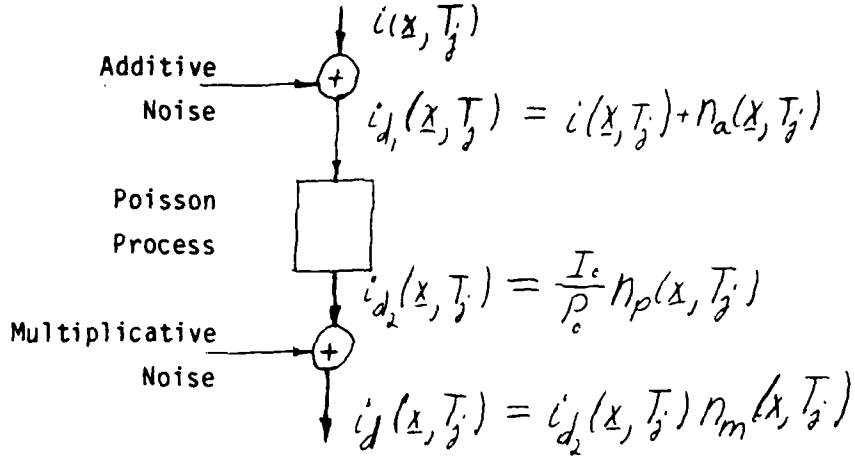

The noise process has a zero mean such that

$$E\{i_d(\underline{x}, T_j)\} = E\{i(\underline{x}, T_j)\}. \tag{11}$$

Let

$n_a(\underline{x}, T_j)$ be an additive noise with zero mean and variance of σ_a^2,
$n_p(\underline{x}, T_j)$ be a Poisson process with means $\overline{n_p(\underline{x}, T_j)}$ and variance $\sigma_p^2(\underline{x}, T_j)$, and
$n_m(\underline{x}, T_j)$ be a multiplicative noise with unity mean and variance σ_m^2.

The mean and variance of the Poisson process are given by

$$\overline{n_p(\underline{x}, T_j)} = \sigma_p^2(\underline{x}, T_j) = \frac{P_o}{I_c}\, \overline{i(\underline{x}, T_j)}, \tag{12}$$

where

P_o is the total photon flux detected, and
I_o is the integral or total expected image intensity.

The three measurement noises are all assumed to be statistically independent among themselves and independent of $i(\underline{x}, T_j)$. They are assumed to be spatially and temporally uncorrelated.

1-3 - The Restoration Algorithm

Sample Image Statistics

For the speckle imaging algorithm, the sample first and second order statistics of a set of images with measurement noise will be used and their relationships to the mean and covariance of the point spread response have to be established.

First Order Sample Statistics: The set of images is composed of N images taken at times, T_j $j=1,\cdots,N$; then the average of the N images gives the first order sample statistics:

$$\hat{\overline{i(\underline{x})}} = \frac{1}{N} \sum_{j=1}^{N} i_d(\underline{x}, T_j). \tag{13}$$

Because of the zero mean of the noise of measurement, the sample mean is unbiased

$$E\{\hat{\overline{i(\underline{x})}}\} = \overline{i(\underline{x})} \tag{14}$$

and when taking the expected value of (9), $\overline{i(\underline{x})}$ is given by:

$$\overline{i(\underline{x})} = \int_{-\infty}^{\infty}\int o(\underline{\lambda})\, \overline{s(\underline{x}-\underline{\lambda})}\, d\underline{\lambda} \tag{15}$$

Fourier transforming (15) changes this integral equation into an

algebraic one

$$\overline{I(\underline{z})} = \theta(\underline{z})\ \overline{S(\underline{z})}, \tag{16}$$

where $\theta(\underline{z})$ is the transform of the object

$\overline{I(\underline{z})}$ is the mean of the Fourier transforms of the images

If $\hat{\underline{I}}(\underline{z})$ is the sample mean of the Fourier transform of the N images; then its expected value is given by

$$E\left\{\hat{\underline{I}}(\underline{z})\right\} = \overline{I(\underline{z})} = \theta(\underline{z})\,\overline{S(\underline{z})}. \tag{17}$$

Unfortunately, these first order statistics contain very little high spatial-frequency information because $\overline{S(\underline{z})}$ has a very low pass nature. Because of this low-pass nature, the inversion of (17) is ill-conditioned: small variations in $\hat{\underline{I}}(\underline{z})$ would result in large variations in the estimation of $\theta(\underline{z})$ and thus, the effect of the measurement noise would be increased.

However, the broad-band nature of the covariance $S_S(\underline{z}_1, \underline{z}_2)$ will allow us to use the second order statistics to restore the images in the high frequency domain.

Second Order Sample Statistics

The following notation will be used for the second order statistics:

- The inverse Fourier transform of $S_S(\underline{z}_1, \underline{z}_2)$, the covariance of the transfer function $S(\underline{z})$, will give $R_S(\underline{x}_1, \underline{x}_2)$, the covariance of the point spread response $s(\underline{x})$.

- The covariance of a set of images in the spatial domain (respectively in the frequency domain) is given by $R_i(\underline{x}_1, \underline{x}_2)$, (respectively $S_i(\underline{z}_1, \underline{z}_2)$) and the sample covariance by $\hat{R}_i(\underline{x}_1, \underline{x}_2)$ (respectively $\hat{S}_i(\underline{z}_1, \underline{z}_2)$).

Taking the covariance of (9) gives

$$R_i(\underline{x}_1, \underline{x}_2) = E\left\{[i(\underline{x}_1,t) - \overline{i(\underline{x}_1)}][i(\underline{x}_2,t) - \overline{i(\underline{x}_2)}]\right\} \quad (18)$$

$$= \int_{-\infty}^{\infty}\int_{-\infty}^{\infty} o(\underline{\lambda}_1)\, o(\underline{\lambda}_2)\, R_S(\underline{x}_1 - \underline{\lambda}_1, \underline{x}_2 - \underline{\lambda}_2)\, d\underline{\lambda}_1\, d\underline{\lambda}_2$$

In this integral equation, the object $o(\underline{\lambda})$ appears as the cartesian product with itself. An unambiguous solution of this non-linear integral equation will require a non-linear solution method. The method will depend on the characteristics of the sample image covariance used in the inversion of (18). Let $\hat{R}_i(\underline{x}_1, \underline{x}_2)$ be the sample covariance function of N images at times T_j, j = 1, ... ,N, then

$$\hat{R}_i(\underline{x}_1, \underline{x}_2) = \frac{1}{N-1}\sum_{j=1}^{N}\left[i_d(\underline{x}_1, T_j) - \hat{\overline{i(\underline{x}_1)}}\right]\left[i_d(\underline{x}_2, T_j) - \hat{\overline{i(\underline{x}_2)}}\right] \quad (19)$$

We are now interested in the relationship between the expected value of the sample covariance, $E\{\hat{R}_i(\underline{x}_1, \underline{x}_2)\}$, and the covariance $R_i(\underline{x}_1, \underline{x}_2)$.

If $\underline{x}_1 \neq \underline{x}_2$, $E\{\hat{R}_i(\underline{x}_1, \underline{x}_2)\} = R_i(\underline{x}_1, \underline{x}_2)$ because the measurement noises are spatially uncorrelated.

If $\underline{x}_1 = \underline{x}_2$, $\hat{R}_i(\underline{x}_1, \underline{x}_2)$ can be expanded in terms of the multiplicative noise and the image corrupted by additive and Poisson noise.

$$\hat{R}_i(\underline{x}_1, \underline{x}_1) = \frac{1}{N-1}\sum_{j=1}^{N}\left(i_{d_2}(\underline{x}_1, T_j) - \hat{\overline{i(\underline{x}_1)}}\right)^2 \quad (20)$$

$$+ \frac{2}{N-1}\sum_{j=1}^{N}\left(n_m(\underline{x}_1, T_j) - 1\right) i_{d_2}(\underline{x}_1, T_j)\left(i_{d_2}(\underline{x}_1, T_j) - \hat{\overline{i(\underline{x}_1)}}\right) + \frac{1}{N-1}\sum_{j=1}^{N} i_{d_2}(\underline{x}_1, T_j)^2\left(n_m(\underline{x}_1, T_j) - 1\right)^2.$$

The mean of the first term adds to the variance the contribution of the additive and Poisson noise. It is equal to

$$E\left\{\frac{1}{N-1}\sum_{j=1}^{N}\left(i_{d_2}(\underline{x}_1,T_j)-\hat{\overline{i'(\underline{x}_1)}}\right)^2\right\}=R_i(\underline{x}_1,\underline{x}_2)+\sigma_a^2+\frac{I_0}{P_0}\overline{i'(\underline{x}_1)}. \quad (21)$$

The mean of the second term is zero because $n_m(\underline{x}_1,T_j)$ has unity mean and is statistically independent of $i_{d_2}(\underline{x}_1,T_j)$. The mean of the last term is equal to the product of the 2nd order non-central moment of $i_{d_2}(\underline{x}_1,T_j)$ and the variance of $n_m(\underline{x}_1,T_j)$,

$$E\left\{\frac{1}{N-1}\sum_{j=1}^{N} i_{d_2}(\underline{x}_1,T_j)^2\left(n_m(\underline{x}_1,T_j)-1\right)^2\right\}=\sigma_m^2\left[R_i(\underline{x}_1,\underline{x}_1)+\sigma_a^2+\frac{I_0}{P_0}\overline{i'(\underline{x}_1)}+\overline{i'(\underline{x}_1)}^2\right] \quad (22)$$

Therefore we obtain:

$$E\left\{\hat{R}_i(\underline{x}_1,\underline{x}_1)\right\}=R_i(\underline{x}_1,\underline{x}_1)+\sigma_a^2+\frac{I_0}{P_0}\overline{i'(\underline{x}_1)} \quad (23)$$
$$+\sigma_m^2\left[R_i(\underline{x}_1,\underline{x}_1)+\sigma_a^2+\frac{I_0}{P_0}\overline{i'(\underline{x}_1)}+\overline{i'(\underline{x}_1)}^2\right]$$

and we can sum up the cases $\underline{x}_1\neq\underline{x}_2$ and $\underline{x}_1=\underline{x}_2$ in a unique formula

$$E\left\{\hat{R}_i(\underline{x}_1,\underline{x}_2)\right\}=R_i(\underline{x}_1,\underline{x}_2)+\delta(\underline{x}_1-\underline{x}_2)\left[\sigma_a^2(1+\sigma_m^2)\right. \quad (24)$$
$$\left.+\frac{I_0}{P_0}\overline{i'(\underline{x}_1)}(1+\sigma_m^2)+\sigma_m^2\left(R_i(\underline{x}_1,\underline{x}_2)+\overline{i'(\underline{x}_1)\,i'(\underline{x}_2)}\right)\right]$$

The difference between $E\{R_i(\underline{x}_1,\underline{x}_2)\}$ and $R_i(\underline{x}_1,\underline{x}_2)$ can be considered as a bias. Once this bias has been subtracted, the sample covariance (18) can be solved for the object using the two broadband dimensions of $R_S(\underline{x}_1,\underline{x}_2)$.

For the assumed case of isoplanatic or spatially invariant imaging, the convolution nature of (18) allows us to use the Fourier transform to rewrite (18) as:

$$S_i(\underline{z}_1,\underline{z}_2)=\Theta(\underline{z}_1)\,\Theta^*(\underline{z}_2)\,S_S(\underline{z}_1,\underline{z}_2). \quad (25)$$

And in the frequency domain, (24) becomes:

$$E\left\{\hat{S}_i(\underline{z}_1,\underline{z}_2)\right\} = S_i(\underline{z}_1,\underline{z}_2) + (1+\sigma_m^2)\left[\sigma_a^2\delta(\underline{z}_1-\underline{z}_2) + \frac{I_o}{P_o}\bar{I}(\underline{z}_1-\underline{z}_2)\right] \quad (26)$$
$$+\sigma_m^2\int_{-\infty}^{\infty}\left[\bar{I}(\underline{z}_1-\underline{\beta})\bar{I}^*(\underline{z}_2-\underline{\beta}) + S_i(\underline{z}_1-\underline{\beta},\underline{z}_2-\underline{\beta})\right]d\underline{\beta}$$

If the noise model is accurate and the parameters are known, the sample covariance can be corrected for the effects of noise. If not, within the constraints of this or another noise model, the parameters can be estimated and used to correct the sample covariance. Let us call $\hat{S}_i^c(\underline{z}_1,\underline{z}_2)$ the corrected sample covariance.

The algorithm previously developed, [1] is an iterative process that uses both the first and second order statistics through equations (17) and (25). If $\theta^l(\underline{z})$ denotes the l-th estimate, then for a particular value of $\underline{z}_1$, equations corresponding (17) and (25) are written as:

$$\theta^{l+1}(\underline{z}_1)\,S(\underline{z}_1) = \hat{\bar{I}}(\underline{z}_1) \quad (27)$$

$$\theta^{l+1}(\underline{z}_1)\left[\theta^{*l}(\underline{z}_2)\,S_s(\underline{z}_1,\underline{z}_2)\right] = \hat{S}_i^c(\underline{z}_1,\underline{z}_2) \quad (28)$$
$$= \hat{S}_i(\underline{z}_1,\underline{z}_2) - \sigma_a^2(1+\sigma_m^2)\,\delta(\underline{z}_1-\underline{z}_2)$$
$$-\frac{I_o}{P_o}\bar{I}(\underline{z}_1-\underline{z}_2)(1+\sigma_m^2)$$
$$-\sigma_m^2\int_{-\infty}^{\infty}\left[\bar{I}(\underline{z}_1-\underline{\beta})\bar{I}^*(\underline{z}_2-\underline{\beta}) + S_i(\underline{z}_1-\underline{\beta},\underline{z}_2-\underline{\beta})\right]d\underline{\beta}$$

where only values of $\underline{z}_2$ near $\underline{z}_1$ are used, $|\underline{z}_1-\underline{z}_2| \le r_o$. Because the sample statistics are used, these equations have errors. The equations for $|\underline{z}_1-\underline{z}_2| > r_o$ are dominated by errors and are discarded. The corresponding components of $\hat{S}_i(\underline{z}_1,\underline{z}_2)$ are not computed, greatly reducing the order of the computation (proportional to M^2 rather than M^4 for M x M images). These equations at a particular value of $\underline{z}_1$, are solved for $\theta^{l+1}(\underline{z}_1)$ in a least squares fashion to give

$$\theta^{\ell}(\underline{z}_1) = \frac{\sum_{|\underline{z}_1-\underline{z}_2|\le r_o} \left[\theta^{*\ell}(\underline{z}_2) S_s(\underline{z}_1,\underline{z}_2)\right]\left[\hat{S}_i^{c}(\underline{z}_1,\underline{z}_2)\right] + \alpha \hat{\bar{I}}(\underline{z}_1)\,\bar{S}(\underline{z}_1)}{\sum_{|\underline{z}_1-\underline{z}_2|\le r_o} \left|O^{*\ell}(\underline{z}_2) S_s(\underline{z}_1,\underline{z}_2)\right|^2 + \alpha\,|S(\underline{z}_1)|^2} \qquad (29)$$

where α is a weighting parameter to control the relative importance of the sample mean and sample covariance (α=0 for $|\underline{z}_1|>r_o$). These equations are solved for each $\underline{z}_1$ starting at the origin proceeding toward the diffraction limit in a spiraling manner.

The parameters of the noise model are estimated (if desired) after (29) has been applied to all $\underline{z}_1$. The estimate is obtained by a least squares solution of

$$\hat{S}_i(\underline{z}_1,\underline{z}_2) = c_o \theta^{\ell}(\underline{z}_1) O^{*\ell}(\underline{z}_2) S_s(\underline{z}_1,\underline{z}_2) \qquad (30)$$
$$+ c_1 \delta(\underline{z}_1-\underline{z}_2) + c_2 B(\underline{z}_1-\underline{z}_2) + c_3 \hat{\bar{I}}(\underline{z}_1-\underline{z}_2)$$

for the coefficients c_o, c_1, c_2, and c_3 where $B(\underline{z}_1-\underline{z}_2)$ is a precalculated approximation to the integral of (28). The coefficients c_1, c_2, and c_3 are used as $\sigma_a^2/(1+\sigma_m^2)$, σ_m^2 and $(1+\sigma_m^2)I_o/P_o$. The square root of c_o is used to scale $\theta^{\ell}(\underline{z}_1)$ before the next iteration.

This iteration using (29) and (30) usually converges after two or three passes. Then the inverse FFT algorithm is used to compute a reconstructed object image. Finally, by varying assumptions concerning the noise processes, we obtain several reconstructions and use them to remove the noise artifacts, which vary between reconstructions.

Finally, our signal-processing method for restoring atmospherically degraded images can be briefly described as follows. We obtain first and second order statistics of the degraded images from 40 to 300 short-exposure (about 10 ms) images. These measured statistics are

then related to the underlying object and atmospheric characteristics by a series of integral equations, which are solved by a combination of "optimal" signal-processing techniques. With Fourier methods, we transform the integral equations into a set of non-linear algebraic equations. An estimate of the undegraded object is then obtained by solving linearized subsets of these equations using least squares techniques. The restoration technique converges quickly, and the required computational effort is roughly proportional to the number of resolution cells in the image.

Figure 1 summarizes the restoration algorithm.

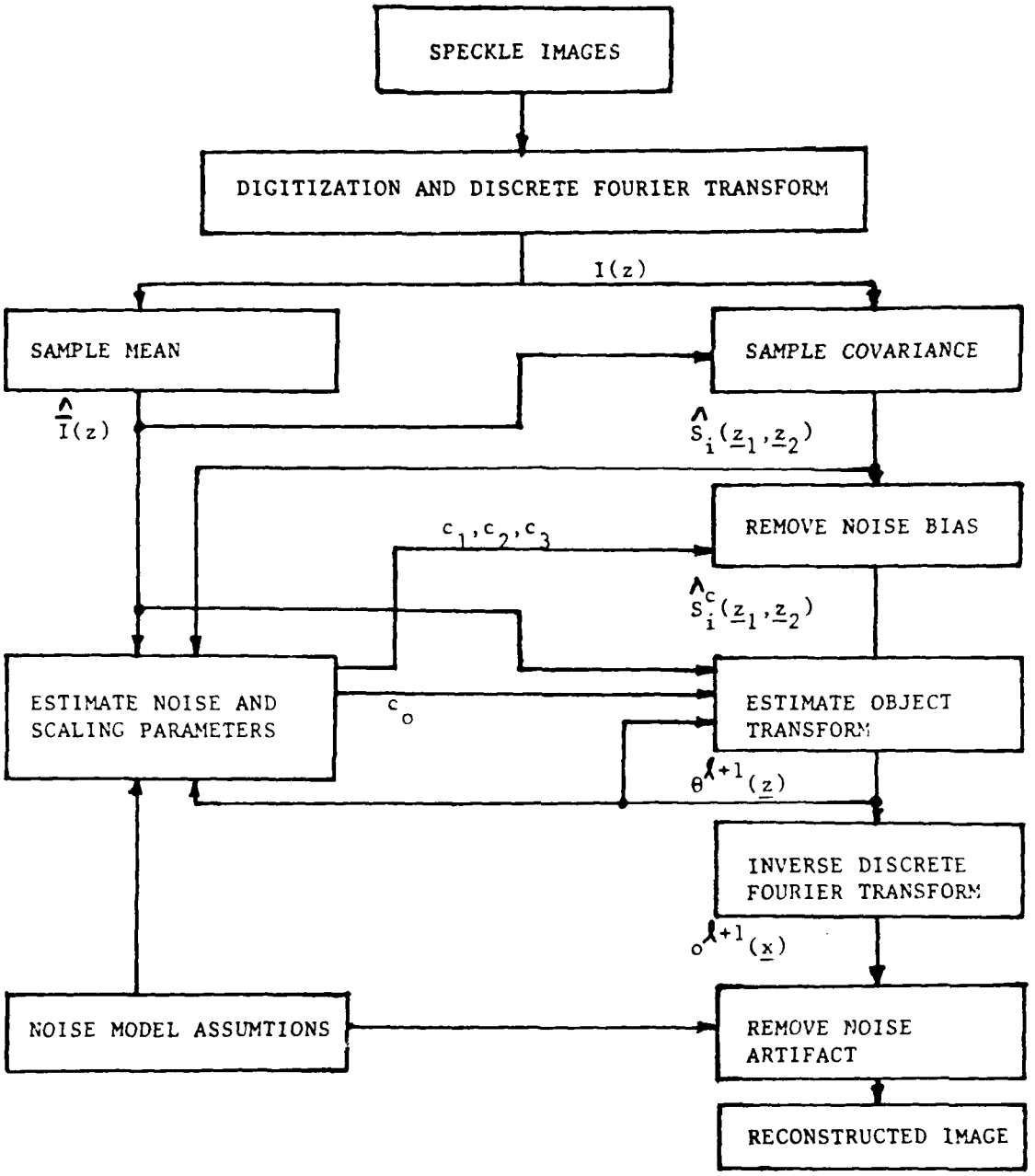

Figure 1 - Algorithm for reconstructing the object image from sample statistics. Once the iterative process converges, a reconstructed object image is computed with the inverse Fourier transform. The final reconstructed image is obtained after several preliminary reconstructions enable us to remove the noise artifacts.

Section 2 - Two Approaches for a New Algorithm

2-1 - A Recursive Least-Squares Algorithm

Our first concept for a recursive algorithm was to simply transform the previously studied least-squares algorithm into a recursive least-squares algorithm.

Let: $I_N(\underline{z}_i)$ be the recorded Nth image in the frequency domain,
$\theta_N^{\ell}(\underline{z}_i)$ be the ℓth estimate of the object obtained with N images,
$\hat{\bar{I}}^N(\underline{z}_i)$ and $\hat{S}_i^N(\underline{z}_1, \underline{z}_2)$ be the first and second order sample statistics computed with the N first images.

A test of convergence is conducted on the sequence $[\theta_N^{\ell}(\underline{z}_i), \ell]$ and for the last iteration, ℓmax, the estimate $\theta_N^{\ell max}(\underline{z}_i)$ is obtained (ℓmax may depend on $\underline{z}_i$). When the next image (N+1) is available, the estimate of the object is initialized for each $\underline{z}_i$ with, $\theta_{N+1}^{0}(\underline{z}) = \theta_N^{\ell max}(\underline{z})$. Then using recursive formulas for the sample statistics, the equation (29) of Section 1 can be rewritten as follows:

$$\theta_{N+1}^{\ell+1}(\underline{z}_i) = \frac{\sum_{|\underline{z}_2 - \underline{z}_1| \le r_0} \left[\theta_{N+1}^{*\ell}(\underline{z}_2) S_S(\underline{z}_1, \underline{z}_2)\right]\left[\hat{S}_i^{C,N+1}(\underline{z}_1, \underline{z}_2)\right] + \alpha \hat{\bar{I}}^{N+1}(\underline{z}_1)\overline{S(\underline{z}_1)}}{\sum_{|\underline{z}_2 - \underline{z}_1| \le r_c} \left|\theta_{N+1}^{*\ell}(\underline{z}_2) S_S(\underline{z}_1, \underline{z}_2)\right|^2 + \alpha\left[\overline{S(\underline{z}_1)}\right]^2} \qquad (31)$$

The first drawback of this real-time algorithm is that it assumes the object and the statistical characteristics of the noise processes are stationary.

Besides, let us examine recursive formulas for the sample statistics of the recorded images. The formulas are given by:

$$\hat{\bar{I}}^{N+1}(\underline{z}_i) = \frac{N}{N+1} \hat{\bar{I}}^N(\underline{z}_i) + \frac{1}{N+1} I_{N+1}(\underline{z}_i) \qquad (32)$$

$$\hat{S}_i^{N+1}(\underline{z}_i, \underline{z}_j) = \frac{N-1}{N} \hat{S}_i^{N}(\underline{z}_i, \underline{z}_j) + \frac{1}{N} I_{N+1}(\underline{z}_i) I_{N+1}^*(\underline{z}_j) \qquad (33)$$

$$\hat{\hat{S}}_i^{N+1}(\underline{z}_i, \underline{z}_j) = \hat{S}_i^{N+1}(\underline{z}_i, \underline{z}_j) - \frac{N+1}{N} \hat{\bar{I}}^{N+1}(\underline{z}_i) \hat{\bar{I}}^{N+1}(\underline{z}_j) \qquad (34)$$

This algorithm would require the storage, at each step N, of the quantities:

$\theta_N^l(\underline{z}_i)$ for each $\underline{z}_i$

$\hat{\bar{I}}^N(\underline{z}_i)$ for each $|\underline{z}_i| \le r_o$

$\hat{S}_i^N(\underline{z}_i, \underline{z}_j)$ for each $\underline{z}_i, \underline{z}_j$ such that $|\underline{z}_i - \underline{z}_j| \le r_o$

For MxM images, the storage requirements would be about 10 to 20 times M^2 and would make the use of a small computer difficult.

If the sample statistics did not have to be stored, a small computer could be used more easily. This would require storing only the current estimate of the object. All the desired information in the sample statistics is ideally contained in the current estimate of the object. The sample statistics recursions (32) and (33) would be replaced in this recursive algorithm by

$$\hat{\bar{I}}^{N+1}(\underline{z}_i) = \frac{N}{N+1} \bar{S}(\underline{z}_i) \theta_N^{l_{max}}(\underline{z}_i) + \frac{1}{N+1} I_{N+1}(\underline{z}_i) \qquad (35)$$

$$\hat{S}_i^{N+1}(\underline{z}_i, \underline{z}_j) = \frac{N-1}{N} S_S(\underline{z}_i, \underline{z}_j) \theta_N^{l_{max}}(\underline{z}_i) \theta_N^{*l_{max}}(\underline{z}_j) + \frac{1}{N} I_{N+1}(\underline{z}_i) I_{N+1}^*(\underline{z}_j)$$

This allows the recursion (31) to be written as

$$\theta_N^{l+1}(\underline{z}_i) = \theta_N^l(\underline{z}_i) + \left[\sum_{|\underline{z}_i - \underline{z}_j| \le r_o} |\theta_N^{*l}(\underline{z}_j) S_S(\underline{z}_i, \underline{z}_j)|^2 + \alpha_l \bar{S}(\underline{z}_i) \right]^{-1} \qquad (36)$$

$$\left[\frac{1}{N-1} \sum_{|\underline{z}_i - \underline{z}_j| \le r_o} [\theta_N^{*l}(\underline{z}_j) S_S(\underline{z}_i, \underline{z}_j)] \Delta \hat{S}_i^c(\underline{z}_i, \underline{z}_j) + \frac{\alpha}{N} \bar{S}(\underline{z}_i) I_N(\underline{z}_i) \right]$$

$$\Delta \hat{S}_i^c(\underline{z}_i, \underline{z}_j) = I_N(\underline{z}_i) I_N^*(\underline{z}_j) - S_S(\underline{z}_i, \underline{z}_j) \theta_N^l(\underline{z}_i) \theta_N^{*l}(\underline{z}_j) - \sigma_a^2 (1+\sigma_m^2) \delta(\underline{z}_i - \underline{z}_j)$$

$$- \frac{I_o}{P_o} \hat{\bar{I}}^N(\underline{z}_i - \underline{z}_j)(1+\sigma_m^2) - \sigma_m^2 \iint_{-\infty}^{\infty} [\hat{\bar{I}}^N(\underline{z}_i - \beta) \hat{\bar{I}}^{N*}(\underline{z}_j - \beta) - \hat{S}_i(\underline{z}_i - \beta, \underline{z}_j - \beta)] d\beta$$

This algorithm is similar in form to a Kalman Filter where Kalman weighting functions have been greatly simplified. A Kalman Filter approach will be taken to obtain a more general result with a better analytic basis for its form.

2-2 - A New Approach: A Kalman Filter Algorithm

The problem of the real-time estimation of the object $\theta(\underline{z}_i)$, in the case of evolution of the object and non-stationarity of the atmospheric characteristics, can be formulated using a Kalman Filter approach.

As for the existing least-squares algorithm, the assumption of isoplanatic imagery will enable us to transform integral equations into algebraic equations and therefore the model in the frequency domain will be preferred to the model in the spatial domain.

The remainder of this paper treats the theoretical formulation of the Kalman Filter and its particularities due to our special case.

However, before studying the Kalman algorithm, a slightly modified notation, taking into account the evolution of the object and of the statistical characteristics of the turbulence, needs to be introduced:

Let the Nth image measured at time T_N be represented in the spatial frequency domain by

$$I_N(\underline{z}_i) = S_{i,N}\ \theta_N(\underline{z}_i) + n_{i,N} \tag{37}$$

where

$I_N(\underline{z}_i)$ is the Fourier transform of the measured image,
$S_{i,N}$ is the optical transfer function,
$\theta_N(\underline{z}_i)$ is the Fourier transform of the object, and
$n_{i,N}$ is the Fourier transform of the measurement noise.

This statement is illustrated by the following block-diagram.

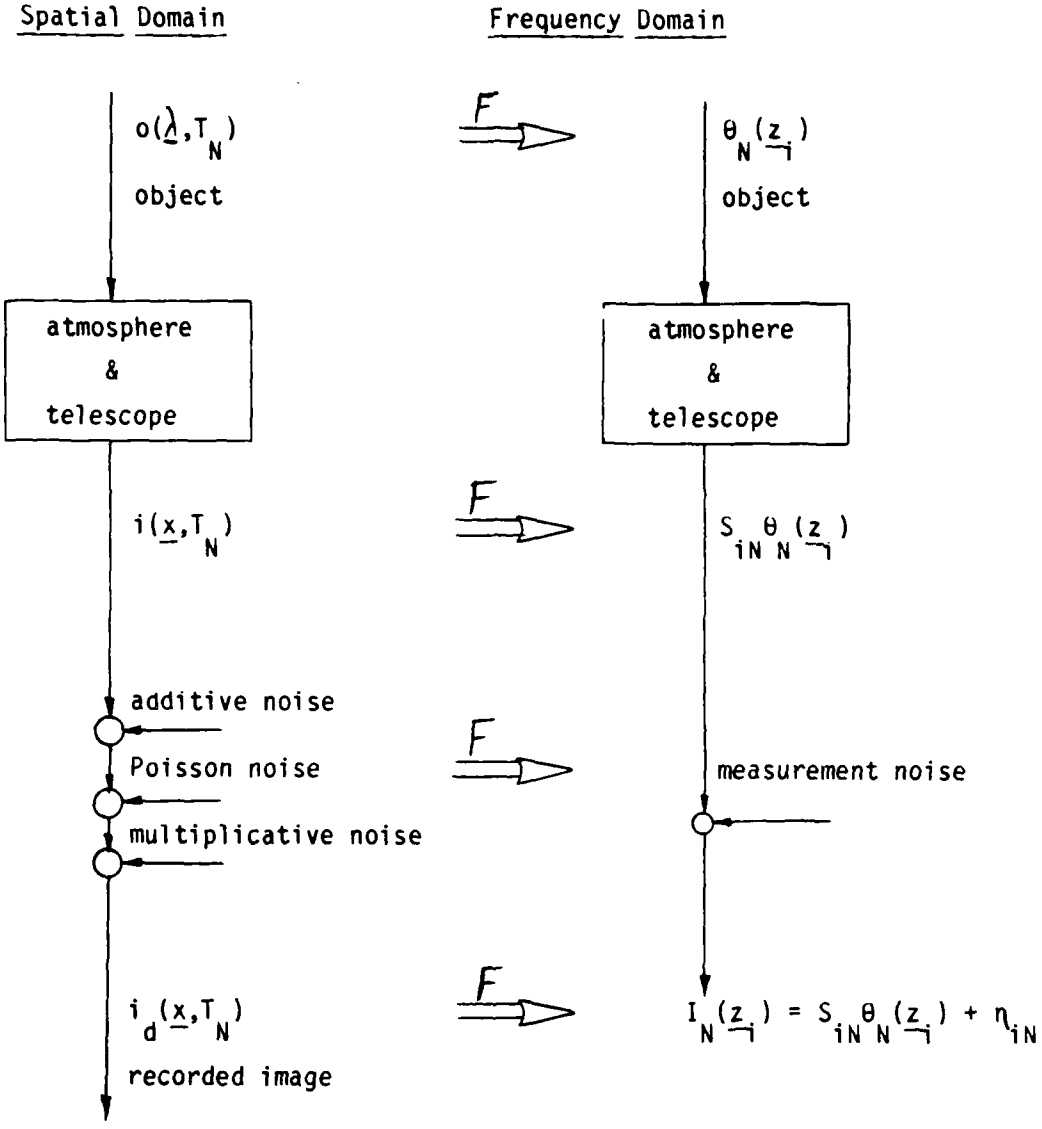

the arrow $\xRightarrow{F}$ symbolizes the two-dimensional Fourier transform

Section 3 - Theoretical Formulation of the Kalman Filter

3-1 - Definition of the State Vector and of the Observations Vectors

Both the real part and imaginary part of the object $\Theta(\underline{z}_i)$ will compose the real state vector $\underline{X}$, which we want to estimate. The state vector can depend on time (we want an algorithm that permits the evolution of the object) and $\underline{X}_N$ will represent the state at time N.

At each time N, we receive a new image. Let us call $\underline{I}_N(\underline{z}_i)$ the Nth image, in the frequency domain, and at the frequency $\underline{z}_i$. This image is received at time N. With this image we can define a vector of observations Y_N. Y_N is composed of measurements $\underline{I}_N(\underline{z}_i)\underline{I}_N^*(\underline{z}_j)$ when $|\underline{z}_i - \underline{z}_j| \leq r_c$; or to be more precise, the real vector Y_N is composed of the real and imaginary parts of $\underline{I}_N(\underline{z}_i)\underline{I}_N^*(\underline{z}_j)$.

3-2 - Equations of the Kalman Filter

The purpose of the Kalman Filter is to build a sequence of estimates of the states ($\underline{X}_N$, N=1,...) from an initial estimate $\underline{X}_{1/0}$ of the state $\underline{X}_1$. Each estimate is a realization of a random process and is then characterized by its statistical properties, in particular the mean and covariance matrix.

Let us call $\underline{X}_{N/N}, N=1,\ldots$ the sequence of estimates, resulting from our Kalman Filter. We shall require for our estimate $X_{N/N}$ to be an unbiased estimate with a minimum covariance matrix $C_{N/N}$.

In order to build $\underline{X}_{N/N}$, we use the information given by the N first images. $X_{N/N}$ is then called the a-posteriori estimate. The information given by the Nth image is stored in the vector Y_N. Using the relation

$$\underline{I}_N(\underline{z}_i) = S_{i,N}\,\Theta_N(\underline{z}_i) + \eta_{i,N} \qquad (38)$$

we can express the observations Y_N as a quadratic function of the state $\underline{X}_N$:

$$Y_N = \mathcal{H}_N(\underline{X}_N) + \vec{n}_N \tag{39}$$

where $\mathcal{H}_N$ is a deterministic quadratic function and $\vec{n}_N$ is a noise vector of zero mean and covariance matrix R_N. This is the observation equation of the Kalman Filter.

The observations do not depend linearly on the state, but follow the quadratic equation (39). In order to obtain the state covariance $C_{N/N}$, we have to use a Taylor series of $\mathcal{H}(\cdot)$ and then introduce the Jacobian matrix H_N. To obtain $C_{N/N}$ as a function of only $C_{N/N-1}$, K_N, and R_N we have to restrict the Taylor series to the first order items.

As shown in the following Section 3-3, the noise of observations is not Gaussian. However, we will use only the first and second-order moments.

These "non-linear observations" and the use of the Jacobian matrix to linearize them about the current estimate results in an algorithm known as the extended Kalman Filter. This solution of will be optimum in the sense of minimum covariance, but not in the sense of maximum likelihood.

Estimation of the state given the first image, $\underline{X}_{1/1}$

If the a-priori state estimate, $\underline{X}_{1/0}$, is unbiased, and if we look for an unbiased estimate of $\underline{X}_{1/1}$ as a linear combination of Y_1 and $\underline{X}_{1/0}$, we can prove that $\underline{X}_{1/1}$ must follow the equation:

$$\underline{X}_{1/1} = \underline{X}_{1/0} + K_1\left(Y_1 - \mathcal{H}(\underline{X}_{1/0})\right). \tag{40}$$

The gain K_1, also called Kalman gain, will be chosen such that the covariance matrix of $\underline{x}_{1/1}$, is minimum.

Let us call $C_{1/0}$ the covariance matrix of $\underline{x}_{1/0}$. Then, expanding (40) about $\underline{x}_{1/0}$ gives

$$\underline{x}_{1/1} - \underline{x}_1 = (I - K_1 H_1)(\underline{x}_{1/0} - \underline{x}_1) + K_1 \vec{n}_1 \tag{41}$$

This relation permits us to calculate $C_{1/1}$ as a function of $C_{1/0}$, K_1, and R_1.

$$C_{1/1} = (I - K_1 H_1) C_{1/0} (I - K_1 H_1)^T + K_1 R_1 K_1^T \tag{42}$$

$C_{1/1}$ is a definite positive symmetric matrix associated with a definite positive quadratic form that will be minimum for

$$K_1 = C_{1/0} H_1^T D_1^{-1} \qquad \text{with} \qquad D_1 = H_1 C_{1/0} H^T + R_1$$

and we shall have:

$$\underline{x}_{1/1} = \underline{x}_{1/0} + K_1 \left(Y_1 - \mathcal{H}_1 (\underline{x}_{1/0}) \right) \tag{43}$$

$$C_{1/1} = C_{1/0} - K_1 H_1 C_{1/0} \tag{44}$$

Prediction of the state at the second image $\underline{x}_{2/1}$ from $\underline{x}_{1/1}$

The evolution of the state between the times N and N+1 is given by an equation of evolution of the following type:

$$\underline{x}_{N+1} = \mathcal{F}(\underline{x}_N, \underline{U}_{N+1}) + \vec{b}_{N+1} \tag{45}$$

where $\mathcal{F}$ is a deterministic function that can house a very general form, where $\underline{U}_{N+1}$ is an input vector and where $\vec{b}_{N+1}$ is a noise vector of zero mean and covariance matrix Q_{N+1}.

To simplify the presentation, we suppose $\mathcal{F}_N$ linear:

$$\underline{x}_{N+1} = F_N \underline{x}_N + G_{N+1} \underline{U}_{N+1} + \vec{b}_{N+1} \tag{46}$$

Using the estimate $\underline{x}_{1/1}$ which is the "best estimate" in the sense of minimum covariance available for $\underline{x}_1$, we can predict the unbiased estimate $\underline{x}_{2/1}$ for $\underline{x}_2$ by:

$$\underline{x}_{2/1} = F_1 \underline{x}_{1/1} + G_2 \underline{U}_2 \tag{47}$$

$\underline{x}_{2/1}$ is called the a-priori estimate of $\underline{x}_2$, its covariance matrix, $C_{2/1}$, is given by

$$C_{2/1} = F_1 C_{1/1} F_1^T + Q_2 \tag{48}$$

Using the second image and repeating the operation we performed to obtain $\underline{x}_{1/1}$ from $\underline{x}_{1/0}$ we obtain a-posteriori estimate of $\underline{x}_2$: $\underline{x}_{1/2}$ and its covariance $C_{2/2}$.

Using alternate filtering and evolution equations, we can compute $(\underline{x}_{N/N}$; N=1,...). The Kalman Filter equations can be summarized by the following set of equations:

Filtering Equations

$$K_N = C_{N/N-1} H_N^T \left(H_N C_{N/N-1} H_N^T + R_N \right)^{-1} \tag{49}$$

$$H_N = \left[\frac{\partial \mathcal{H}_N(\underline{x})}{\partial \underline{x}} \Big|_{\underline{x} = \underline{x}_{N/N-1}} \right]$$

$$\underline{x}_{N/N} = \underline{x}_{N/N-1} + K_N \left(Y_N - \mathcal{H}(\underline{x}_{N/N-1}) \right)$$

$$C_{N/N} = C_{N/N-1} - K_N H_N C_{N/N-1}$$

Evolution Equations

$$\underline{X}_{N+1/N} = F_N \underline{X}_N + G_{N+1} \underline{U}_{N+1} \tag{50}$$

$$C_{N+1/N} = F_N C_{N/N} F_N^T + Q_{N+1}$$

3-3 - Particularities of the Noise of Observations - $\vec{n}_N$ and Form of the Equation of Observation

Another particularity of this Kalman Filter is the model of the noise of observations $\vec{n}_N$. This noise results from a combination of noises of different sources:

Noise due to the turbulence of the atmosphere which is modeled by a random transfer function of the telescope, $S_{i,N}$ at the frequency z_i

Noise of measurement $\eta_{i,N}$ (additive, multiplicative and Poisson noise).

In order to understand the noise process, we can use a block-diagram and some simplified notation.

Given a time N, we can omit the index N appearing in the notation and we define x_i and y_i as follows:

$$x_i = \Theta_N(z_i) \tag{51}$$

$$y_i = I_N(z_i) \tag{52}$$

Block Diagram

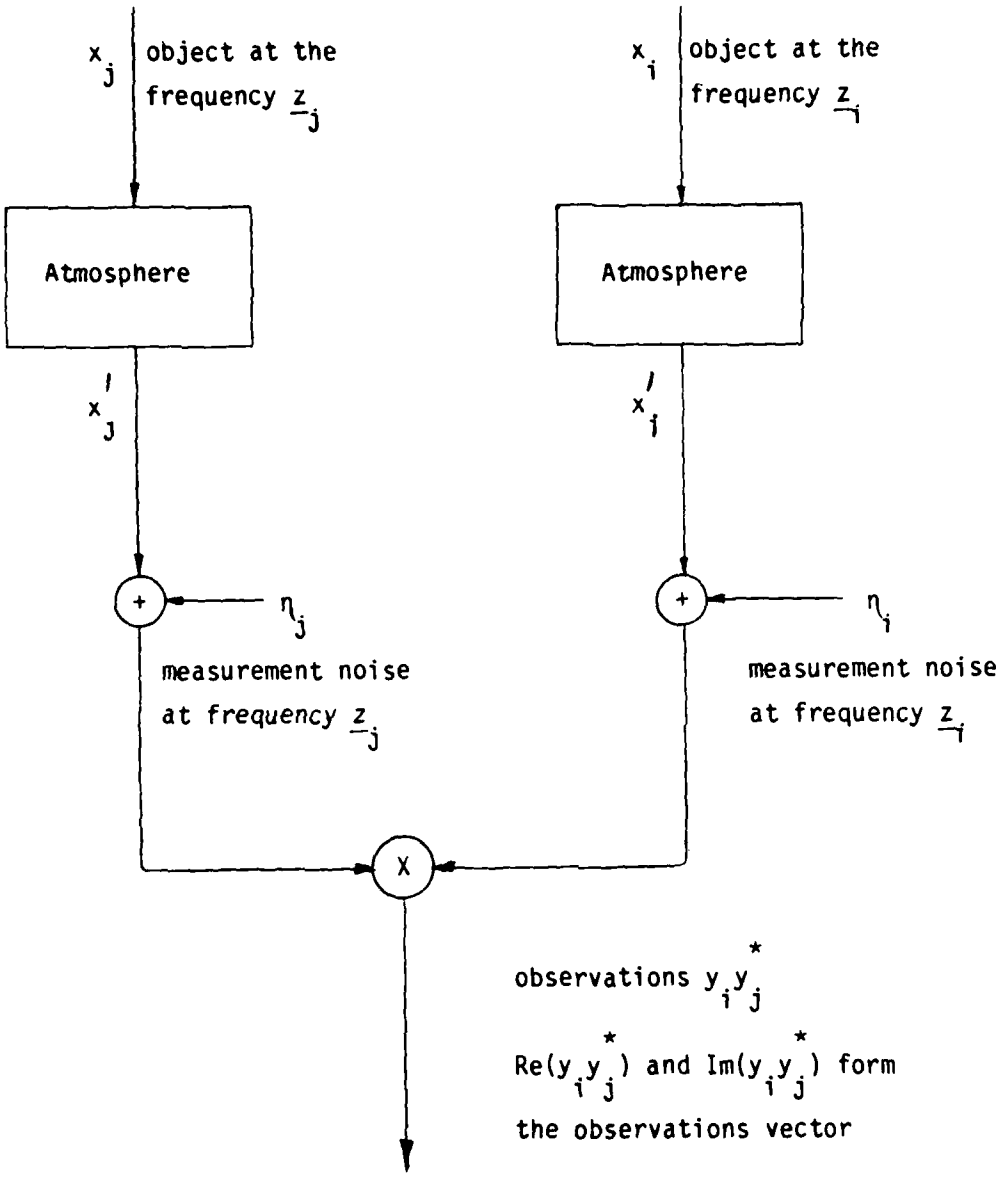

x_i' is the image received by the telescope at the frequency $\underline{z}_i$. The real and imaginary parts of x_i are elements of the state vector. y_i is the measured image at the frequency $\underline{z}_i$.

By definition of the transfer function S_i at the frequency $\underline{z}_i$, we have

$$x_i' = S_i \, x_i \tag{53}$$

and by definition of the noise of measurement

$$y_i = x_i' + n_i \, , \tag{54}$$

$$y_i = S_i x_i + n_i \, . \tag{55}$$

To help understand the form of the observation equation and the particularities of the noise $\vec{n}_N$, it is interesting to calculate $y_i y_j^*$

$$y_i y_j^* = (S_i x_i + n_i)(S_j x_j + n_j)^* \tag{56}$$

$$y_i y_j^* = x_i x_j^* S_i S_j^* + n_i n_j^* + x_i S_i n_j^* + x_j^* S_j^* n_i$$

To go from this expression of $y_i y_j^*$ to the equation of observations $Y_N = \mathcal{H}_n(\underline{x}_N) + \vec{n}_N$, we use the relation,

$$y_i y_j^* = E(y_i y_j^*) + (y_i y_j^* - E(y_i y_j^*)) \tag{57}$$

where E(p) denotes the expected value of the random process p.

The real and imaginary parts of the terms $E(y_i y_j^*)$ will compose the

elements of the deterministic vector $\mathcal{H}(\underline{x}_n)$. Also, the real and imaginary parts of $(y_i y_j^* - E(y_i y_j^*))$ will compose the elements of the noise vector $\vec{n}_N$.

Therefore, by construction $\mathcal{H}_N(\underline{x}_N)$ will be deterministic and the noise vector $\vec{n}_N$ will have a zero mean.

Calculation of $E(y_i y_j^*)$; form of the function $\mathcal{H}_n$ and matrix H_N

The two random processes, noise of turbulence and noise of measurements, are statistically independent. Also, the noise of measurement has zero mean. This allows $E(y_i y_j^*)$ to be simplified,

$$E(y_i y_j^*) = x_i x_j^* E(s_i s_j^*) + E(\eta_i \eta_j^*) \qquad (58)$$

The parameters of the complex function $\mathcal{H}_N(\underline{x}_N)$ are composed of the second-order moments of the noises of turbulence and measurement: $E(s_i s_j^*)$ and $E(\eta_i \eta_j^*)$.

Knowing that $E(s_i s_j^*)$ is a real number, the elements of $\mathcal{H}_N(\underline{x}_n)$ will have one of the following forms:

$$Re(x_i x_j^*)E(s_i s_j^*) + Re(E(\eta_i \eta_j^*)) = \left(Re(x_i)Re(x_j) + Im(x_i)Im(x_j)\right)E(s_i s_j^*) + Re(E(\eta_i \eta_j^*))$$

or

$$Im(x_i x_j^*)E(s_i s_j^*) + Im(E(\eta_i \eta_j^*)) = \left(Re(x_j)Im(x_i) - Re(x_i)Im(x_j)\right)E(s_i s_j^*) + (E(\eta_i \eta_j^*))$$

Then, the derivatives of these expressions with respect to the real or imaginary parts of x_i or x_j will give the elements of the Jacobian matrix H_N. These elements will be one of the following types:

$$Re(x_j)E(s_i s_j^*),\ \pm Re(x_i)E(s_i s_j^*),\ Im(x_j)E(s_i s_j^*),\ \pm Im(x_i)E(s_i s_j^*),\ \text{or } 0.$$

The second-order moments of the noise of turbulence are the parameters

of the Jacobian matrix H_N.

The Noise $\vec{n}_N$ and its Covariance Matrix R_N

The elements of $\vec{n}_N$ are given by the real and imaginary parts of

$$y_i y_j^* - E(y_i y_j^*) = x_i x_j^* (S_i S_j^* - E(S_i S_j^*) + \eta_i \eta_j^* - E(\eta_i \eta_j^*)) + x_i S_i \eta_j^* + x_j^* S_j^* \eta_i \quad (59)$$

Some statistical properties of the noise $\vec{n}_N$ will be given for the covariance matrix of $\vec{n}_N$, R_N, which is involved in the Kalman equations.

The elements of R_N will be of one of the three following forms:

$$E\left(Re(y_i y_j^* - E(y_i y_j^*))\, Re(y_k y_l^* - E(y_k y_l^*))\right) = \frac{1}{2} Re\left[Cov(y_i y_j^*, y_k y_l^*) + Cov(y_i y_j^*, y_k^* y_l)\right]$$

$$E\left(Re(y_i y_j^* - E(y_i y_j^*))\, Im(y_k y_l^* - E(y_k y_l^*))\right) = \frac{1}{2} Im\left[Cov(y_i y_j^*, y_k y_l^*) - Cov(y_i y_j^*, y_k^* y_l)\right]$$

$$E\left(Im(y_i y_j^* - E(y_i y_j^*))\, Im(y_k y_l^* - E(y_k y_l^*))\right) = -\frac{1}{2} Re\left[Cov(y_i y_j^*, y_k y_l^*) - Cov(y_i y_j^*, y_k^* y_l)\right]$$

The general formula for $Cov(y_i y_j^*, y_k y_l^*)$ is developed in Appendix 1 and will permit us to calculate the matrix R_N.

The general formula for $Cov(y_i y_j^*, y_k y_l^*)$ is

$$Cov(y_i y_j^*, y_k y_l^*) = x_i x_j^* x_k x_l^* \left(E(S_i S_j^* S_k S_l^*) - E(S_i S_j^*) E(S_k S_l^*)\right) \quad (60)$$
$$+ x_j^* x_l^* E(S_j^* S_l^*) E(\eta_i \eta_k) + x_i x_l^* E(S_i S_l^*) E(\eta_j^* \eta_k)$$
$$+ x_j^* x_k E(S_j^* S_k) E(\eta_i \eta_l^*) + x_i x_k E(S_i S_k) E(\eta_j^* \eta_l)$$
$$+ x_l^* E(S_l^*) E(\eta_i \eta_j^* \eta_k) + x_k E(S_k) E(\eta_i \eta_j^* \eta_l^*)$$
$$+ x_j^* E(S_j^*) E(\eta_k \eta_l^* \eta_i) + x_i E(S_i) E(\eta_k \eta_l^* \eta_j^*)$$
$$+ E(\eta_i \eta_j^* \eta_k \eta_l^*) - E(\eta_i \eta_j^*) E(\eta_k \eta_l^*)$$

The following table gives the orders of various moments in the terms of $\mathrm{Cov}(y_i y_j^*, y_k y_l^*)$.

	For the noise of turbulence	and for the noise of measurement
in terms of the 1st line	4	no moment
in terms of 2nd and 3rd lines	2	2
in terms of the 4th and 5th lines	1	3
in terms of 6th line	no moment	4

We can notice first that the sum of the orders of the moments of the noise and turbulence and of the noise of measurement is always equal to four, and second that third-order moments of the noise of turbulence have disappeared because they were multiplied by the first-order moment of the noise of measurement, that is by zero.

Conclusion

The calculation of the second-order moments of the noise of observation $\vec{n}_N$ will require the knowledge of the 1st, 2nd, 3rd and 4th order moments of the noises of turbulence and measurement. This is due to the nonlinearity of the observation equations.

3-4 - Particularities of the Covariance Matrix of the State Vector

One particularity of the state vector comes from the fact that it contains real and imaginary parts of complex numbers; and this particularity will confer a special structure to its covariance matrix.

Let us consider $\underline{x}_N$ the state vector at the time N and an estimate of it $\underline{\hat{x}}_n$. The covariance is given by

$$C_n = E\left[(\hat{\chi}_n - \chi_n)(\hat{\chi}_n - \chi_n)^T\right]. \tag{61}$$

C_n is equal to $C_{n/n}$ if $\hat{\chi}_n = \hat{\chi}_{n/n}$ or to $C_{n/n-1}$ if $\hat{\chi}_n = \hat{\chi}_{n/n-1}$. χ_N is composed of the real and imaginary parts of $\theta_n(\underline{z}_i)$ and we can also define the complex vector $\underline{\theta}_N$ whose elements are $\theta_N(\underline{z}_i)$. An estimate of $\underline{\theta}_N$ is given by $\hat{\underline{\theta}}_N$. The dimension of χ_n and $\hat{\chi}_n$ is twice the dimension of $\underline{\theta}_n$ and $\hat{\underline{\theta}}_N$.

We can also define two complex matrices C_N and $\tilde{C}_N$ as follows:

$$C_N = E\left[(\hat{\underline{\theta}}_n - \underline{\theta}_N)(\hat{\underline{\theta}}_n - \underline{\theta}_N)^T\right] \tag{62}$$

$$\tilde{C}_n = E\left[(\hat{\underline{\theta}}_n - \underline{\theta}_n)(\hat{\underline{\theta}}_n - \underline{\theta}_n)^{*T}\right]$$

If p and q are some elements of $\underline{\theta}_N$, then C_N will be composed of terms of the form Cov(p,q) and $\tilde{C}_n$ will be composed of terms of the form $\mathrm{Cov}(p,q^*)$.

Also, C_N is composed of terms of the following form:

$$\mathrm{Cov}(\mathrm{Re}(p), \mathrm{Re}(q)) = \tfrac{1}{2}\mathrm{Re}\left[\mathrm{cov}(p,q) + \mathrm{Cov}(p,q^*)\right] \tag{63}$$

$$\mathrm{Cov}(\mathrm{Re}(p), \mathrm{Im}(q)) = \tfrac{1}{2}\mathrm{Im}\left[\mathrm{cov}(p,q) - \mathrm{Cov}(p,q^*)\right]$$

$$\mathrm{Cov}(\mathrm{Im}(p), \mathrm{Im}(q)) = -\tfrac{1}{2}\mathrm{Re}\left[\mathrm{cov}(p,q) - \mathrm{Cov}(p,q^*)\right]$$

We want to express C_N as a function of C_n and $\tilde{C}_N$. Then, assume that the elements of χ_N are ordered as follows:

$$\chi_N = \begin{bmatrix} \mathrm{Re}(\underline{\theta}_N) \\ \hline \mathrm{Im}(\underline{\theta}_N) \end{bmatrix}. \tag{64}$$

C_N is equal to the block-matrix,

$$C_N = \left[\begin{array}{c|c} A_N & B_N^T \\ \hline B_N & D_N \end{array}\right]. \tag{65}$$

Using the sets of formulas (62) and (63) we can show that,

$$A_N = \frac{1}{2} Re\left[G_N + \tilde{G}_N\right] \tag{66}$$

$$D_N = -\frac{1}{2} Re\left[G_N - \tilde{G}_N\right] \tag{67}$$

$$B_N = \frac{1}{2} Im\left[G_N - \tilde{G}_N\right] \tag{68}$$

Because $Im(G_N)$ is a symmetric matrix and $Im(\tilde{G}_N)$ is an antisymmetric matrix, we can rewrite (68) and (65) as

$$B_N^T = \frac{1}{2}\left[Im\left[G_N + \tilde{G}_N\right]\right] \tag{69}$$

and

$$C_N = \left[\begin{array}{c|c} \frac{1}{2} Re(G_N + \tilde{G}_N) & \frac{1}{2} Im(G_N + \tilde{G}_N) \\ \hline \frac{1}{2} Im(G_N - \tilde{G}_N) & -\frac{1}{2} Re(G_N - \tilde{G}_N) \end{array}\right] \tag{70}$$

Separating the terms concerning G_N and $\tilde{G}_N$ we obtain

$$C_N = \frac{1}{2}\left[\begin{array}{c|c} Re(G_N) & Im(G_N) \\ \hline Im(G_N) & -Re(G_N) \end{array}\right] + \frac{1}{2}\left[\begin{array}{c|c} Re(\tilde{G}_N) & Im(\tilde{G}_N) \\ \hline -Im(\tilde{G}_N) & Re(\tilde{G}_N) \end{array}\right] \tag{71}$$

Section 4 - Particular problems of the application of a Kalman Filter to Speckle Imaging

4-1 - Decomposition of our Large-Scale System into Subsystems

When implementing a Kalman algorithm to treat speckle images, the first problem we meet is a problem of dimension.

A typical dimension of a digitized image has been 256 by 256 elements (pixels). We will use the discrete Fourier transforms of the measured images as input data at a discrete set of two-dimensional frequencies $\underline{z}_i (z_{i1}, z_{i2})$. Using the symmetry properties of the Fourier transform and the aperture limits will reduce the set of frequencies that must be treated. The result of estimating the object, in the frequency domain, is also a discrete set of values of the Fourier transform of the object. This set will have the same dimension as the one concerning the image and will be treated by the same FFT algorithm to restore the estimate of the object in the spatial domain. Then, the state of our Kalman Filter, , will typically have about 51,500 elements ($256 \times 256 \times \pi/4$).

This is a large-scale system that will require a specific algorithm of decomposition. However, the decomposition of the whole system into several subsystems of reasonable size will come naturally when examining the structure of the observations. As a matter of fact, the measurement $y_i y_j^*$ does not bring any useful information whenever $|\underline{z}_i - \underline{z}_j| > r_0$. Thus, when we want to estimate a particular x_i, we shall select a subsystem, $\mathcal{S}_{x_i}$, from the full system composed of all the x_j's such that $y_i y_j^*$ is one of the measurements used in the full system.

Then the state vector of the subsystem $\mathcal{S}_{x_i}$ is a vector restricted to the real and imaginary parts of the x_j's such that $|\underline{z}_i - \underline{z}_j| \leq r_0$ and the observations vector is composed of all the measurements $y_i y_j^*$ that can

be formed with the $\chi_{i'2}$ and $\chi_{j'2}$ belonging to the state vector of the subsystem.

Since r_c is very small compared to the aperture R, the dimension of the state of the subsystem is very small compared to the dimension of the state of the full system.

This decomposition is actually an approximation. Let us go back to the full system and let us consider three frequencies $\underline{z}_i$, $\underline{z}_j$, and $\underline{z}_k$ such that: $|\underline{z}_i - \underline{z}_j| \leq r_o$, $|\underline{z}_j - \underline{z}_k| \leq r_o$, and $|\underline{z}_i - \underline{z}_k| > r_o$.

Then, the two measurements $y_i y_j^*$ and $y_i y_k^*$ will belong to the vector of observations of the full system, but not $y_i y_k^*$.

However, the measurement $y_j y_k^*$ will be helpful for the estimation of χ_j and this estimation of χ_j will affect the estimation of χ_i, by the intermediary of the observation $y_i y_j^*$. Therefore, $y_j y_k^*$, which is an observation of the subsystem $\mathcal{S}_{\chi_k}$, will affect the estimation of χ_i even if $|\underline{z}_i - \underline{z}_k|$ is greater than r_o. Thus, the subsystems $\mathcal{S}_{\chi_i}$ and $\mathcal{S}_{\chi_k}$ are not independent even if $|\underline{z}_i - \underline{z}_k| > r_o$.

This shows that the Kalman filter propogates the information given by a particular measurement $y_j y_k^*$ along the whole set of frequencies $\underline{z}_i$ and that the estimation of χ_i will be affected by the whole set of measurements

$$y_{jN}\, y_{kN}^* = I_N(\underline{z}_j)\, I_N^*(\underline{z}_k), \quad N = 1, 2, \cdots$$

whatever $\underline{z}_i$, $\underline{z}_j$, and $\underline{z}_k$ may be. Obviously, the dependence of the estimation of χ_i upon the measurements $(y_{jN} y_{kN}^*)$, $N = 1, 2 \cdots$ will be more or less important depending on the distances $|\underline{z}_i - \underline{z}_j|$ and $|\underline{z}_i - \underline{z}_k|$.

The Effect of Propagation of the Information on the Covariance Matrix of the State of the Kalman Filter

If we initialize χ_i using the first image and the information this image gives with the measurements $y_i y_j^*$ such that $|z_i - z_j| \leq r_o$, then the covariance matrix of the state will be initialized by a matrix with a band structure and the width of the band will depend on the number of frequencies inside the circle of radius r_o.

As a result of the phenomena of propagation, if we run the Kalman Filter, the width of the band of the covariance matrix will increase with each new image and some covariance terms will appear between two estimates χ_i and χ_k such that $|\underline{z}_i - \underline{z}_k| > r_o$.

Implication on the Choice of the Subsystems

The algorithm on the subsystems $\mathcal{S}_{\chi_i}$ must restore this propagation of the information in order to use each observation as much as possible. To achieve this goal, we must make an adequate choice for the subsystems.

Assume that we make the following choice of subsystems. We partition the set of frequencies $\underline{z}_i$ into "circles" of radius r_o such that each $\underline{z}_i$ (respectively χ_i) belongs to one and only one "circle" (respectively subsystem). The treatment of one subsystem $\mathcal{S}_{\chi_i}$, associated with a subset of frequencies, will provide the estimates of all the χ_j's such that $|\underline{z}_i - \underline{z}_j| \leq r_o$. Then the treatment of all the subsystems will provide an estimate of the whole object.

Nevertheless, with this choice of subsystems, we would not restore the phenomena of propagation of the information along the set of frequencies because we would make two subsystems appear independent, whereas they are not in the full system. Also, the use of measurements would not be optimal: the estimation of χ_j belonging to

$\mathcal{S}_{x_j}$ and of χ_k belonging to $\mathcal{S}_{x_i}$, such that $\mathcal{S}_{x_j}$ is different from $\mathcal{S}_{x_i}$ but $|\underline{z}_j - \underline{z}_k| \leq r_o$, would not use the observation $y_j y_k^*$. This discarding of the measurements that correspond to crossproducts of state elements in separate subsystems is undesirable. Because such a choice is inappropiate, we must chose a sequence of subsystems that retains these measurements. There are several closely related viewpoints which allow the use of the needed measurements.

First, we can choose a sequence of K subsystems $\mathcal{S}(1), \mathcal{S}(2), \ldots \mathcal{S}(K)$ such that two adjacent subsystems $\mathcal{S}(m)$ and $\mathcal{S}(m+1)$ have a common part in their state vector. Then the part of the object, which is common to $\mathcal{S}(m)$ and $\mathcal{S}(m+1)$ and estimated by the Kalman filter on the subsystem $\mathcal{S}(m)$, will be used by the Kalman filter on $\mathcal{S}(m+1)$. Thus, using the a-posteriori estimate for $\mathcal{S}(m)$, we shall improve the a-priori estimate for $\mathcal{S}(m+1)$.

Second, we can expand the observations vector used with a given subsystem $\mathcal{S}_{x_i}$ to include all measurements that involve at least one element of the state vector. Then, all of the data will be used.

Finally, we can view all of these subsystem constructions as particular cases of treating the observations of the full system in subgroups and restricting the elements of the state vector being updated. The updates are then treated in a sequence which treats all of the observations and all of the state vector. The subgroups of either the observations or the state vector or both must overlap.

This overlapping characteristic of the algorithm will propagate the information on the estimation of the state. Thus, the state estimates will be interdependent and correlated. However, the corresponding terms of the covariance will still be zero and the norm of the covariance will be larger than computed by the full system.

Let us illustrate the first viewpoint by a one-dimensional example.

Let us consider a set of Fourier transforms of one-dimensional images. The set of frequencies has been discretized into M discrete frequencies separated by intervals of constant length ; $z_0 = 0$, z_1, ... z_{m-1}. We choose the subsystems so that the state of the subystem $\mathcal{S}(I+1)$ is obtained from the state of the subsystem $\mathcal{S}(I)$ by dropping the object at the frequency z_{I-1}, and inserting the object at the frequency z_{I+K-1}.

The treatment of $\mathcal{S}(1)$ will provide an estimate of $x_0, x_1, \cdots, x_{K-1}$.

The treatment of $\mathcal{S}(2)$ will provide an estimate of $x_1, x_2, \cdots, x_K$.

The treatment of $\mathcal{S}(3)$ will provide an estimate of $x_2, x_3, \cdots, x_{K+1}$.

After the treatment of $\mathcal{S}(1)$, we keep the estimate of x_0 because it has been made using all the information $y_0 y_0^*, y_0 y_1^*, \ldots y_0 y_{K-1}^*$. We also use the estimates of x_1, x_2, ... x_{K-1} as the a-priori estimates for the Kalman Filter of $\mathcal{S}(2)$. The estimate of x_1, we obtained with $\mathcal{S}(1)$ did not use the information given by $y_1 y_K^*$.

Then, with $\mathcal{S}(2)$ we shall again estimate x_1, now using $y_1 y_K^*$. The result will contain information about $y_0 y_1^*$ given through the a-priori estimation of x_1, and information about $y_1 y_1^*$, $y_1 y_2^*$, ... $y_1 y_K^*$ given through the observations vector of $\mathcal{S}(2)$. We can repeat this operation until the Kalman filter has been applied to the last subsystem. We start again with the treatment of $\mathcal{S}(1)$ when we receive a new image. Such an algorithm will use the important measurement information and will propagate the information along the set of frequencies.

If the discretization of the Fourier transforms of the images is very fine, corresponding to a large field of view, we shall have too many points inside a circle of radius r_0 and the state of any subsystem may still be too large to be treated easily and quickly by a mini-computer. In this case, we can either reduce the field of view and treat subsections of available images, or formulate the Kalman filter using a more restricted update of the state vector.

4-2 - The Kalman Gain Matrix

Computing the Kalman gain matrix usually requires most of the computational effort associated with the filtering equations. A straight forward treatment of the Kalman gain equation for the full system would require the inversion of an enormous matrix whose order is the same as the observations vector. Fortunately, by using the decompostion into subsystems, the order of the matrix that needs to be inverted is greatly reduced. However, because of the high number of images and subsystems, the computation effort required for inversion would still be quite large.

The required computational effort can be reduced further if we forego some of the generality of the Kalman formulation. We shall assume that our system has no dynamics. By "no dynamics", we mean that the equation of evolution $\underline{\chi}_{k+1} = \underline{\mathcal{F}}(\underline{\chi}_k, \underline{U}_{k+1}) + \vec{b}$ becomes $\underline{\chi}_{k+1} = \underline{\chi}_k$. This simplification restricts the class of objects being estimated to constant images described by the general diffraction limited Fourier transform. Although we do not allow any evolution for the object, we allow the statistical characteristics of the noises of turbulence and measurement to change. For example, changes in the seeing conditions and measurement conditions are quite common.

How much the required computational effort can be reduced depends on the degree to which the Kalman gain calculation can be simplified. Two alternatives will be explored briefly. First, the Kalman gain calculation will be approximated by a difference equation. Second, further simplifying assumptions will be used to allow the Kalman gain to be precomputed to various degrees.

Simplification of the Notation

As the system has no dynamics, the evolution equations of the Kalman Filter become,

for the state:

$$\underline{\chi}_{N+1/N} = \underline{\chi}_{N/N} \tag{72}$$

for its covariance:

$$C_{N+1/N} = C_{N/N} \tag{73}$$

The a-priori variables at time N+1 are equal to the a-posteriori variables at time N. Therefore, we can get rid of the double index notation and $\underline{\chi}_N$ and C_N would now represent the a-posteriori variables, which result from the Kalman filter at time N. The word estimate, if nothing else is precisely expressed, will refer to the a-posteriori estimate.

With the new notation, the filtering equations become:

Gain:

$$K_N = C_{N-1} H_N^T D_N^{-1} \tag{74}$$

$$D_N^{-1} = \left(H_N C_{N-1} H_N^T + R_N\right)^{-1}$$

$$H_N = \left[\frac{\partial \mathcal{H}(\underline{\chi})}{\partial \underline{\chi}}\right]_{\underline{\chi} = \underline{\chi}_{N+1}}$$

State:

$$\underline{\chi}_N = \underline{\chi}_{N-1} + K_N\left(Y_N - \mathcal{H}(\underline{\chi}_{N-1})\right) \tag{75}$$

Covariance:

$$C_N = C_{N-1} - K_N H_N C_{N-1} \tag{76}$$

Development of a Difference Equation for the Kalman Gain

Let us now consider the equations of the gain giving K_N and K_{N+1} :

$$K_N = C_{N-1} H_N^T D_N^{-1} \tag{77}$$

$$K_{N+1} = C_N H_{N+1}^T D_{N+1}^{-1} \tag{78}$$

And, in order to develop a difference equation for the gain, let us define the following matrices:

$$\Delta H_{N+1} = H_{N+1} - H_N \tag{79}$$

$$\Delta R_{N+1} = R_{N+1} - R_N \tag{80}$$

$$\Delta C_N = C_{N-1} - C_N \tag{81}$$

$$\Delta (D_{N+1}^{-1}) = D_{N+1}^{-1} - D_N^{-1} \tag{82}$$

H_{N+1} and H_N (respectively R_{N+1} and R_N) are computed with the a-priori estimates of the state times N+1 and N, $\hat{x}_N$ and $\hat{x}_{N-1}$. Then, ΔH_{N+1} (respectively ΔR_{N+1}) will depend on the variation of the state estimate between times N-1 and N, but it can also depend on the variation of the noise moments between times N and N+1 as these moments are the parameters of the Jacobian matrix (respectively the covariance matrix R).

We must notice the minus sign in (81). The Kalman Filter causes a decrease in the covariance matrix of the state estimate at each iteration.

As we shall see later, the last one among these variation matrices, $\Delta(D_{N+1}^{-1})$ can be approximated in the first order by a linear function of the matrices ΔH_{N+1}, ΔR_{N+1} and ΔC_N.

The equation (78) can now be rewritten as follows:

$$K_{N+1} = (C_{N-1} - \Delta C_N)(H_N + \Delta H_{N+1})^T (D_N^{-1} + \Delta(D_{N+1}^{-1})) \tag{83}$$

and assuming small variations, if we only keep the first order terms, we obtain

$$K_{N+1} = K_N - (\Delta C_N) H_H^T D_N^{-1} + C_{N-1} (\Delta H_{N+1})^T D_N^{-1} + C_{N-1} H_N^T \Delta (D_{N+1}^{-1}) \quad (84)$$

This is the first step to the difference equation we are looking for, and we now need to develop the expression of $\Delta (D_{N+1}^{-1})$ as a function of ΔH_{N+1}, ΔR_{N+1} and ΔC_N. Expanding D_{N+1} and keeping only the first order terms, we obtain:

$$D_{N+1} = D_N \left(I - D_N^{-1} \left(H_N \Delta C_N H_N^T - \Delta H_{N+1} C_{N-1} H_N^T - H_N C_{N-1} \Delta H_{N+1}^T - \Delta R_{N+1} \right) \right) \quad (85)$$

If we denote by ΔM_{N+1} the following matrix:

$$\Delta M_{N+1} = D_N^{-1} \left(H_N \Delta C_N H_N^T - \Delta H_{N+1} C_{N-1} H_N^T - H_N C_{N-1} \Delta H_{N+1}^T - \Delta R_{N+1} \right), \quad (86)$$

we obtain

$$D_{N+1}^{-1} = \left(I - \Delta M_{N+1} \right)^{-1} D_N^{-1} \quad (87)$$

If we use the following approximation:

$$\left(I - \Delta M_{N+1} \right)^{-1} \simeq I + \Delta M_{N+1}, \quad (88)$$

we obtain

$$\Delta (D_{N+1}^{-1}) = \Delta M_{N+1} D_N^{-1} \quad (89)$$

The difference equation for the Kalman gain becomes

$$K_{N+1} = K_N + \left[- \Delta C_N H_N^T + C_{N-1} \Delta H_{N+1}^T + C_{N-1} H_N^T \Delta M_{N+1} \right] D_N^{-1} \quad (90)$$

with

$$\Delta M_{N+1} = D_N^{-1} \left[H_N \Delta C_N H_N^T - \Delta H_{N+1} C_{N-1} H_N^T - H_N C_{N-1} \Delta H_{N+1}^T - \Delta R_{N+1} \right] \quad (91)$$

This recursive formula will permit calculating K_{N+1} from K_N, D_N^{-1}, ΔC_N,

ΔH_{N+1}, and ΔR_{N+1}.

Then assuming we know D_N^{-1}, we will not have to calculate D_{N+1}^{-1} by a matrix inversion in order to obtain K_{N+1}. With the Kalman gain K_{N+1} we can easily get the state estimate $\underline{X}_{N+1}$, its covariance C_{N+1}, the variation matrices, and finally D_{N+1}^{-1}.

Precomputed Kalman Gain Matrices

Finally, we will examine conditions under which the Kalman Gain matrix and state covariance can be partially or fully precomputed. The Kalman gain and state covariance depend on each other, but only the Kalman gain is required for the state estimation recursion. First, we will determine the conditions which reduce the Kalman filter to the recursive least squares algorithm of Section 2. Then, we will consider the effect of removing some of these simplifying conditions.

The recursive least squares algorithm (36) updates the state at only one frequency and uses all the observations within r_0 of that frequency. Under these conditions, the Kalman filter has a two element state vector and a larger observation vector. The Kalman gain and state covariance equations can be rewritten in the form where the matrix inversion lemma has not been applied,

$$K_N = \left[C_{N-1}^{-1} + H^T R^{-1} H\right]^{-1} H^T R^{-1} \tag{92}$$

$$C_N = \left[C_{N-1}^{-1} + H^T R^{-1} H\right]^{-1} \tag{93}$$

Assuming that the atmospheric and measurment statistics are stationary gives constants for the covariance R and the moments used in calculating observation function $\mathcal{H}_N(\underline{X}_N)$ and its Jacobian H_N. Assuming, that the Taylor series from which the Jacobian is obtained is expanded about the correct result rather than the current estimate yields a constant H_N. Under these conditions, the state covariance and Kalman

gain equations can be solved to yield

$$C_N = \frac{1}{N}\left[H^T R^{-1} H\right]^{-1} \tag{94}$$

$$K_N = \frac{1}{N}\left[H^T R^{-1} H\right]^{-1} H^T R^{-1} \tag{95}$$

The resulting recursion becomes

$$\begin{bmatrix} Re(\theta_N(Z_i)) \\ Im(\theta_N(Z_i)) \end{bmatrix} = \begin{bmatrix} Re(\theta_{N-1}(Z_i)) \\ Im(\theta_{N-1}(Z_i)) \end{bmatrix} + K_N\left(Y_N - \mathcal{H}(\theta_{N-1}(Z_i))\right) \tag{96}$$

where the current estimate can be used to evaluate the Kalman gain expression.

This result is directly analogous to the least squares recursion (36) of Section 2, but further simplification is required to complete the comparison. The difference of observations and their predictions are the same for both recursions,

$$\Delta S_i^C(Z_i, Z_j) = Y_N - \mathcal{H}(\theta_{N-1}(Z_i)) \tag{97}$$

Each row of the Jacobian matrix is the partial derivative of one of the observations with respect to the state and has one of three forms:

1. for $y_i y_i^*$; $\left[Re\left(\theta_{N-1}^*(Z_i) S_S(Z_i, Z_j)\right), Im\left(\theta_{N-1}^*(Z_i) S_S(Z_i, Z_j)\right)\right]^T$
2. for $Re[y_i y_j^*]$; $\left[Re\left(\theta_{N-1}^*(Z_j) S_S(Z_i, Z_j)\right), Im\left(\theta_{N-1}^*(Z_i) S_S(Z_i, Z_j)\right)\right]$
3. for $Im[y_i y_j^*]$; $\left[Im\left(-\theta_{N-1}^*(Z_j) S_S(Z_i, Z_j)\right), Re\left(\theta_{N-1}^*(Z_i) S_S(Z_i, Z_j)\right)\right]$

If the observations are assumed to be independent with the same variance, R is given by

$$R = \sigma_R^2 \, I. \tag{98}$$

Now the Kalman gain matrix of (96) is quite close to the gain matrix

of (36). The recursion derived from (97) and written in a form similar to (36) is

$$\begin{bmatrix} Re(\theta_{N+1}(\underline{z}_i)) \\ Im(\theta_{N+1}(\underline{z}_i)) \end{bmatrix} = \begin{bmatrix} Re(\theta_N(\underline{z}_i)) \\ Im(\theta_N(\underline{z}_i)) \end{bmatrix} + C_N H^T \Delta S_i^C \qquad (99)$$

where

$$H^T \Delta S_i^C = \begin{bmatrix} Re(A) \\ Im(A) \end{bmatrix},$$

$$C_N = \frac{1}{N} \begin{bmatrix} B - (Im(\theta^*(\underline{z}_i)) S_S(\underline{z}_i, \underline{z}_i))^2, & Re(\theta^*(\underline{z}_i)) Im(\theta^*(\underline{z}_i)) S_S^2(\underline{z}_i, \underline{z}_i) \\ Re(\theta^*(\underline{z}_i)) Im(\theta^*(\underline{z}_i)) S_S^2(\underline{z}_i, \underline{z}_i), & B - (Re(\theta^*(\underline{z}_i)) S_S(\underline{z}_i, \underline{z}_i))^2 \end{bmatrix}^{-1},$$

$$A = \sum_{|\underline{z}_i - \underline{z}_j| \le r_o} \theta_N^*(\underline{z}_j) S_S(\underline{z}_i, \underline{z}_j) \Delta S_i^C(\underline{z}_i, \underline{z}_j),$$

$$B = \sum_{|\underline{z}_i - \underline{z}_j| \le r_o} \left| \theta_N^*(\underline{z}_j) S_S(\underline{z}_i, \underline{z}_j) \right|^2.$$

Note that (36) used a diagonal matrix inversely proportional to B for the covariance of the state C_N which provides the same normalization for both the real and imaginary parts of the estimate and does not cross couple them. Also, we have not treated lower frequencies, $|\underline{z}_i| < r_o$, in (99).

Increasing the dimension of the state vector does not substantially change the recursion (96). The Kalman gain can still be derived a-priori and evaluated using the current estimate. If we assume that the observation statistics vary only by a multiplicative constant, we only have to compute a scalar weighting factor to replace the 1/N factor in (96).

If we allow the observation statistics to vary more generally, the Kalman gain cannot be derived a-priori. However, if we assume some

restrictive description of how the statistics vary, we can approximate the Kalman gain a-priori. In particular, assume that the observation statistics are slowly varying. For example, the seeing conditions as described by the mean optical transfer function $\overline{S(\underline{z})}$ or r_o, could be slowly varying. Then, $\overline{S(\underline{z})}$ could be estimated over intervals less than the decorrelation time of the seeing conditions and used in the recursion (95) that assumes stationarity.

Conclusion

We have developed a Kalman formulation for the Speckle Imaging problem. The intent was to develop a formulation that would allow the use of mini-computers for Speckle Imaging. This was accomplished by using decompositions of the full system into manageable subsystems. These subsystems result from natural decompositions based on the very limited area of coherence in the aperture caused by atmospheric turbulence. Thus, the limitation of nature which requires that Speckle Imaging is needed aids in making the numeric solution manageable.

Although this formulation was developed under very general conditions for the image and disturbance models, we have examined simplifications and approximations which reduce the computational requirements. These simplified Kalman filters approach a recursive version of the least squares algorithm previously developed.

Appendix 1 - Calculation of the Terms used in the Formation of R_N, the Covariance Matrix of the Noise of Observations $\vec{n}_N$

A - Calculation of the variance and covariance terms of the real and imaginary parts of two complex random processes

If E(r) is the expected value of a real random process r, we naturally define the expected value of a complex random process by:

$$E(p) = E(\,Re(p)\,) + j\,E(\,Im(p)\,)$$

Then, we can define the complex covariance of two complex random processes p and q by:

$$Cov(p,q) = E(\,(p - E(p))\,(\,(q - E(q))\,)$$

Using to the definition of $E(\cdot)$, we can commute the operation $E(\cdot)$ with any of the following ones: $Re(\cdot)$, $Im(\cdot)$, and conjugation. Therefore, we can develop the two following calculations:

1) $$Cov(p,q) = Cov(Re(p),Re(q)) - Cov(Im(p),Im(q)) + j\,Cov(Re(p),Im(q)) + j\,Cov(Im(p),Re(q))$$

2) $$Cov(p,q^*) = Cov(Re(p),Re(q)) + Cov(Im(p),Im(q)) - j\,Cov(Re(p),Im(q)) + j\,Cov(Im(p),Re(q))$$

Combining $Cov(p,q)$ and $Cov(p,q^*)$ we find the three following formulas:

$$Cov\left[Re(p),Re(q)\right] = \frac{1}{2}\,Re\left[Cov(p,q) + Cov(p,q^*)\right]$$

$$Cov\left[Re(p),Im(q)\right] = \frac{1}{2}\,Im\left[Cov(p,q) + Cov(p,q^*)\right]$$

$$Cov\left[Im(p),Im(q)\right] = -\frac{1}{2}\,Re\left[Cov(p,q) - Cov(p,q^*)\right]$$

We shall apply these formulas to $p = y_i y_j^*$ and $q = y_k y_l^*$ and develop below a general formula for:

$$\mathrm{Cov}(p,q) = \mathrm{Cov}(\, y_i y_j^* \,,\, y_k y_l^* \,)$$

and then

$$\mathrm{Cov}(p,q^*) = \mathrm{Cov}(\, y_i y_j^* \,,\, y_l y_k^* \,)$$

To obtain Cov(p,q) from Cov(p,q), we shall interchange the two indices l and k.

B - "Complex Covariance" of the Two Random Complex Processes $y_i y_j^*$ and $y_k y_l^*$

We want to calculate

$$\mathrm{Cov}(\, y_i y_j^* \,,\, y_k y_l^* \,) = E(y_i y_j^* y_k y_l^*) - E(y_i y_j^*)\, E(y_k y_l^*)$$

with

$$y_m + x_m s_m + \eta_m \qquad \text{for } m = i,\ j,\ k,\ \text{or } l.$$

Expanding $pq = y_i y_j^* y_k y_l^*$ gives

$$\begin{aligned} pq = {} & x_i x_j^* x_k x_l^* s_i s_j^* s_k s_l^* + \eta_i \eta_j^* \eta_k \eta_l^* \\ & + x_i x_j^* s_i s_j^* \eta_k \eta_l^* + x_k x_l^* s_k s_l^* \eta_i \eta_j^* \\ & + \underline{x_i x_j^* s_i s_j^* (\eta_k x_l^* s_l^* + \eta_l^* x_k s_k)} \\ & + \underline{x_k x_l^* s_k s_l^* (\eta_i x_j^* s_j^* + \eta_j^* x_i s_i)} \\ & + \eta_i \eta_j^* (\eta_k x_l^* s_l^* + \eta_l^* x_k s_k) + \eta_k \eta_l^* (\eta_i x_j^* s_j^* + \eta_j^* x_i s_i) \\ & + (\eta_i x_j^* s_j^* + \eta_j^* x_i s_i)(\eta_k x_l^* s_l^* + \eta_l^* x_k s_k). \end{aligned}$$

To calculate E(pq), we take the sum of the expected value of each term of the previous sum and we use the statistically independent of the noise of turbulence and the noise of measurement. Also, because of the zero-mean of the noise of measurement, the two underlined terms have a zero mean. Then, the moments of p and q are:

$$
\begin{aligned}
E(pq) = {} & x_i x_j^* x_k x_l^* E(s_i s_j^* s_k s_l^*) + x_i x_j^* E(s_i s_j^*) E(n_k n_l^*) \\
& + x_k x_l^* E(s_k s_l^*) E(n_i n_j^*) + x_j x_l^* E(s_j s_l^*) E(n_i n_k) \\
& + x_i x_l^* E(s_i s_l^*) E(n_j^* n_k) + x_j^* x_k E(s_j^* s_k) E(n_i n_l^*) \\
& + x x_k E(s_i s_k) E(n_j^* n_l^*) + E(n_i n_j^* n_k n_l^*) \\
& + x_l^* E(s^*) E(n_i n_j^* n_k) + x_k E(s_k) E(n_i n_j^* n_l^*) \\
& + x_j^* E(s_j^*) E(n_i n_k n_l^*) + x_i E(s_i) E(n_j^* n_k n_l^*)
\end{aligned}
$$

$$E(p) = x_i x_j^* E(s_i s_j^*) + E(n_i n_j^*)$$

$$E(q) = x_k x_l^* E(s_k s_l^*) + E(n_k n_l^*)$$

Combining these equations we obtain the general "complex covariance":

$$
\begin{aligned}
Cov(y_i y_j^* y_k y_l^*) = {} & x_i x_j^* x_k x_l^* [E(s_i s_j^* s_k s_l^*) - E(s_i s_j^*) E(s_k s_l^*)] \\
& + x_j^* x_l^* E(s_j^* s_l^*) E(n_i n_k) + x_i x_l^* E(s_i s_l^*) E(n_j^* n_k) \\
& + x_j^* x_k E(s_j^* s_k) E(n_i n_l^*) + x_i x_k E(s_i s_k) E(n_j^* n_l^*) \\
& + x_l^* E(s_l^*) E(n_i n_j^* n_k) + x_k E(s_k) E(n_i n_j^* n_l^*) \\
& + x_j^* E(s_j^*) E(n_i n_k n_l^*) + x_i E(s_i) E(n_j^* n_k n_l^*) \\
& + E(n_i n_j^* n_k n_l^*) - E(n_i n_j^*) E(n_k n_l^*)
\end{aligned}
$$

REFERENCES

1. J. W. Sherman, "Speckle Imaging Using the Principle Value Decomposition Method", SPIE Proceedings, Vol. 149 (1978).

2. R. L. Fante, "Some Results on the Imaging of Incoherent Sources Through Turbulence", J. Opt. Soc. Am., 66, 574 (1976).

NONISOPLANATIC IMAGING THROUGH A TURBULENT ATMOSPHERE

Craig K. Rushforth

David O. Anderton

University of Utah

September 30, 1981

ABSTRACT

This report deals with astronomical imaging through a turbulent atmosphere when the commonly-made assumption of isoplanicity is not valid. Integral equations are developed which relate the object to the mean and autocorrelation function of a series of short-exposure images. Useful approximations to certain functions describing the effects of the atmosphere are developed and tested using extensive numerical computations. These approximations lead to a considerable simplification in the analysis of the effects of nonisoplanatic imaging.

1. Introduction

The purpose of this report is to describe the effects of atmospheric turbulence on astronomical imaging when the object is so large that the imaging is not isoplanatic. We begin by reviewing the equations which describe optical imaging under the usual conditions of Fraunhofer diffraction. We then develop some equations which relate the object to the first and second moments of the image. Under certain conditions which are frequently encountered in practice, these equations are well conditioned and can be solved to yield a reasonable estimate of the object. The imaging equations have been developed by Sherman [1] and this report is an extension of his analysis.

Unless further assumptions and approximations are made, the imaging equations will involve complicated functions and time-consuming numerical integration. A key contribution of the research described in this report is the development of useful and accurate approximations which allow us to obtain closed-form analytical results which describe the effects of nonisoplanatic imaging. Results obtained using the approximate model are compared with the corresponding results obtained using numerical integration in order to assess the accuracy of the approximation. As we shall demonstrate, the approximate model yields very accurate results over a wide and useful range of parameter values. Furthermore, bounds on the spatial frequencies for which the model is valid are established, and these bounds are related to physical phenomena.

The imaging configuration with which we are concerned is

shown in Fig. 1. When the object is incoherent, the image intensity distribution is given by the superposition integral

$$I(x) = \int_{-\infty}^{\infty} \int O(y)\, s(x, y)\, d^2y \qquad (1)$$

where

x is the angular position (in radians) in the image plane,

y is the angular position (in radians) in the object plane,

I(x) is the image intensity distribution,

O(y) is the object intensity distribution,

and

s(x,y) is the point-spread function of the atmosphere-telescope system.

We assume that the conditions for Fraunhofer diffraction apply [2]. Under these conditions, the complex amplitudes in the object and aperture planes, and those in the aperture and image planes, are related by Fourier transforms. The Green's function for a point source at angular position y in the object plane is given by

$$U(x, y) = A \int_{-\infty}^{\infty} \int F(z, y) \exp\{jkz \cdot (y - x)\}\, d^2z \qquad (2)$$

where

z is the aperture position in meters,

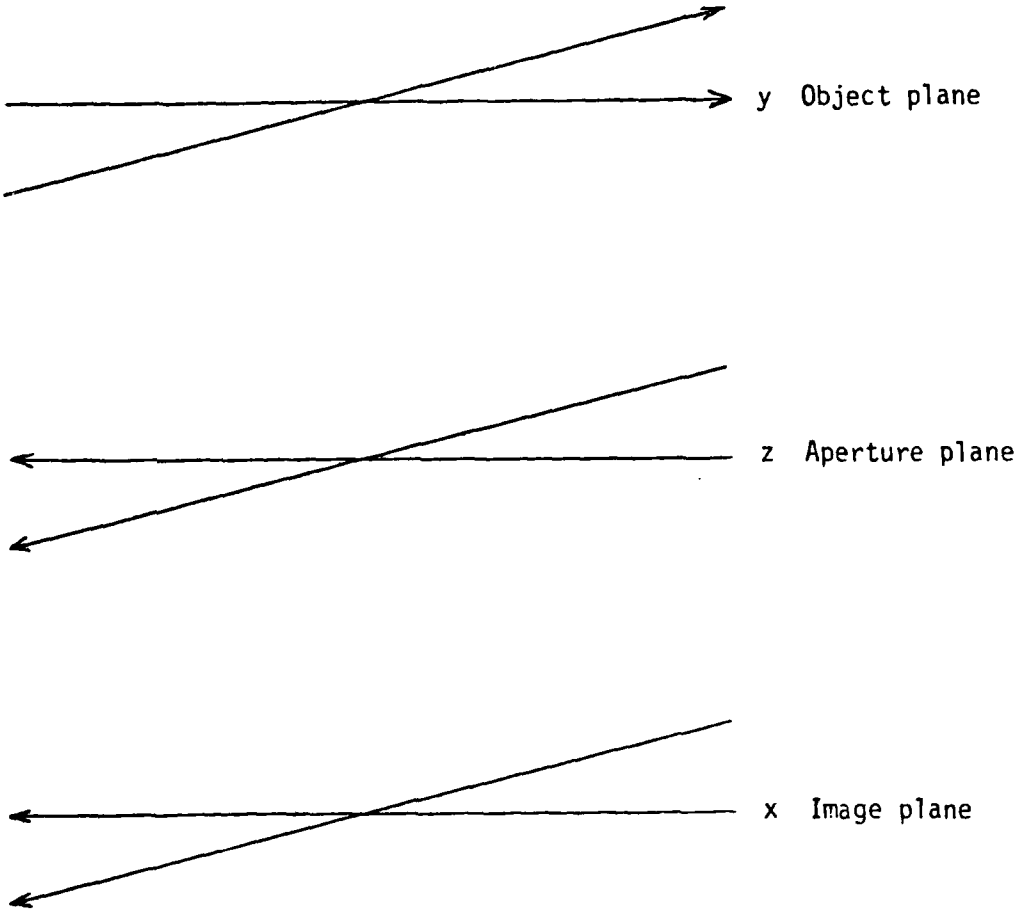

Fig. 1. The imaging configuration.

A is a scale factor,

$U(x,y)$ is the complex amplitude at angular position x in the image plane resulting from a point source at y in the object plane,

k is the wave number,

and

$F(z, y)$ is the complex amplitude at z in the aperture plane resulting from a point source at y in the object plane.

We write $F(z, y)$ in the form

$$F(z, y) = \psi(z, y)\, a(z) \exp\{j\theta(z)\} \tag{3}$$

where

$\psi(z, y)$ is the complex transmittance function of the atmosphere,

$a(z)$ is the pupil function of the aperture,

and

$\theta(z)$ is the phase aberration function of the lens.

The transmittance function $\psi(z, y)$ can be expressed in the form

$$\psi(z, y) = \exp\{\chi(z, y) + j\phi(z, y)\} \tag{4}$$

where

$\chi(z, y)$ is the log amplitude disturbance

and

$\phi(z, y)$ is the phase disturbance due to the atmosphere.

In terms of the quantities defined above, the incoherent point-spread function becomes [2]

$$s(x, y) = U(x, y)\, U^*(x, y)$$

$$= |A|^2 \int_{-\infty}^{\infty}\int \int_{-\infty}^{\infty}\int F(\beta + \omega, y)\, F^*(\beta, y) \tag{5}$$

$$\cdot \exp\{-jk\omega \cdot (x - y)\}\, d^2\beta\, d^2\omega.$$

F, and therefore s, are of course sample functions of random processes which must be described in terms of their statistical properties. We turn in the next section to the development of expressions which relate the first and second moments of the image intensity distribution to the object intensity distribution and to the statistical properties of the atmosphere.

2. First- and Second-Order Image Statistics

Sherman [1] has derived expressions for the mean and the autocorrelation function of the image intensity distribution under the assumption that $\chi(\cdot, \cdot)$ and $\phi(\cdot, \cdot)$ are Gaussian random processes. Similar results have been obtained by Fante [3] and others. We briefly review these results in this section. Detailed derivations are contained in Appendix A.

Taking expected values of both sides of (1) yields

$$E\{I(x)\} = \int_{-\infty}^{\infty}\int O(y)\, E\{s(x, y)\}\, d^2y. \tag{6}$$

The mean point-spread function has been shown to be [1, 3]

$$E\{s(x, y)\} = |A|^2 \int_{-\infty}^{\infty}\int \exp\{-D(\omega, 0)/2\} \cdot \exp\{-jk\omega \cdot (x - y)\}$$

$$\cdot \int_{-\infty}^{\infty}\int a(\beta + \omega)\, a(\beta) \exp\{j\theta(\beta + \omega) - j\theta(\beta)\}\, d^2\omega\, d^2\beta. \tag{7}$$

where $D(\Delta, \delta)$ is the two-point wave-structure function whose properties will be discussed in some detail in section 3.

The autocorrelation function of the image intensity distribution is given by

$$E\{I(x_1)I(x_2)\} = \int_{-\infty}^{\infty}\int \int_{-\infty}^{\infty}\int O(y_1)O(y_2) \cdot E\{s(x_1,y_1)\, s(x_2,y_2)\}\, d^2y_1 d^2y_2 \tag{8}$$

where

$$E\{s(x_1,y_1)s(x_2,y_2)\} = |A|^4 \int_{-\infty}^{\infty}\int \int_{-\infty}^{\infty}\int \int_{-\infty}^{\infty}\int \int_{-\infty}^{\infty}\int P(\beta_1,\omega_1,\beta_2,\omega_2)$$

$$\cdot M(\beta_1,\omega_1,y_1,\beta_2,\omega_2,y_2) \exp\{-jk\omega_1 \cdot (x_1 - y_1) - jk\omega_2(x_2 - y_2)\}$$

$$\cdot d^2\beta_1\, d^2\beta_2\, d^2\omega_1\, d^2\omega_2. \tag{9}$$

The quantities P( ) and M( ) in (9) are defined by

$$P(\beta_1,\omega_1,\beta_2,\omega_2) = a(\beta_1 + \omega_1)\, a(\beta_1)\, a(\beta_2)\, a(\beta_2 - \omega_2)$$

$$\cdot \exp\{j\theta(\beta_1 + \omega_1) - j\theta(\beta_1) + j\theta(\beta_2) - j\theta(\beta_2 - \omega_2)\} \tag{10}$$

and

$$M(\beta_1, \omega_1, y_1, \beta_2, \omega_2, y_2) =$$

$$\exp\left\{-\frac{1}{2}\left(\begin{array}{l} D(\omega_1, 0) + D(\omega_2, 0) \\ + D[\beta_1 - \beta_2 + \omega_1 + \omega_2, h(y_1 - y_2)] \\ + D[\beta_1 - \beta_2, h(y_1 - y_2)] - D[\beta_1 - \beta_2 + \omega_1, h(y_1 - y_2)] \\ - D[\beta_1 - \beta_2 + \omega_2, h(y_1 - y_2)] \end{array}\right)\right\}. \tag{11}$$

The derivation of (9) to (11) neglects terms involving the autocorrelation of $\chi(\cdot, \cdot)$ and the cross-correlation of $\chi(\cdot, \cdot)$ and $\phi(\cdot, \cdot)$. Fante [3] has argued that the impact of these terms is small. For further details on these derivations, see Appendix A.

$P(\beta_1, \omega_1, \beta_2, \omega_2)$ describes the effects of the finite aperture and of lens aberrations on the second-order statistics of the image, while $M(\beta_1, \omega_1, y_1, \beta_2, \omega_2, y_2)$ describes the effects of atmospheric turbulence. Sherman [2] has argued that lens aberrations can be neglected if turbulence is strongest near the ground in the sense that

$$\int_0^{\Delta h} C_n^2(h)\, dh > \int_{h'}^{h'+\Delta h} C_n^2(h)\, dh \tag{12}$$

where $C_n^2(h)$ is the refractive index structure constant at height h. We will assume condition (12) to be valid for all C_n^2 profiles of interest, and will therefore neglect the effects of aberrations in the remainder of the report.

We introduce the following changes of variables:

$$\bar{\beta} = \frac{\beta_1 + \beta_2}{2} ; \quad \Delta\beta = \frac{\beta_1 - \beta_2}{2} ;$$

$$\bar{y} = \frac{y_1 + y_2}{2} ; \quad \Delta y = \frac{y_1 - y_2}{2} ;$$

$$\bar{\omega} = \frac{\omega_1 - \omega_2}{2} ; \quad \Delta\omega = \frac{\omega_1 + \omega_2}{2} . \tag{13}$$

Making these variable changes and neglecting lens aberrations in (10) and (11) yield the equations

$$P'(\bar{\beta}, \Delta\beta, \bar{\omega}, \Delta\omega) = a(\bar{\beta} + \Delta\beta + \bar{\omega} + \Delta\omega)\, a(\bar{\beta} + \Delta\beta)\, a(\bar{\beta} - \Delta\beta) \cdot a(\bar{\beta} - \Delta\beta + \bar{\omega} - \Delta\omega) \tag{14}$$

and

$$M'(\bar{\omega}, \Delta\omega, \Delta\beta, \Delta y) =$$

$$\exp\left\{-\frac{1}{2}\left(\begin{array}{l} D(\bar{\omega} + \Delta\omega, 0) + D(\bar{\omega} - \Delta\omega, 0) \\ + D(2\Delta\beta + 2\Delta\omega, 2h\Delta y) + D(2\Delta\beta, 2h\Delta y) \\ - D(2\Delta\beta + \Delta\omega + \bar{\omega}, 2h\Delta y) - D(2\Delta\beta + \Delta\omega - \bar{\omega}, 2h\Delta y) \end{array}\right)\right\} . \tag{15}$$

We now turn to a more detailed discussion of the two-point wave-structure function $D(\cdot, \cdot)$.

3. The Two-Point Source Wave-Structure Function

Kon and Feizulin [4] have derived the following expression for the two-point source wave-structure function:

$$D(\Delta, \delta) = 0.033 \left(\frac{6}{5}\right) \Gamma\left(\frac{1}{6}\right) \pi^2 k^2 K_m^{-5/3} \int_0^H C_n^2(h) \cdot \left[{}_1F_1\left(-\frac{5}{6}, 1, \frac{-K_m^2 (L - h)^2 \left|\Delta + \frac{h}{L - h}\delta\right|^2}{4L^2}\right) - 1 \right] dh \tag{16}$$

where

- Δ is the distance between test points in the aperture plane (meters),
- δ is the distance between source points in the object plane (meters),
- k is the electromagnetic wave number,
- K_m is $5.91/l_o$, where l_o is the inner-scale size of the turbulence,
- H is the height of the turbulent medium,
- $C_n^2(h)$ is the refractive index structure constant at height h,
- L is the distance from object to aperture plane,
- ${}_1F_1$ is Kummer's function (a confluent hypergeometric function).

Kummer's function is the confluent hypergeometrc function [5]

$${}_1F_1(a, b, z) = 1 + \frac{az}{b} + \frac{(a)(a + 1)\, z^2}{(b)(b + 1)\, 2!} + \frac{(a)(a + 1)(a + 2)\, z^3}{(b)(b + 1)(b + 2)\, 3!} + \cdots \tag{17}$$

This is a very messy function to work with, and we seek reasonable approximations. In the literature [6], it has been common practice to develop approximate expressions for ${}_1F_1(a, b, z)$ for the limiting cases $|z| \ll 1$ and $|z| \gg 1$. We observe that for $|z| \ll 1$, we may neglect the higher order terms:

$$ {}_1F_1(a, b, z) \approx 1 + \frac{az}{b}, \qquad |z| \ll 1, \tag{18} $$

$$ {}_1F_1(a, b, z) - 1 \approx \frac{az}{b}, \qquad |z| \ll 1. \tag{19} $$

For $|z| \gg 1$, we employ the asymptotic expression [5] valid for $\mathrm{Re}[z] < 0$:

$$ {}_1F_1(a, b, z) \approx \frac{\Gamma(b)}{\Gamma(b - a)} (-z)^{-a}, \qquad |z| \gg 1. \tag{20} $$

Since, in the problem at hand, $a < 0$ and $z < 0$, ${}_1F_1(a, b, z)$ is an increasing function of z. For $|z|$ sufficiently large we have

$$ {}_1F_1(a, b, z) - 1 \approx \frac{\Gamma(b)}{\Gamma(b - a)} (-z)^{-a}, \qquad |z| \gg 1. \tag{21} $$

Fante [3] has used these limiting values of Kummer's function to derive approximations to (16). His approximate expressions are

$$ D(\Delta, \delta) \approx k^2 \int_0^H C_n^2(h)\, d\left(\frac{L - h}{L} \Delta + \frac{h}{L} \delta\right) dh \tag{22} $$

where

$$d(\rho) = \begin{cases} 3.25\ l_o^{-1/3}\ |\rho|^2, & |\rho| \ll 0.17\ l_o \\ 2.92\ |\rho|^{5/3}, & |\rho| \gg 0.17\ l_o \end{cases} . \qquad (23)$$

Upon introducing the imaging problem in section 1, we used angular rather than linear units. To reflect this in the structure function, we define the angular position vector δ' as

$$\delta' \equiv \frac{\delta}{L} . \qquad (24)$$

We also assume that the objects are astronomical and hence that $L \gg H$. With this assumption and the change of variables shown above, we find that

$$D(\Delta, h\delta') \approx k^2 \int_0^H C_n^2(h)\ d(\Delta + h\delta')\ dh. \qquad (25)$$

A key issue is the behavior of $d(\rho)$ when $\rho \approx 0.17\ l_o$. Thus far we have only developed approximations valid in the regions $|\rho| \ll 0.17\ l_o$ and $|\rho| \gg 0.17\ l_o$. It is not known at this point which of the two approximations models the behavior of $d(\rho)$ in the region of uncertainty. Indeed, it is not known if either approximation is valid in this intermediate region. To determine more closely the behavior of $D(\Delta, h\delta')$, ${}_1F_1(a, b, z)$ was computed numerically by summing terms in the hypergeometric series. The result was compared to the quadratic approximation and to the 5/3-

power approximation ((19) and (21), respectively). The results of the numerical analysis of Kummer's function are detailed in Appendix B. In brief, it was found that the quadratic approximation (19) begins to diverge rapidly beyond the breakpoint $\rho = 0.17\ l_o$, while the 5/3-power approximation closely follows Kummer's function over the entire range tested. We conclude that the quadratic law is valid only for very small arguments and that the 5/3-power approximation is reasonable for all z. Henceforth, we will use the 5/3-power approximation of $d(\rho)$ for all values of ρ.

With an analytical expression for the wave structure function, we are ready to consider the concept of the atmospheric cutoff frequency ω_c. We associate ω_c with the spatial frequencies that can be recovered from the blurred image by long-term averaging. The cutoff ω_c is determined by the first-order statistics and is generally defined [7] as the value of ω that results in an exponent of -1 in the function $\exp\,[-1/2\ D(\omega, 0)]$. That is,

$$\exp\left[-\frac{1}{2}\,D(\omega_c, 0)\right] = \exp\,[-1]. \tag{26}$$

Solving for ω_c algebraically, we obtain

$$\omega_c = \left[\frac{2}{2.92\ k^2\ \mu_o}\right]^{3/5} \tag{27}$$

where we have defined μ_o to be the zero-order moment of the refractive index structure constant

$$\mu_o \equiv \int_0^H C_n^2(h)\, dh. \tag{28}$$

In general, we define the n^{th}-order moment μ_n to be

$$\mu_n \equiv \int_0^H h^n\, C_n^2(h)\, dh. \tag{29}$$

These moments will be useful in later developments.

4. Imaging Equations

Substituting the expression for the structure function given by (25) into (15), we obtain the following expression for the mutual coherence function $M'(\bar{\omega}, \Delta\omega, \Delta\beta, \Delta y)$:

$$M'(\bar{\omega}, \Delta\omega, \Delta\beta, \Delta y) =$$

$$\exp\left[-\frac{k^2}{2}\int_0^H C_n^2(h)\left(\begin{array}{l} d(\bar{\omega}+\Delta\omega) + d(\bar{\omega}-\Delta\omega) \\ + d(2\Delta\beta+2h\Delta y+2\Delta\omega) + d(2\Delta\beta+2h\Delta y) \\ - d(2\Delta\beta+2h\Delta y+\Delta\omega-\bar{\omega}) - d(2\Delta\beta+2h\Delta y+\Delta\omega+\bar{\omega}) \end{array}\right) dh\right]. \tag{30}$$

We make the following observations about the mutual coherence function:

1. For frequencies satisfying $|\bar{\omega}|^2 + |\Delta\omega|^2 < \omega_c^2$, the mutual coherence is essentially independent of $\Delta\beta$ and Δy, and the entire aperture appears to be spatially coherent. That is,

$$M'(\bar{\omega}, \Delta\omega, \Delta\beta, \Delta y) \approx M_c(\bar{\omega}, \Delta\omega).$$

2. For spatial frequencies satisfying $|\Delta\omega| >> \omega_c$, $|\bar{\omega}| >> \omega_c$, the mutual coherence is nearly zero:

$$M'(\bar{\omega}, \Delta\omega, \Delta\beta, \Delta y) \approx 0.$$

3. For spatial frequencies satisfying $|\Delta\omega| < \omega_c$, $|\bar{\omega}| >> \omega_c$, there is nonzero coherence in the region $|2\Delta\beta + \Delta\omega| < \omega_c$ and $|\Delta y| < \Delta y_c$. In this case the aperture is spatially coherent in regions the size of ω_c, provided that the two source points are not separated by a distance greater than Δy_c.

The ability to recover the high spatial frequency information from the second-order statistics of a set of speckle images depends upon the nature of the mutual coherence function in case 3 (i.e., $|\bar{\omega}| >> \omega_c$, $|\Delta\omega| < \omega_c$). In the remainder of this report we will concentrate on analyzing the coherence function under these conditions.

We will now consider the effects of the turbulence on the image. As discussed previously, we neglect lens aberrations. We have shown that

$$E\{I(x_1)I(x_2)\} = \int_{-\infty}^{\infty}\int_{-\infty}^{\infty} O(y_1)O(y_2)E\{s(x_1,y_1)s(x_2,y_2)\}\, d\, y_1^2 d\, y_2^2 \qquad (8)$$

where

$$E\{s(x_1, y_1)s(x_2, y_2)\} = 4|A|^4 \iint_{-\infty}^{\infty} \iint_{-\infty}^{\infty} \iint_{-\infty}^{\infty} \iint_{-\infty}^{\infty} P'(\bar{\omega}, \Delta\omega, \bar{\beta}, \Delta\beta)$$

$$\cdot M'(\bar{\omega}, \Delta\omega, \Delta\beta, \Delta y)\, d^2\bar{\beta}\, d^2\Delta\beta \exp\left[-jk\omega_1\right.$$

$$\left.\cdot (x_1 - y_1) - jk\omega_2 \cdot (x_2 - y_2)\right] d^2\omega_1\, d^2\omega_2, \tag{9}$$

$$P'(\bar{\omega}, \Delta\omega, \bar{\beta}, \Delta\beta) = a(\bar{\beta} + \Delta\beta + \bar{\omega} - \Delta\omega)\, a(\bar{\beta} + \Delta\beta)\, a(\bar{\beta} - \Delta\beta)$$

$$\cdot a(\bar{\beta} - \Delta\beta + \bar{\omega} - \Delta\omega), \tag{14}$$

and

$$M'(\bar{\omega}, \Delta\omega, \Delta\beta, \Delta y) =$$

$$\exp\left[-\frac{k^2}{2}\int_0^H C_n^2(h) \begin{pmatrix} d(\bar{\omega}+\Delta\omega) + d(\bar{\omega}-\Delta\omega) \\ + d(2\Delta\beta+2h\Delta y+2\Delta\omega) + d(2\Delta\beta+2h\Delta y) \\ - d(2\Delta\beta+2h\Delta y+\Delta\omega-\bar{\omega}) - d(2\Delta\beta+2h\Delta y+\Delta\omega+\bar{\omega}) \end{pmatrix} dh\right]. \tag{30}$$

To simplify the notation we introduce the function

$$N(\bar{\omega}, \Delta\omega, \Delta y) \equiv \iint_{-\infty}^{\infty} \iint_{-\infty}^{\infty} M'(\bar{\omega}, \Delta\omega, \Delta\beta, \Delta y)\, P'(\bar{\omega}, \Delta\omega, \bar{\beta}, \Delta\beta)\, d^2\bar{\beta}\, d^2\Delta\beta \tag{31}$$

The integration over $\Delta\beta$ effectively samples the function $P'(\bar{\omega}, \Delta\omega, \bar{\beta}, \Delta\beta)$ at $\Delta\beta = -\Delta\omega/2$. Hence

$$N(\bar{\omega},\ \Delta\omega,\ \Delta y) \approx \iint_{-\infty}^{\infty} P'\left(\bar{\omega},\ \Delta\omega,\ \bar{\beta},\ \Delta\beta = -\frac{\Delta\omega}{2}\right) d^2\bar{\beta}$$

$$\cdot \iint_{-\infty}^{\infty} M'(\bar{\omega},\ \Delta\omega,\ \Delta\beta,\ \Delta y)\ d^2\Delta\beta. \qquad (32)$$

For convenience we define

$$F_4(\bar{\omega},\ \Delta\omega) \equiv \iint_{-\infty}^{\infty} P'\left(\bar{\omega},\ \Delta\omega,\ \bar{\beta},\ \Delta\beta = -\frac{\Delta\omega}{2}\right) d^2\bar{\beta}$$

$$= \iint_{-\infty}^{\infty} a\left(\bar{\beta} + \bar{\omega} + \frac{\Delta\omega}{2}\right) a\left(\bar{\beta} - \frac{\Delta\omega}{2}\right) a\left(\bar{\beta} + \frac{\Delta\omega}{2}\right)$$

$$\cdot a\left(\bar{\beta} + \bar{\omega} - \frac{\Delta\omega}{2}\right)\ d^2\bar{\beta} \qquad (33)$$

and

$$M_o(\bar{\omega},\ \Delta\omega,\ \Delta y) \equiv \iint_{-\infty}^{\infty} M'(\bar{\omega},\ \Delta\omega,\ \Delta\beta,\ \Delta y)\ d^2\Delta\beta. \qquad (34)$$

From (8), (9), (14), and (31)-(34), we find that

$$E\{I(x_1)I(x_2)\} = 4|A|^4 \iint_{-\infty}^{\infty}\iint_{-\infty}^{\infty} O(y_1)\ O(y_2) \iint_{-\infty}^{\infty}\iint_{-\infty}^{\infty} M_o(\bar{\omega},\ \Delta\omega,\ \Delta y)$$

$$\cdot F_4(\bar{\omega},\ \Delta\omega)\ \exp[-jk\omega_1 \cdot (x_1 - y_1) - jk\omega_2$$

$$\cdot (x_2 - y_2)]\ d^2\omega_1\ d^2\omega_2\ d^2y_1\ d^2y_2. \qquad (35)$$

This equation is valid for $|\bar{\omega}| >> \omega_c$, and $|\Delta\omega| < \omega_c$.

We may express $O(y)$ and $M_o(\bar{\omega},\ \Delta\omega,\ \Delta\omega)$ as inverse Fourier

transforms:

$$O(y) = \left(\frac{2\pi}{k}\right)^2 \iint_{-\infty}^{\infty} \tilde{O}(\omega') \exp\left[-jk\omega' \cdot y\right] d^2\omega', \tag{36}$$

$$M_o(\bar{\omega}, \Delta\omega, \Delta y) = \left(\frac{2\pi}{k}\right)^2 \iint_{-\infty}^{\infty} \tilde{M}_o(\bar{\omega}, \Delta\omega, \Delta\omega') \exp\left[-jk\Delta\omega' \cdot \Delta y\right] d^2\Delta\omega'. \tag{37}$$

Substituting these expressions for $O(y)$ and $M_o(\bar{\omega}, \Delta\omega, \Delta y)$ into (35) and simplifying yields

$$E\{I(x_1)I(x_2)\} = 4|A|^4 \frac{(2\pi)^8}{(k)^4} \iint_{-\infty}^{\infty} \iint_{-\infty}^{\infty} \iint_{-\infty}^{\infty} \tilde{O}\left(\omega_1 - \frac{\Delta\omega'}{2}\right) \tilde{O}\left(\omega_2 + \frac{\Delta\omega'}{2}\right)$$

$$\cdot \tilde{M}_o(\bar{\omega}, \Delta\omega, \Delta\omega')\, d^2\Delta\omega'\, F_4(\bar{\omega}, \Delta\omega)$$

$$\cdot \exp\left[-jk\omega_1 \cdot x_1 - jk\omega_2 \cdot x_2\right] d^2\omega_1\, d^2\omega_2. \tag{38}$$

Or, taking the Fourier transform of both sides of this equation,

$$F\{E[I(x_1)I(x_2)]\} \equiv W(\omega_1, \omega_2)$$

$$= 4|A|^4 \frac{(2\pi)^4}{(k)^2} \iint_{-\infty}^{\infty} \tilde{O}\left(\omega_1 - \frac{\Delta\omega'}{2}\right) \tilde{O}\left(\omega_2 + \frac{\Delta\omega'}{2}\right)$$

$$\cdot \tilde{M}_o(\bar{\omega}, \Delta\omega, \Delta\omega')\, F_4(\bar{\omega}, \Delta\omega)\, d^2\Delta\omega' \tag{39}$$

From (38) and (39) we conclude that the effect of nonisoplanatism is to smooth the second-order statistics in the $\Delta\omega'$ plane. The behavior of the smoothing function $\tilde{M}_o(\bar{\omega}, \Delta\omega, \Delta\omega')$ in the $\Delta\omega'$ plane determines the feasibility of solving (38) for the Fourier transform of the object $\tilde{O}(\omega)$. If

$$\Delta\omega'_c < \omega_c, \tag{40}$$

then the integral equation (38) is well conditioned.

In the remainder of this report we shall consider the impact of the mutual coherence function $M'(\bar{\omega}, \Delta\omega, \Delta\beta, \Delta y)$ and the smoothing function $\tilde{M}_o(\bar{\omega}, \Delta\omega, \Delta\omega')$ on the second-order statistics. Some key issues include:

1. Is it possible to find simple analytical expressions for $M'(\bar{\omega}, \Delta\omega, \Delta\beta, \Delta y)$ and $\tilde{M}_o(\bar{\omega}, \Delta\omega, \Delta\omega')$?
2. How does the random process $C_n^2(h)$ affect $M'(\bar{\omega}, \Delta\omega, \Delta\beta, \Delta y)$? What are the pertinent properties of $C_n^2(h)$ that impact the imaging?
3. What generalizations can be made about the impact of the smoothing function $\tilde{M}_o(\bar{\omega}, \Delta\omega, \Delta\omega')$ on the imaging?

5. The Effects on Nonisoplanatism

In this section we will explore the effects of nonisoplanatism by deriving reasonable closed form approximations for $M_o(\bar{\omega}, \Delta\omega, \Delta y)$ and $\tilde{M}_o(\bar{\omega}, \Delta\omega, \Delta\omega')$. We shall temporarily assume that

$$|\bar{\omega}| >> \omega_c,\ |\Delta\omega| < \omega_c,\ |2\Delta\beta + \Delta\omega| < \omega_c,\ |\Delta y| < y_c; \qquad (41)$$

these conditions will be explored in more detail later. We begin by reviewing (30):

$$M'(\bar{\omega}, \Delta\omega, \Delta\beta, \Delta y) =$$

$$\exp\left\{-\frac{k^2}{2}\int_0^H C_n^2(h)\left(\begin{array}{l} d_1(\bar{\omega}+\Delta\omega) + d_2(\bar{\omega}-\Delta\omega) \\ + d_3(2\Delta\beta + 2h\Delta y + 2\Delta\omega) + d_4(2\Delta\beta + 2h\Delta y) \\ - d_5(2\Delta\beta+2h\Delta y+\Delta\omega-\bar{\omega}) - d_6(2\Delta\beta+2h\Delta y+\Delta\omega+\bar{\omega}) \end{array}\right) dh\right\} \qquad (30)$$

where

$$d(\rho) = 2.92\ |\rho|^{5/3}. \qquad (23)$$

We have numbered the $d(\cdot)$ functions with subscripts to expedite the discussion.

The conditions set forth in (41) insure that $|\bar{\omega}|$ is large while $|\Delta\beta|$, $|\Delta\omega|$, and $|\Delta y|$ are small. For the moment we will assume that $|\bar{\omega}|$ dominates the other terms in the arguments of $d_1(\cdot)$, $d_2(\cdot)$, $d_5(\cdot)$, and $d_6(\cdot)$. This assumption is suspect since the term Δy is always multiplied by h, which may take on large values $(2 \cdot 10^4)$ in the range of integration [0, H]. However, we shall tacitly accept the assumption that $|h\Delta y| < |\bar{\omega}|$ at this stage. Later on, we shall explore the limitations and consequences of this

assumption.

With the assumption that $|\bar{\omega}|$ dominates the other terms in the arguments of $d_1(\cdot)$, $d_2(\cdot)$, $d_5(\cdot)$, and $d_6(\cdot)$, we may expand each of these functions in a power series by employing the binomial expansion [5]

$$(1 + x)^{\alpha} = 1 + \alpha x + \frac{\alpha(\alpha - 1)}{2!} x^2 + \frac{\alpha(\alpha - 1)(\alpha - 2)}{3!} x^3 + \ldots,$$

$$|x| < 1. \tag{42}$$

For the problem at hand,

$$\begin{aligned} d(\bar{\omega} + \delta) &= 2.92\ |\bar{\omega} + \delta|^{5/3} \\ &= 2.92\ [(\bar{\omega} + \delta) \cdot (\bar{\omega} + \delta)]^{5/6} \\ &= 2.92 \left[\bar{\omega} \cdot \bar{\omega} \left(1 + \frac{2\delta \cdot \bar{\omega}}{\bar{\omega} \cdot \bar{\omega}} + \frac{\delta \cdot \delta}{\bar{\omega} \cdot \bar{\omega}}\right)\right]^{5/6} \end{aligned} \tag{43}$$

As before, the dot denotes inner product. We have assumed for each function that $|\bar{\omega}| > |\delta|$, so we may expand the term in parenthesis in a binomial series with

$$x = \frac{2\delta \cdot \bar{\omega}}{\bar{\omega} \cdot \bar{\omega}} + \frac{\delta \cdot \delta}{\bar{\omega} \cdot \bar{\omega}} \tag{44}$$

The resulting expression for $d(\bar{\omega} + \delta)$ is

$$d(\bar{\omega} + \delta) = 2.92\ (\bar{\omega} \cdot \bar{\omega})^{5/6} \left[1 + \frac{5\delta \cdot \bar{\omega}}{3\bar{\omega} \cdot \bar{\omega}} + \frac{\delta \cdot \delta}{\bar{\omega} \cdot \bar{\omega}} \left(\frac{5}{6} - \frac{5}{18} \cos^2\theta\right) + \ldots\right] \tag{45}$$

where θ is the angle between δ and $\bar{\omega}$. We can approximate $d(\bar{\omega} + \delta)$ by neglecting cubic and higher order terms:

$$d(\bar{\omega} + \delta) \approx 2.92 \left(\bar{\omega} \cdot \bar{\omega}\right)^{5/6}\left[1 + \frac{5\delta \cdot \bar{\omega}}{3\bar{\omega} \cdot \bar{\omega}} + \frac{\delta \cdot \delta}{\bar{\omega} \cdot \bar{\omega}}\left(\frac{5}{6} - \frac{5}{18}\cos^2\theta\right)\right]. \tag{46}$$

Making the appropriate substitutions for δ, we arrive at the following approximate expressions for $d_1(\cdot)$, $d_2(\cdot)$, $d_5(\cdot)$, and $d_6(\cdot)$:

$$d_1(\bar{\omega} + \Delta\omega) \approx 2.92 \left(\bar{\omega} \cdot \bar{\omega}\right)^{5/6}\left[1 + \frac{5\Delta\omega \cdot \bar{\omega}}{3\bar{\omega} \cdot \bar{\omega}} + \frac{\Delta\omega \cdot \Delta\omega}{\bar{\omega} \cdot \bar{\omega}}\left(\frac{5}{6} - \frac{5}{18}\cos^2\theta_1\right)\right] \tag{47}$$

$$d_2(\bar{\omega} - \Delta\omega) \approx 2.92 \left(\bar{\omega} \cdot \bar{\omega}\right)^{5/6}\left[1 - \frac{5\Delta\omega \cdot \bar{\omega}}{3\bar{\omega} \cdot \bar{\omega}} + \frac{\Delta\omega \cdot \Delta\omega}{\bar{\omega} \cdot \bar{\omega}}\left(\frac{5}{6} - \frac{5}{18}\cos^2\theta_2\right)\right] \tag{48}$$

$$d_5(2\Delta\beta + 2h\Delta y + \Delta\omega - \bar{\omega}) \approx 2.92 \left(\bar{\omega} \cdot \bar{\omega}\right)^{5/6} \left[1 - \frac{5(2\Delta\beta+2h\Delta y+\Delta\omega) \cdot \bar{\omega}}{3\bar{\omega} \cdot \bar{\omega}} + \frac{(2\Delta\beta + 2h\Delta y + \Delta\omega) \cdot (2\Delta\beta + 2h\Delta y + \Delta\omega)}{\bar{\omega} \cdot \bar{\omega}}\left(\frac{5}{6} - \frac{5}{18}\cos^2\theta_3\right)\right] \tag{49}$$

$$d_6(2\Delta\beta + 2h\Delta y + \Delta\omega + \bar{\omega}) \approx 2.92 \left(\bar{\omega} \cdot \bar{\omega}\right)^{5/6} \left[1 + \frac{5(2\Delta\beta+2h\Delta y+\Delta\omega) \cdot \bar{\omega}}{3\,\bar{\omega} \cdot \bar{\omega}} + \frac{(2\Delta\beta + 2h\Delta y + \Delta\omega) \cdot (2\Delta\beta + 2h\Delta y + \Delta\omega)}{\bar{\omega} \cdot \bar{\omega}}\left(\frac{5}{6} - \frac{5}{18}\cos^2\theta_4\right)\right] \tag{50}$$

where

θ_1 = angle between $\bar{\omega}$ and $\Delta\omega$

θ_2 = angle between $\bar{\omega}$ and $-\Delta\omega$

θ_3 = angle between $-\bar{\omega}$ and $(2\Delta\beta + 2h\Delta y + \Delta\omega)$

θ_4 = angle between $+\bar{\omega}$ and $(2\Delta\beta + 2h\Delta y + \Delta\omega)$.

We note that

$$\theta_1 = \pi - \theta_2$$

$$\theta_3 = \pi - \theta_4$$

and from the trigonometric identity $\cos(\pi - \theta) = -\cos\theta$, we conclude that

$$\cos^2\theta_1 = \cos^2\theta_2$$

$$\cos^2\theta_3 = \cos^2\theta_4$$

We next observe that the mutual coherence function $M'(\bar{\omega}, \Delta\omega, \Delta\beta, \Delta y)$ will be maximized for fixed $\bar{\omega}$ and $\Delta\omega$ when $(2\Delta\beta + 2h\Delta y) \approx -\Delta\omega$. This leads us to conclude that over the region where $M'(\bar{\omega}, \Delta\omega, \Delta\beta, \Delta y)$ is most significant, the term $(2\Delta\beta + 2h\Delta y + \Delta\omega)$ will be nearly colinear with $\Delta\omega$. Hence:

$$\cos^2\theta_1 = \cos^2\theta_2 \approx \cos^2\theta_3 = \cos^2\theta_4$$

In the remainder of this report we shall employ the approximation above, and we will refer to θ_1 as simply θ.

Unfortunately, we cannot expand $d_3(\cdot)$ and $d_4(\cdot)$ by the binomial expansion since we cannot guarantee that any term in the argument will dominate for either function. However, we recognize that $d_3(\cdot)$ and $d_4(\cdot)$ will only profoundly impact the shape of the mutual coherence function M' when the magnitude of the argument is close to ω_c. Hence, we will approximate $d_3(\rho)$ and $d_4(\rho)$ by a simpler function that is a good fit in some sense when $\rho \approx \omega_c$. The choice for the approximating function is

$$d(\rho) \approx c_1\rho \cdot \rho + c_o \tag{51}$$

where c_1 and c_o are constants selected to "optimize" the fit for $|\rho| \approx \omega_c$. The motivation for this quadratic approximating function will become apparent shortly. Applying this approximation to $d_3(\cdot)$ and $d_4(\cdot)$, we have

$$d_3(2\Delta\beta + 2h\Delta y + 2\Delta\omega) \approx c_1(2\Delta\beta + 2h\Delta y + 2\Delta\omega) \cdot (2\Delta\beta + 2h\Delta y + 2\Delta\omega) + c_o, \tag{52}$$

$$d_4(2\Delta\beta + 2h\Delta y) \approx c_1(2\Delta\beta + 2h\Delta y) \cdot (2\Delta\beta + 2h\Delta y) + c_o. \tag{53}$$

To simplify the notation we introduce the following functions:

$$f_1(\bar{\omega}, \Delta\omega, \Delta\beta, \Delta y) \equiv d_1(\bar{\omega} + \Delta\omega) + d_2(\bar{\omega} - \Delta\omega)$$

$$- d_5(2\Delta\beta + 2h\Delta y + \Delta\omega - \bar{\omega}) - d_6(2\Delta\beta + 2h\Delta y + \Delta\omega + \bar{\omega}), \quad (54)$$

$$f_2(\Delta\omega, \Delta\beta, \Delta y) \equiv d_3(2\Delta\beta + 2h\Delta y + 2\Delta\omega) + d_4(2\Delta\beta + 2h\Delta y). \quad (55)$$

With this notation we can express (30) as

$$M'(\bar{\omega}, \Delta\omega, \Delta\beta, \Delta y) = \exp\left\{-\frac{k^2}{2}\int_0^H C_n^2(h) \cdot [f_1(\bar{\omega}, \Delta\omega, \Delta\beta, \Delta y) + f_2(\Delta\omega, \Delta\beta, \Delta y)]\, dh\right\} \quad (56)$$

Combining (47)-(50) and (52)-(53) with (54) and (55), we obtain

$$f_1(\bar{\omega}, \Delta\omega, \Delta\beta, \Delta y) \approx -19.47\left(1 - \frac{1}{3}\cos^2\theta\right)(\bar{\omega} \cdot \bar{\omega})^{-1/6}\,[\Delta\beta \cdot \Delta\beta +$$

$$(2h\Delta y + \Delta\omega) \cdot \Delta\beta + h\Delta\omega \cdot \Delta y + h^2\Delta y \cdot \Delta y], \quad (57)$$

$$f_2(\Delta\omega, \Delta\beta, \Delta y) \approx c_1\,[8\Delta\beta \cdot \Delta\beta + (16h\Delta y + 8\Delta\omega) \cdot \Delta\beta + 4\Delta\omega \cdot \Delta\omega$$

$$+ 8h\Delta\omega \cdot \Delta y + 8h^2\Delta y \cdot \Delta y] + 2c_o. \quad (58)$$

Substituting these approximate expressions for $f_1(\bar{\omega}, \Delta\omega, \Delta\beta, \Delta y)$ and $f_2(\Delta\omega, \Delta\beta, \Delta y)$ into (56), we obtain

$$M'(\bar{\omega}, \Delta\omega, \Delta\beta, \Delta y) \approx$$

$$\exp\left\{-\frac{k^2}{2}\int_0^H C_n^2(h)\left(\begin{array}{l} c_1\left[8\Delta\beta \cdot \Delta\beta + (16h\Delta y + 8\Delta\omega)\cdot\Delta\beta \right. \\ \left. + 4\Delta\omega\cdot\Delta\omega + 8h\Delta\omega\cdot\Delta y + 8h^2\Delta y\cdot\Delta y\right] + 2c_o \\ - 19.47\left(1-\frac{1}{3}\cos^2\theta\right)(\bar{\omega}\cdot\bar{\omega})^{-1/6}\left[\Delta\beta\cdot\Delta\beta \right. \\ \left. + (2h\Delta y + \Delta\omega)\cdot\Delta\beta + h\Delta\omega\cdot\Delta y + h^2\Delta y\cdot\Delta y\right] \end{array}\right) dh\right\}. \tag{59}$$

Employing the definition of the moments of the refractive index structure constant $C_n^2(h)$ given in (29), we may perform the integration with respect to h. Computing the integral and collecting terms involving $\Delta\beta \cdot \Delta\beta$ and $\Delta\beta$ yields

$$M'(\bar{\omega}, \Delta\omega, \Delta\beta, \Delta y) \approx$$

$$\exp\left\{-\frac{k^2}{2}\left[\begin{array}{l} \left[8c_1\mu_o - 19.47\left(1-\frac{1}{3}\cos^2\theta\right)(\bar{\omega}\cdot\bar{\omega})^{-1/6}\,\mu_o\right]\Delta\beta\cdot\Delta\beta \\ + \left[16c_1\mu_1\Delta y + 8c_1\mu_o\Delta\omega - 19.47\left(1-\frac{1}{3}\cos^2\theta\right)(\bar{\omega}\cdot\bar{\omega})^{-1/6}\left(2\mu_1\Delta y \right.\right. \\ \left.\left. + \mu_o\Delta\omega\right)\right]\cdot\Delta\beta + \left[c_1\left(8\mu_2\Delta y\cdot\Delta y + 4\mu_o\Delta\omega\cdot\Delta\omega + 8\mu_1\Delta\omega\cdot\Delta y\right) + 2c_o\mu_o \right. \\ \left. -19.47\left(1-\frac{1}{3}\cos^2\theta\right)(\bar{\omega}\cdot\bar{\omega})^{-1/6}\left(\mu_1\Delta\omega\cdot\Delta y + \mu_2\Delta y\cdot\Delta y\right)\right] \end{array}\right]\right\}. \tag{60}$$

To make this seemingly complicated expression more tractable, we will make the following definitions:

$$\eta_1 \equiv 4c_1\mu_o - 9.73\left(1-\frac{1}{3}\cos^2\theta\right)(\bar{\omega}\cdot\bar{\omega})^{-1/6}\,\mu_o, \tag{61}$$

$$\eta_2 \equiv 8c_1\mu_1\Delta y + 4c_1\mu_o\Delta\omega - 9.73\left(1 - \frac{1}{3}\cos^2\theta\right)(\bar{\omega}\cdot\bar{\omega})^{-1/6} \cdot (2\mu_1\Delta y + \mu_o\Delta\omega), \tag{62}$$

$$\eta_3 \equiv c_1(4\mu_2\Delta y\cdot\Delta y + 4\mu_1\Delta\omega\cdot\Delta y + 2\mu_o\Delta\omega\cdot\Delta\omega) + c_o\mu_o - 9.73\left(1 - \frac{1}{3}\cos^2\theta\right)(\bar{\omega}\cdot\bar{\omega})^{-1/6}(\mu_1\Delta\omega\cdot\Delta y + \mu_2\Delta y\cdot\Delta y). \tag{63}$$

We note that η_2 is a vector while η_1 and η_3 are scalars. With these definitions (60) can be expressed very simply as

$$M'(\bar{\omega}, \Delta\omega, \Delta\beta, \Delta y) \approx \exp\left\{-k^2\eta_1\left[\Delta\beta\cdot\Delta\beta + \eta_2\cdot\Delta\beta/\eta_1 + \eta_3/\eta_1\right]\right\}. \tag{64}$$

Since this expression involves only quadratic and linear terms in $\Delta\beta$, we may perform the integration with respect to $\Delta\beta$ called for in (34). Hence, with the approximations we have made, we may obtain an approximate analytical expression for $M_o(\bar{\omega}, \Delta\omega, \Delta y)$. This was the prime motive for approximating the $d(\cdot)$ functions by quadratic polynomials.

Completing the square in the exponent of (64) and performing the integration with respect to $\Delta\beta$, we derive the following approximation of $M_o(\bar{\omega}, \Delta\omega, \Delta y)$:

$$M_o(\bar{\omega},\ \Delta\omega,\ \Delta y) = \int_{-\infty}^{\infty}\int M'(\bar{\omega},\ \Delta\omega,\ \Delta\beta,\ \Delta y)\ d^2\Delta\beta$$

$$= \sqrt{\frac{2\pi^2}{k^2\eta_1}}\ \exp\ \{-k^2(\eta_3 - \eta_2 \cdot \eta_2/4\eta_1)\}. \qquad (65)$$

The term $(\eta_3 - \eta_2 \cdot \eta_2/4\eta_1)$ can be evaluated by direct substitution of (61)-(63). The result is

$$(\eta_3 - \eta_2 \cdot \eta_2/4\eta_1) = \gamma_1 \left(\mu_2 - \mu_1^2/\mu_o\right) \Delta y \cdot \Delta y + \gamma_2\mu_o\Delta\omega \cdot \Delta\omega + c_o\mu_o, \qquad (66)$$

where we have made the following definitions to maintain the simplicity of the notation:

$$\gamma_1 \equiv 4c_1 - 9.73\left(1 - \frac{1}{3}\cos^2\theta\right)(\bar{\omega}\cdot\bar{\omega})^{-1/6}, \qquad (67)$$

$$\gamma_2 \equiv c_1 + 2.43\left(1 - \frac{1}{3}\cos^2\theta\right)(\bar{\omega}\cdot\bar{\omega})^{-1/6}. \qquad (68)$$

Finally, substituting (66) into (65),

$$M_o(\bar{\omega},\ \Delta\omega,\ \Delta y) = \sqrt{\frac{2\pi^2}{k^2\gamma_1\mu_o}}\ \exp\ \left\{-k^2\gamma_1\left(\mu_2 - \mu_1^2/\mu_o\right)\Delta y \cdot \Delta y\right\}$$

$$\cdot\ \exp\ \left\{-k^2\gamma_2\mu_o\Delta\omega \cdot \Delta\omega\right\}\ \exp\ \left\{-k^2c_o\mu_o\right\}. \qquad (69)$$

From (69) we see that $M_o(\bar{\omega},\ \Delta\omega,\ \Delta y)$ behaves as a Gaussian function in both the Δy and $\Delta\omega$ directions. We may take advantage of this by defining

$$\Delta y_c^2 \equiv \left[k^2\gamma_1\left(\mu_2 - \mu_1^2/\mu_o\right)\right]^{-1},$$

$$\Delta\omega_c^2 \equiv \left[k^2\gamma_2\mu_o\right]^{-1}.$$

Equation (69) becomes

$$M_o(\bar{\omega}, \Delta\omega, \Delta y) = \sqrt{\frac{2\pi^2}{k^2\gamma_1\mu_o}} \exp\left\{-\Delta y \cdot \Delta y/\Delta y_c^2\right\} \exp\left\{-\Delta\omega \cdot \Delta\omega/\Delta\omega_c^2\right\}$$
$$\cdot \exp\left\{-k^2 c_o \mu_o\right\}. \qquad (70)$$

Equation (70) involves only a quadratic term in Δy and hence the Fourier transform implied by (37) can be calculated in closed form. The result is

$$\tilde{M}_o(\bar{\omega}, \Delta\omega, \Delta\omega') = \iint_{-\infty}^{\infty} M_o(\bar{\omega}, \Delta\omega, \Delta y) \exp\left[jk\Delta\omega' \cdot \Delta y\right] d^2\Delta y$$

$$= 2\pi^2 \sqrt{\frac{\Delta y_c^2}{k^2\gamma_1\mu_o}} \exp\left\{-\Delta\omega \cdot \Delta\omega/\Delta\omega_c^2\right\}$$
$$\cdot \exp\left\{-k^2\Delta y_c^2\Delta\omega' \cdot \Delta\omega'/4\right\} \exp\left\{-k^2 c_o\mu_o\right\}. \qquad (71)$$

Defining

$$\omega_c' \equiv 2/k\Delta y_c, \qquad (72)$$

we have

$$\tilde{M}_o(\bar{\omega}, \Delta\omega, \Delta\omega') = 2\pi^2 \sqrt{\frac{\Delta y_c^2}{k^2 \gamma_1 \mu_o}} \exp\left\{-\Delta\omega \cdot \Delta\omega/\Delta\omega_c^2\right\}$$

$$\cdot \exp\left\{-\Delta\omega' \cdot \Delta\omega'/(\Delta\omega_c')^2\right\} \exp\left\{-k^2 c_o \mu_o\right\}. \tag{73}$$

Hence, we have found approximate analytical expressions for $M_o(\bar{\omega}, \Delta\omega, \Delta y)$ and $\tilde{M}_o(\bar{\omega}, \Delta\omega, \Delta\omega')$.

We now consider the problem of selecting the coefficients c_1 and c_o. These coefficients are selected so that

$$d(\rho) \approx c_1 \rho \cdot \rho + c_o \tag{51}$$

when $\rho \approx \omega_c$. The coefficients c_o and c_1 were calculated and compared using a variety of methods. The details of these calculations are relegated to Appendix C. The following values for c_1 and c_o were found to be reasonable choices:

$$c_1 = 3\left(k^2 \mu_o\right)^{1/5}, \tag{74}$$

$$c_o = 0. \tag{75}$$

Substituting these values into our previous results, we obtain

$$M_o(\bar{\omega}, \Delta\omega, \Delta y) \approx \sqrt{\frac{2\pi^2}{k^2 \gamma_1 \mu_o}} \exp\left\{-\Delta y \cdot \Delta y/\Delta y_c^2\right\} \exp\left\{-\Delta\omega \cdot \Delta\omega/\Delta\omega_c^2\right\} \tag{76}$$

and

$$\tilde{M}_o(\bar{\omega},\ \Delta\omega,\ \Delta\omega') \approx 2\pi^2 \sqrt{\frac{\Delta y_c^2}{k^2 \gamma_1 \mu_o}} \exp\left\{-\Delta\omega \cdot \Delta\omega/\Delta\omega_c^2\right\} \cdot \exp\left\{-\Delta\omega' \cdot \Delta\omega'/(\Delta\omega_c')^2\right\} \tag{77}$$

with

$$\gamma_1 = 12\left(k^2\mu_o\right)^{1/5} - 9.73\left(1 - \frac{1}{3}\cos^2\theta\right)(\bar{\omega}\cdot\bar{\omega})^{-1/6}, \tag{78}$$

$$\gamma_2 = 3\left(k^2\mu_o\right)^{1/5} + 2.43\left(1 - \frac{1}{3}\cos^2\theta\right)(\bar{\omega}\cdot\bar{\omega})^{-1/6}, \tag{79}$$

$$\Delta\omega_c = \sqrt{\frac{1}{k^2\gamma_2\mu_o}}, \tag{80}$$

$$\Delta y_c = \sqrt{\frac{1}{k^2\gamma_1\left(\mu_2 - \mu_1^2/\mu_o\right)}}, \tag{81}$$

and

$$\Delta\omega_c' = 2\sqrt{\gamma_1\left(\mu_2 - \mu_1^2/\mu_o\right)}. \tag{82}$$

The validity of the approximations used to derive (76) and (77) were tested by comparing the value of $M_o(\bar{\omega}, \Delta\omega, \Delta y)$ predicted by (76) with the value computed by numerical integration of (30).

The two results were compared for a family of values of $\bar{\omega}$, $\Delta\omega$, and Δy. The details of the numerical analysis and the technical aspects of the numerical integration are included in section 6 and Appendix D of this report. However, initial numerical results showed that (76) closely approximated the value obtained through numerical integration of (30) for large $|\bar{\omega}|$ $(|\bar{\omega}| > 10\omega_c)$. As $|\bar{\omega}|$ was decreased (76) became an increasingly poor model for $M_o(\bar{\omega}, \Delta\omega, \Delta y)$. The model completely broke down as $|\bar{\omega}| \to \omega_c$. The approximations used to derive (76) assumed that $|\bar{\omega}| >> \omega_c$; hence, it is not surprising that the expression for $M_o(\bar{\omega}, \Delta\omega, \Delta y)$ ceases to be accurate for $|\bar{\omega}| \approx \omega_c$. We will analyze this problem in more detail to find the lower bound on $|\bar{\omega}|$ for which our model is valid. This lower bound will quantify the previous somewhat nebulous requirement that $|\bar{\omega}| >> \omega_c$.

We return to (34). $M_o(\bar{\omega}, \Delta\omega, \Delta y)$ was found by integrating $M'(\bar{\omega}, \Delta\omega, \Delta\beta, \Delta y)$ with respect to $\Delta\beta$ over the infinite $\Delta\beta$ plane. We should note here that the integration over the aperture plane is actually limited by the size of the aperture. Thus, physically the integral always converges. However, in deriving (35) we argued that the effects of the finite aperture could be separated from the integration over $\Delta\beta$ by sampling $P'(\bar{\omega}, \Delta\omega, \bar{\beta}, \Delta\beta)$ at $\Delta\beta = -\Delta\omega/2$. We now explore the consequences of this approximation and, in particular we determine the range of $\bar{\omega}$ for which the approximation is reasonable. For the integral in (34) to exist, $M'(\bar{\omega}, \Delta\omega, \Delta\beta, \Delta y)$ must vanish for sufficiently large $|\Delta\beta|$. We shall explore the behavior of $M'(\bar{\omega}, \Delta\omega, \Delta\beta, \Delta y)$ for very large $\Delta\beta$. From (30)

it is apparent that for very large $\Delta\beta$, the terms $d_3(\cdot)$, $d_4(\cdot)$, $d_5(\cdot)$, and $d_6(\cdot)$ approximately cancel each other and we have

$$M'(\bar{\omega}, \Delta\omega, \Delta\beta, \Delta y) \approx \exp\left\{-\frac{k^2}{2}\int_0^H C_n^2(h)\,[d(\bar{\omega}+\Delta\omega) + d(\bar{\omega}-\Delta\omega)]\,dh\right\},$$

$$|\Delta\beta| \text{ very large.} \tag{83}$$

We are not interested here in the $\Delta\omega$ dependence so we set $\Delta\omega = 0$. Substituting (23) into (83),

$$M'(\bar{\omega}, \Delta\omega, \Delta\beta, \Delta y) \approx \exp\left\{-2.92\,k^2\int_0^H C_n^2(h)\,dh\,|\bar{\omega}|^{5/3}\right\}$$

$$= \exp\left\{-2.92\,k^2\mu_o\,|\bar{\omega}|^{5/3}\right\}. \tag{84}$$

From (84) we observe that if $|\bar{\omega}|$ is not large enough, then $M'(\bar{\omega}, \Delta\omega, \Delta\beta, \Delta y)$ will not effectively vanish for large $|\Delta\beta|$ and the integration over the $\Delta\beta$ plane is not defined. We hasten to add that (84) indicates that $M'(\bar{\omega}, \Delta\omega, \Delta\beta, \Delta y)$ does not strictly vanish for large $|\Delta\beta|$ but rather approaches some constant value. We must quantify what we mean by effectively vanishing. Numerical analysis has shown good correlation between (76) and the numerical integration of (30) if $|\bar{\omega}|$ is large enough to insure that the asymptotic value predicted in (84) is on the order of 10^{-6} or smaller. We can now compute the lower bound on $|\bar{\omega}|$ subject to this condition. The lower bound will be denoted by $\bar{\omega}_{c1}$, and is calculated from the condition

$$\exp\left\{-2.92\ k^2 \mu_o\ |\bar{\omega}_{c1}|^{5/3}\right\} = 10^{-6}.$$

Solving for $\bar{\omega}_{c1}$, we find that

$$\bar{\omega}_{c1} = \left(\frac{13.8}{2.92\ k^2 \mu_o}\right)^{3/5} \approx 3\ \omega_c. \tag{85}$$

We have established $\bar{\omega}_{c1}$ as a lower bound on $|\bar{\omega}|$. Our model for $M_o(\bar{\omega}, \Delta\omega, \Delta y)$ is valid for $|\bar{\omega}| > \omega_{c1}$. We can also interpret physically the behavior of $M'(\bar{\omega}, \Delta\omega, \Delta\beta, \Delta y)$ in the region $\omega_c < |\bar{\omega}| < \omega_{c1}$. In section 4 we noted that for spatial frequencies satisfying $|\bar{\omega}|^2 + |\Delta\omega|^2 < \omega_c^2$, the entire aperture appears to be spatially coherent. Furthermore, for spatial frequencies satisfying $|\Delta\omega| < \omega_c$ and $|\bar{\omega}| >> \omega_c$, the aperture is spatially coherent in regions the size of ω_c (for source points separated by $\Delta y < \Delta y_c$). The region $\omega_c < |\bar{\omega}| < \omega_{c1}$ is in the transition zone between the regions of complete and partial coherence.

There is one remaining issue that must be resolved. In the course of deriving (76) and (77), we assumed that $|\bar{\omega}| > |h\Delta y|$, knowing that this assumption was suspect. The preliminary numerical analysis mentioned above has shown additional discrepancies between (76) and the values calculated from numerical integration of (30) for values of $|\bar{\omega}|$ larger than $\bar{\omega}_{c1}$. The region in which the discrepancy was significant was generally confined to $\bar{\omega}_{c1} < |\bar{\omega}| < 5\bar{\omega}_{c1}$. For larger values of $|\bar{\omega}|$, (76) was valid. We should point out that the width of this troublesome region is

highly dependent upon the model used for the refractive index structure constant $C_n^2(h)$. The width is largest for $C_n^2(h)$ profiles with very weak turbulence at higher altitudes.

The discrepancy is in the Δy plane only. For values of $\bar{\omega}$ in the troublesome region, $M_o(\bar{\omega}, \Delta\omega, \Delta y)$ no longer appears to be a Gaussian in Δy but rather the sum of a Gaussian and a constant. The value of the constant decreases with increasing $|\bar{\omega}|$. The problem is due to the fact that under these conditions $|\bar{\omega}|$ does not dominate $|h\Delta y|$ and the truncated binomial expansions used in the derivation of (76) are not accurate.

To quantify the effects we have observed, we seek an alternative approximation to $M'(\bar{\omega}, \Delta\omega, \Delta\beta, \Delta y)$ that is valid for large $|h\Delta y|$. Unfortunately, we have not been successful in determining an approximation that preserves integrability with respect to h. Hence, we must sacrifice generality here and assume some model for the $C_n^2(h)$ profile. To expedite the integration over h, we will use the simple double-impulse model for $C_n^2(h)$ shown in Fig. 2.

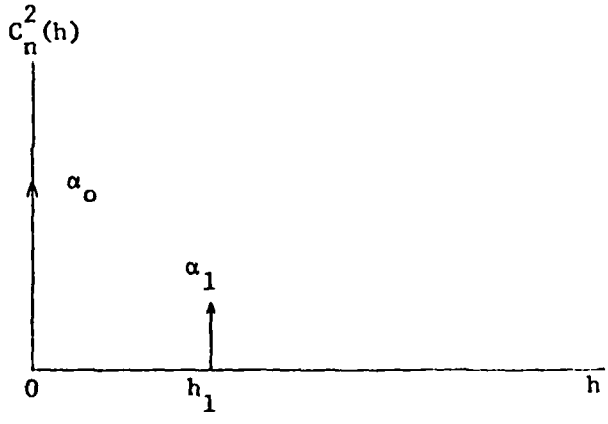

Fig. 2. The double impulse model for $C_n^2(h)$.

We model $C_n^2(h)$ by

$$C_n^2(h) = \alpha_o \delta(h) + \alpha_1 \delta(h - h_1),$$

$$\alpha_o > \alpha_1. \tag{86}$$

The impulse at h = 0 represents turbulence near the ground while the impulse at $h = h_1$ represents turbulence in the upper atmosphere. The height h_1 of the second impulse is in general variable, but in this report we will associate h_1 with the "tropopausal bump" sometimes observed at a height of 10^4 m [8]. We require that $\alpha_o > \alpha_1$ to satisfy (12).

The double impulse model allows the trivial evaluation of the integration with respect to h. Substituting the double impulse model into (10) and integrating over h yields

$$M'(\bar{\omega}, \Delta\omega, \Delta\beta, \Delta y) =$$

$$\exp\left\{-\frac{k^2}{2}\left[\alpha_o\begin{pmatrix} d_1(\bar{\omega}+\Delta\omega) + d_2(\bar{\omega}-\Delta\omega) \\ + d_3(2\Delta\beta + 2\Delta\omega) + d_4(2\Delta\beta) \\ - d_5(2\Delta\beta + \Delta\omega - \bar{\omega}) - d_6(2\Delta\beta + \Delta\omega + \bar{\omega}) \end{pmatrix} + \alpha_1\begin{pmatrix} d_7(\bar{\omega}+\Delta\omega) + d_8(\bar{\omega}-\Delta\omega) \\ + d_9(2\Delta\beta + 2h_1\Delta y + 2\Delta\omega) + d_{10}(2\Delta\beta + 2h_1\Delta y) \\ - d_{11}(2\Delta\beta+2h_1\Delta y+\Delta\omega-\bar{\omega}) - d_{12}(2\Delta\beta+2h_1\Delta y+\Delta\omega+\bar{\omega}) \end{pmatrix}\right]\right\} \tag{87}$$

AD-A115 887 ANALYTIC INFORMATION PROCESSING INC DANVILLE CA F/G 20/6
RESEARCH AND DEVELOPMENT IN SPECKLE IMAGING.(U)
NOV 81 J W SHERMAN F49620-80-C-0032
UNCLASSIFIED AFOSR-TR-82-0361 NL

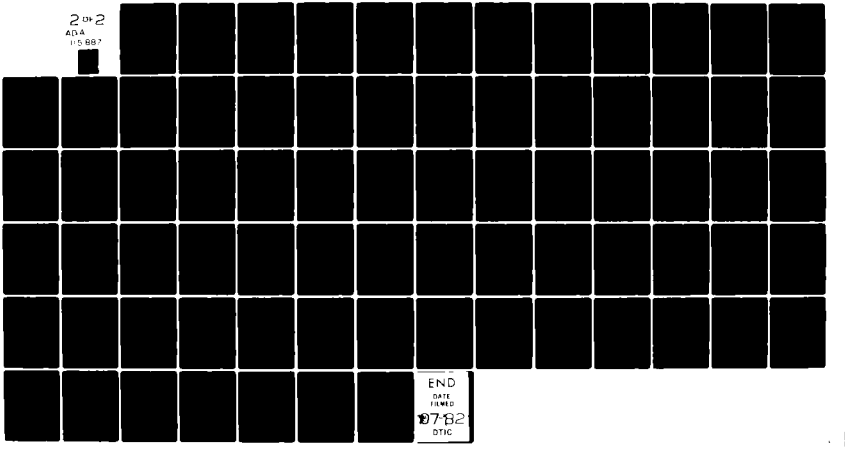

Once again we will approximate each of the $d(\cdot)$ functions by quadratics. However, here we are interested in large values of $|h_1 \Delta y|$, so we will assume that $|h_1 \Delta y|$ dominates the other terms in the arguments of $d_9(\cdot)$ to $d_{12}(\cdot)$. Previously, we have shown that

$$d(\rho) \approx c_1 \rho \cdot \rho + c_o \qquad (\rho \approx \omega_c) \tag{51}$$

and

$$d(\bar{\omega} + \delta) \approx 2.92\ (\bar{\omega} \cdot \bar{\omega})^{5/6} \left[1 + \frac{5\delta \cdot \bar{\omega}}{3\bar{\omega} \cdot \bar{\omega}} + \frac{\delta \cdot \delta}{\bar{\omega} \cdot \bar{\omega}}\left(\frac{5}{6} - \frac{5}{18}\cos^2\theta\right)\right]. \tag{46}$$

Similarly,

$$d\left(2h_1 \Delta y + \delta\right) \approx 2.92\left(4h_1^2 \Delta y \cdot \Delta y\right)^{5/6}\left[1 + \frac{5h_1 \delta \cdot \Delta y}{12h_1^2 \Delta y \cdot \Delta y} + \frac{\delta \cdot \delta}{4h_1^2 \Delta y \cdot \Delta y} \cdot \left(\frac{5}{6} - \frac{5}{18}\cos^2\psi\right)\right]. \tag{88}$$

where ψ is the angle between Δy and δ. We are interested here in the qualitative behavior of $M'(\bar{\omega}, \Delta\omega, \Delta\beta, \Delta y)$ as $|h\Delta y|$ becomes very large. To simplify the analysis, we will neglect the angular dependence ψ and set $\cos^2\psi = 1$. We approximate $d_3(\cdot)$ and $d_4(\cdot)$ by (51), $d_1(\cdot)$, $d_2(\cdot)$, $d_5(\cdot)$, $d_6(\cdot)$, $d_7(\cdot)$, and $d_8(\cdot)$ by (46), and $d_9(\cdot)$, $d_{10}(\cdot)$, $d_{11}(\cdot)$, and $d_{12}(\cdot)$ by (88). In Appendix C, c_o is shown to be nearly zero. Making these substitutions in (87), we obtain

$$M'(\bar{\omega},\ \Delta\omega,\ \Delta\beta,\ \Delta y) \approx$$

$$\exp\left\{-k^2\left(\begin{array}{l}\left[4c_1 - 6.49(\bar{\omega}\cdot\bar{\omega})^{-1/6}\right]\alpha_o\Delta\beta\cdot\Delta\beta + \left[4c_1 - 6.49(\bar{\omega}\cdot\bar{\omega})^{-1/6}\right]\alpha_o\Delta\omega\cdot\Delta\beta \\ + 2c_1\alpha_o + 1.62(\bar{\omega}\cdot\bar{\omega})^{-1/6}\alpha_1\Big]\ \Delta\omega\cdot\Delta\omega \\ + \left[2.92(\bar{\omega}\cdot\bar{\omega})^{-1/6}\alpha_1 - 1.62\left(4h_1^2\Delta y\cdot\Delta y\right)^{-1/6}(\bar{\omega}\cdot\bar{\omega}-\Delta\omega\cdot\Delta\omega)\ \alpha_1\right]\end{array}\right)\right\}. \tag{89}$$

This equation is quadratic in $\Delta\beta$. Completing the square and integrating over the $\Delta\beta$ plane yields

$$M_o(\bar{\omega},\ \Delta\omega,\ \Delta y) \approx$$

$$\sqrt{\frac{2\pi^2}{k^2\gamma'\alpha_o}}\exp\left\{-k^2\left[3\left(k^2\mu_o\right)^{1/5}\alpha_o + 1.62(\bar{\omega}\cdot\bar{\omega})^{-1/6}\mu_o\right]\Delta\omega\cdot\Delta\omega\right\}$$

$$\exp\left\{-k^2\left[2.92(\bar{\omega}\cdot\bar{\omega})^{5/6}\alpha_1 - 1.62\left(4h_1^2\Delta y\cdot\Delta y\right)^{-1/6}(\bar{\omega}\cdot\bar{\omega}-\Delta\omega\cdot\Delta\omega)\alpha_1\right]\right\} \tag{90}$$

where γ' is given by:

$$\gamma' = 12\left(k^2\mu_o\right)^{1/5} - 6.49\ (\bar{\omega}\cdot\bar{\omega})^{-1/6}. \tag{91}$$

The Δy dependence is no longer Gaussian, and we emphasize that this approximation is valid only for very large $|h_1\Delta y|$. In particular, setting $\Delta\omega = 0$ and taking the limit as $|h_1\Delta y| \to \infty$,

$$\lim_{|h_1\Delta y|\to\infty} M_o(\bar{\omega},\ 0,\ \Delta y) = \sqrt{\frac{2\pi^2}{k^2\gamma'\alpha_o}}\exp\left\{-2.92\ k^2\ \alpha_1\ |\bar{\omega}|^{5/3}\right\}. \tag{92}$$

Equation (76) predicts that $M_o(\bar{\omega}, 0, \Delta y) \to 0$ as $|h_1 \Delta y| \to \infty$. However, (91) predicts that $M_o(\bar{\omega}, 0, \Delta y) \to g(\bar{\omega}, \alpha_o, \alpha_1, h_1) \neq 0$ as $|h_1 \Delta y| \to \infty$. We also note that as $|\bar{\omega}|$ increases, the value of g decreases. To bound the region where this effect is significant, we propose to neglect g when $|\bar{\omega}| > \bar{\omega}_{c2}$. We define $\bar{\omega}_{c2}$ as

$$\exp \left\{-2.92\, k^2 \alpha_1 \, |\bar{\omega}_{c2}|^{5/3}\right\} = \exp\{-2\} \tag{93}$$

Solving for $\bar{\omega}_{c2}$ yields

$$\bar{\omega}_{c2} = \left(\frac{2}{2.92\, k^2 \alpha_1}\right)^{3/5}. \tag{94}$$

It is more convenient to express $\bar{\omega}_{c2}$ as a multiple of ω_c. Using (27), we obtain

$$\bar{\omega}_{c2} = \left(1 + \frac{\alpha_o}{\alpha_1}\right)^{3/5} \omega_c. \tag{95}$$

Equation (95) bounds the region where the noted phenomenon is significant. The effect is significant for spatial frequencies $\bar{\omega}$ such that $\bar{\omega}_{c1} < |\bar{\omega}| < \bar{\omega}_{c2}$. We note that

$$\bar{\omega}_{c1} \approx 3\, \omega_c \tag{96}$$

$$\bar{\omega}_{c2} \approx K\omega_c \tag{97}$$

where K depends upon the ratio of surface-to-high-altitude turbu-

lence. Some values of K are tabulated in Table 1.

Table 1. Representative values of K as a function of the ratio α_o/α_1.

α_o/α_1	K
100	15.9
10	4.2
8	3.7
4	2.3
2	1.5

We now make a key observation. If $\alpha_o/\alpha_1 \leq 5.2$ (i.e., if α_1 is at least 20 percent of α_o), then $\bar{\omega}_{c2} \leq \bar{\omega}_{c1}$ and (76) is valid for all $|\bar{\omega}| > \bar{\omega}_{c1}$. On the other hand, if $\alpha_o/\alpha_1 > 5.2$, then there will be a nonvanishing region in which the Gaussian model in Δy must be replaced by a Gaussian plus constant model. However, the width of this region *does not become* significant until $\alpha_o/\alpha_1 > 10$.

At this point it is useful to partition the $\bar{\omega}$ plane into four regions:

a. $|\bar{\omega}| < \omega_c$

b. $\omega_c < |\bar{\omega}| < \bar{\omega}_{c1}$

c. $\bar{\omega}_{c1} < |\bar{\omega}| < \bar{\omega}_{c2}$

d. $\bar{\omega}_{c2} < |\bar{\omega}|$

Under the assumptions $|\Delta\omega| < \omega_c$, $|2\Delta\beta + \Delta\omega| < \omega_c$ and $|\Delta y| < \Delta y_c$, in region (a) the entire aperture appears coherent. Region (b) is the transition zone from complete to partial coherence. In region (c), $M_o(\bar{\omega}, \Delta\omega, \Delta y)$ is best modeled by the product of a Gaussian in $\Delta\omega$ and a Gaussian plus constant in Δy. In region (d) $M_o(\bar{\omega}, \Delta\omega, \Delta y)$ may be modeled by the product of a Gaussian in $\Delta\omega$ and a Gaussian in Δy. We have shown that region (c) vanishes for moderate to strong upper atmospheric turbulence.

Equations (89) and (90) are strictly valid only for the double-impulse model of $C_n^2(h)$. However, the analysis should extend to more general $C_n^2(h)$ profiles. The key result is contained in (92). We conclude for the general case that if some appropriate measure of the turbulence in the upper atmosphere is much less than the corresponding measure of turbulence near the surface (i.e., less than 10 percent), then there will exist a nonvanishing region (c) $\bar{\omega}_{c1} < |\bar{\omega}| < \bar{\omega}_{c2}$ where our models for $M_o(\bar{\omega}, \Delta\omega, \Delta y)$ and $\tilde{M}_o(\bar{\omega}, \Delta\omega, \Delta\omega')$ given by (76) and (77) will not be valid. For the double-impulse model of $C_n^2(h)$, we can predict the size of the region and the form of the deviation from (76) and (77). In the more general case, the exact form of the deviation cannot be predicted by a closed form expression. We note that, physically, the phenomenon we have described is the transition of the imaging problem from the isoplanatic case to the nonisoplanatic case.

One reasonable technique for measuring the relative amounts

of upper atmospheric and surface turbulence for an arbitrary sample function of $C_n^2(h)$ is to compute the moments μ_o, μ_1, and μ_2 of the sample function and then convert these values into an equivalent double-impulse model. Equation (95) can then be applied to determine the approximate value of $\bar{\omega}_{c2}$. For example, consider Hufnagel's simple model [9] for $C_n^2(h)$:

$$C_n^2(h) = \begin{cases} \dfrac{1.5 \cdot 10^{-13}}{h} & h < 20{,}000 \\ 0 & h > 20{,}000 \end{cases} . \qquad (98)$$

The moments of this profile can be easily computed:

$$\mu_o = 1.64 \cdot 10^{-12},$$

$$\mu_1 = 3.00 \cdot 10^{-9},$$

$$\mu_2 = 3.00 \cdot 10^{-5}.$$

An equivalent double-impulse profile would have parameters

$$\alpha_o = 1.34 \cdot 10^{-12},$$

$$\alpha_1 = 3.00 \cdot 10^{-13},$$

$$h_1 = 10^4.$$

Computing $\bar{\omega}_{c2}$, we find that

$$\bar{\omega}_{c2} \approx 2.8\ \omega_c .$$

We conclude that region (c) vanishes for this profile and (76) and (77) are valid approximations for all $|\bar{\omega}| > 3\omega_c$.

In general, region (c) is significant only for atmospheric models with extremely weak high altitude turbulence. From the above analysis of Hufnagel's simple model and other published profiles of $C_n^2(h)$, it appears reasonable to conclude that models with such extremely weak high altitude turbulence are not often encountered in practice.

Returning to the questions posed before embarking upon this series of derivations, we find that simple analytical expressions can be found that approximate $M_o(\bar{\omega}, \Delta\omega, \Delta y)$ and $\tilde{M}_o(\bar{\omega}, \Delta\omega, \Delta\omega')$. Our models for these two functions are given by (76) and (77). We find that $C_n^2(h)$ influences $M_o(\bar{\omega}, \Delta\omega, \Delta y)$ and $\tilde{M}_o(\bar{\omega}, \Delta\omega, \Delta\omega')$ through the zero, first, and second moments $(\mu_o, \mu_1, \text{ and } \mu_2)$. These are the salient parameters of the refractive index structure constant, and aside from condition (12) the general shape of the sample function is unimportant. We will discuss the impact of the smoothing function $\tilde{M}_o(\bar{\omega}, \Delta\omega, \Delta\omega')$ on the imaging statistics in section 8 of this report.

6. Numerical Verification of the M_o Model

In this section of the report, we will summarize the results

of numerical analysis performed to test the validity of the closed form expression for M_o. The integration over $\Delta\beta$ called for in (34) was computed numerically and compared with the value predicted by our model. Only one-dimensional problems were considered to keep the numerical routines tractable. The details of the numerical integration algorithm are discussed in Appendix D. The one-dimensional equations for $M_o(\bar{\omega}, \Delta\omega, \Delta y)$ are given in Appendix E.

The calculation of $M_o(\bar{\omega}, \Delta\omega, \Delta y)$ requires two integrations: the first with respect to h, and the second with respect to $\Delta\beta$. Initially, the numerical complexity of the integration routine was simplified by presuming the double impulse model for $C_n^2(h)$ (Fig. 2). This supposition makes the integration over h trivial.

Three double-impulse models were considered. They differ in the ratio of upper-to-lower atmospheric turbulence (i. e., $C_n^2(h_1)/C_n^2(0)$). The model parameters are summarized in Table 2.

Table 2. Parameters of the three double-impulse models.

$C_n^2(h)$ model	α_o	α_1	h_1
1%	10^{-12}	10^{-14}	10^4
10%	10^{-12}	10^{-13}	10^4
25%	10^{-12}	$2.5 \cdot 10^{-13}$	10^4

We refer to the three profiles as the 1 percent, 10 percent, and 25 percent models, where the percentage is the ratio of upper-to-lower atmospheric turbulence $((\alpha_1/\alpha_o) \cdot 100)$. In each case we set the height of the second impulse, h_1, at 10,000 meters. The various

atmospheric cutoff frequencies $(\omega_c, \bar{\omega}_{c1}, \bar{\omega}_{c2})$ for the three $C_n^2(h)$ profiles are tabulated in Table 3.

Table 3. Cutoff frequencies for the three double-impulse models.

$C_n^2(h)$ Model	ω_c	$\bar{\omega}_{c1}$	$\bar{\omega}_{c2}$
1%	0.050	0.150	0.797
10%	0.047	0.141	0.198
25%	0.044	0.132	0.116

All three models have comparable values of ω_c and $\bar{\omega}_{c1}$. However, the value of $\bar{\omega}_{c2}$ varies considerably among the three models. This is due to the wide variation in the relative amounts of upper-atmospheric turbulence in the three models. The 1 percent model implies extremely weak upper-atmospheric turbulence and hence the value of $\bar{\omega}_{c2}$ is large. The 10 and 25 percent models imply moderate and moderate-to-strong upper-atmospheric turbulence and have correspondingly smaller values of $\bar{\omega}_{c2}$. Indeed, for the 25 percent model, region c has vanished (section 5).

The values of $M_o(\bar{\omega}, \Delta\omega, \Delta y)$ computed from (E2) and by the numerical integration of (30) were compared for many (350) combinations of $\bar{\omega}$, $\Delta\omega$, Δy. The correlation was found to be very good, with errors generally less than 10 percent until $M_o(\bar{\omega}, \Delta\omega, \Delta y)$ approached zero.

Some typical results are plotted in Figs. 3-5. In each plot cross sections in the $\Delta\omega$ and the Δy directions are shown, with the

other parameters fixed. The numerical integration data are plotted in a dashed line, while the values predicted by (E2) are plotted in a solid line.

Figures 3a,b-5a,b illustrate the roll-off of $M_o(\bar{\omega}, \Delta\omega, \Delta y)$ in the $\Delta\omega$ direction with $\Delta y = 10^{-7}$ rads. Since $\Delta y << \Delta y_c$, there is effectively no attenuation of $M_o(\bar{\omega}, \Delta\omega, \Delta y)$ due to the separation Δy of the image points. Similarly, Figs. 3c,d-5c,d illustrate the roll-off of $M_o(\bar{\omega}, \Delta\omega, \Delta y)$ in the Δy direction with $\Delta\omega = 10^{-3}$ meters. Since $\Delta\omega << \omega_c$, there is effectively no attenuation of $M_o(\bar{\omega}, \Delta\omega, \Delta y)$ due to the difference in aperture spatial frequencies $\Delta\omega$. Figures 6a-6b are analogous to 5a and 5b except that a much larger value of Δy was selected $(\Delta y = 3 \cdot 10^{-6})$ to illustrate the cross section in $\Delta\omega$ when Δy is sufficiently large to contribute to the attenuation. Also, Figs. 6c and 6d are analogous to 5c and 5d except for the selection of a larger value of $\Delta\omega$ $(\Delta\omega = 3 \cdot 10^{-1})$, to illustrate the cross section in Δy when $\Delta\omega$ is sufficiently large to contribute to the attenuation.

Figures 7a and 7b demonstrate the rapid degradation in the model for $M_o(\bar{\omega}, \Delta\omega, \Delta y)$ (E2) for $\bar{\omega} < \bar{\omega}_{c1}$. From Table 3, for the 25 percent profile, $\bar{\omega}_{c2} = 0.116$ meters. Figures 7a and 7b are plots of the $\Delta\omega$ and Δy cross section, with $\bar{\omega} = 0.100$ meters. For this value of $\bar{\omega}$ slightly less than $\bar{\omega}_{c1}$, the degradation in our model is already apparent. Other numerical results indicate that the breakdown of the model is rapid and severe for $\bar{\omega} < \bar{\omega}_{c1}$.

There is strong motivation to further verify the model for $M_o(\bar{\omega}, \Delta\omega, \Delta y)$ by generalizing the numerical comparisons made above

to more general sample functions of $C_n^2(h)$. Unfortunately, the computational complexity of the "nested" integration implied in (30) can rapidly become overwhelming even for reasonably "well-behaved" profiles. Rather than tackle this more comprehensive problem, we have tested a sampled version of Hufnagel's simple model:

$$C_n^2(h) = \begin{cases} \dfrac{1.5 \cdot 10^{-13}}{h} & h \leq 20{,}000 \\ 0 & h > 20{,}000 \end{cases} . \qquad (99)$$

This profile was sampled at 1 km intervals resulting in the multiple impulse model shown in Fig. 8 with

$$\alpha_o = \int_0^{500} \frac{1.5 \cdot 10^{-13}}{h}\, dh,$$

$$\alpha_i = \int_{(2i-1)500}^{(2i+1)500} \frac{1.5 \cdot 10^{-13}}{h}\, dh \qquad 1 \leq i \leq 19,$$

$$\alpha_{20} = \int_{19,500}^{20,000} \frac{1.5 \cdot 10^{-13}}{h}\, dh.$$

The corresponding $\Delta\omega$ and Δy cross-sectional plots generated by the numerical integration of (34) with this profile and the values predicted by (E1) are shown in Figs. 9a-9d. This model has a significant level of upper-atmospheric turbulence, and so (E1) was used rather than (E2). Once again, the dashed line represents data calculated by numerical integration while the solid line represents

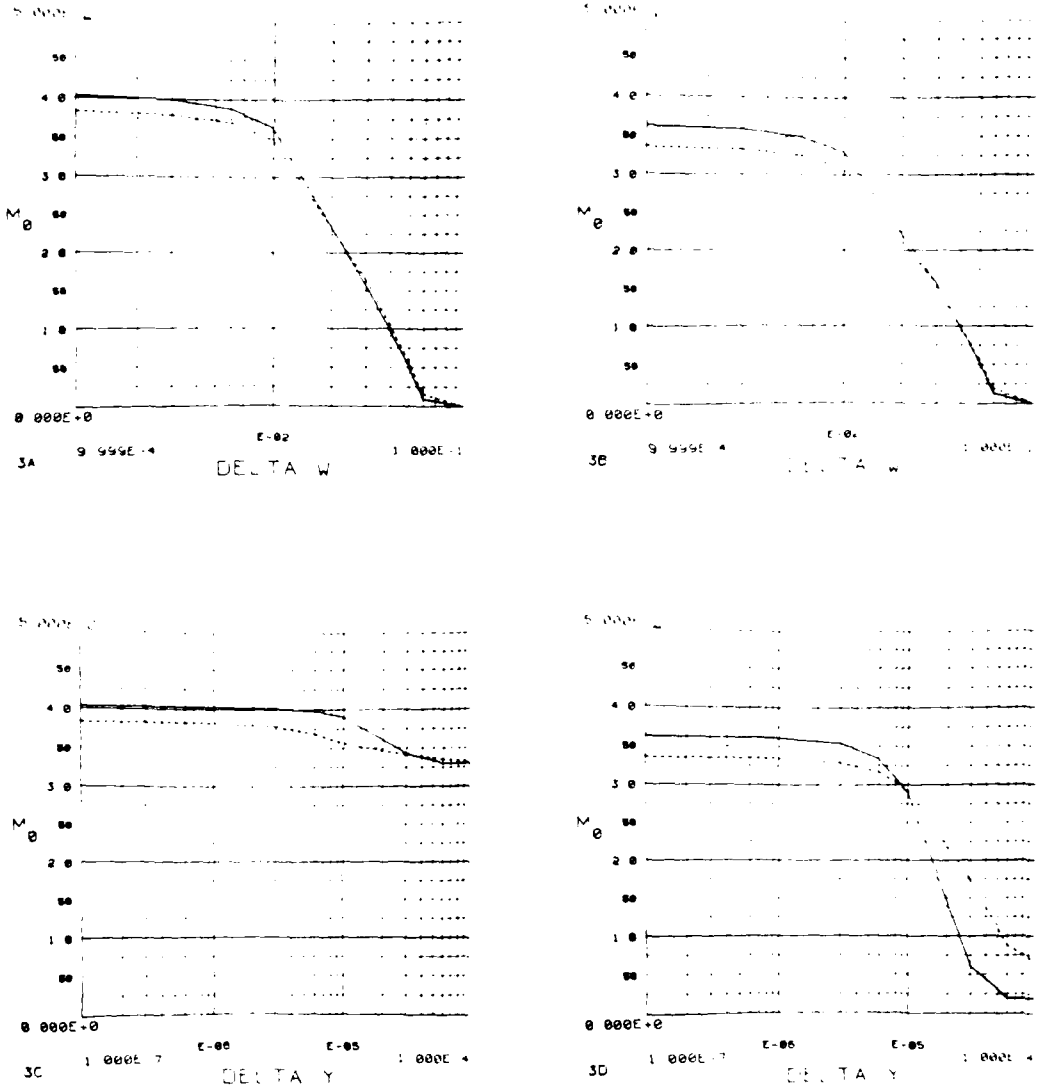

Fig. 3. A comparison of (E2) with the numerical integration of (34) for the 1 percent $C_n^2(h)$ profile (solid line - (E2); dashed line - numerical integration).

(a) $\bar{\omega} = 0.2$, $\Delta y = 10^{-7}$
(b) $\bar{\omega} = 1$, $\Delta y = 10^{-7}$
(c) $\bar{\omega} = 0.2$, $\Delta\omega = 10^{-3}$
(d) $\bar{\omega} = 1$, $\Delta\omega = 10^{-3}$

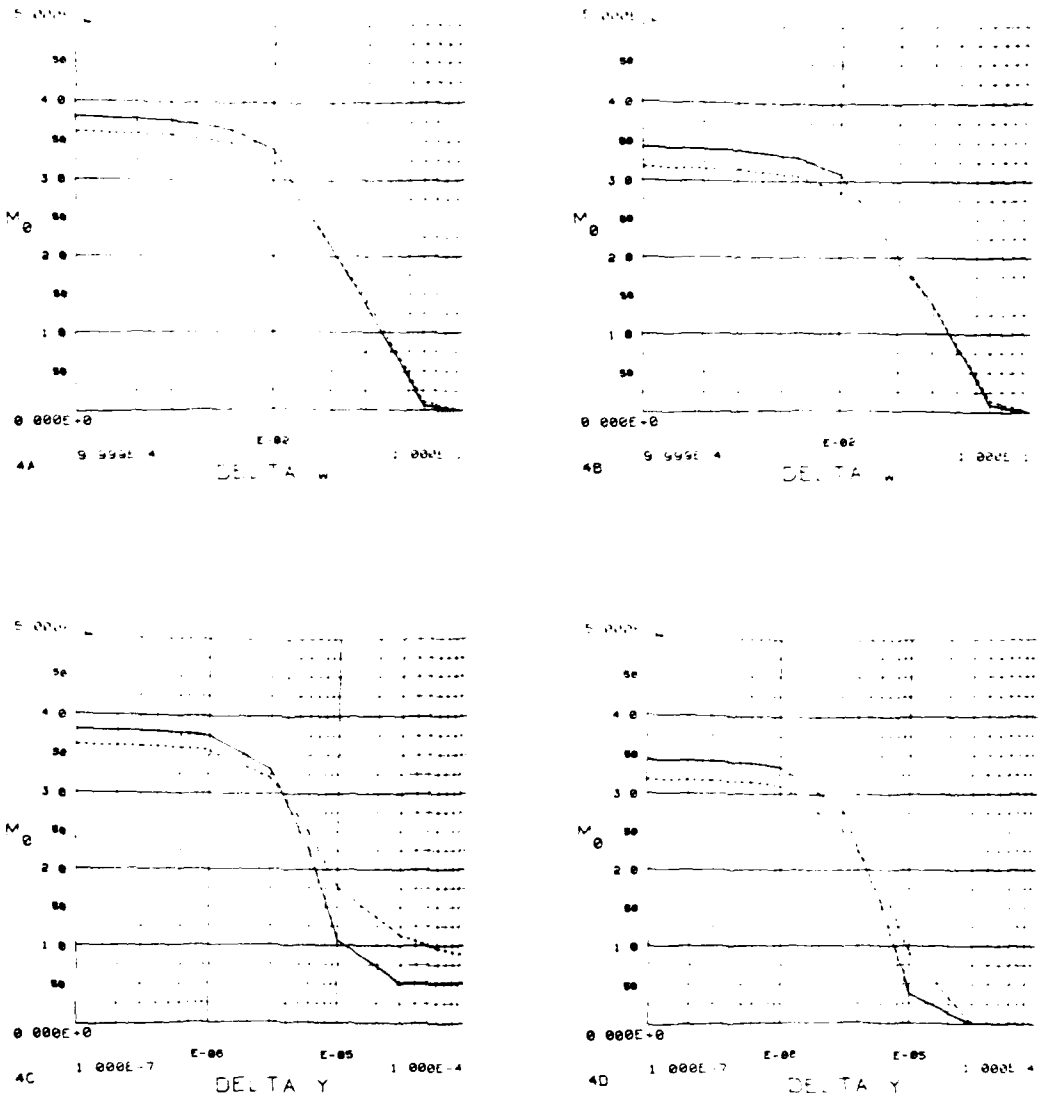

Fig. 4. A comparison of (E2) with the numerical integration of (34) for the 10 percent $C_n^2(h)$ profile (solid line - (E2); dashed line - numerical integration).

(a) $\bar{\omega} = 0.2$; $\Delta y = 10^{-7}$
(b) $\bar{\omega} = 1$, $\Delta y = 10^{-7}$
(c) $\bar{\omega} = 0.2$; $\Delta\omega = 10^{-3}$
(d) $\bar{\omega} = 1$; $\Delta\omega = 10^{-3}$

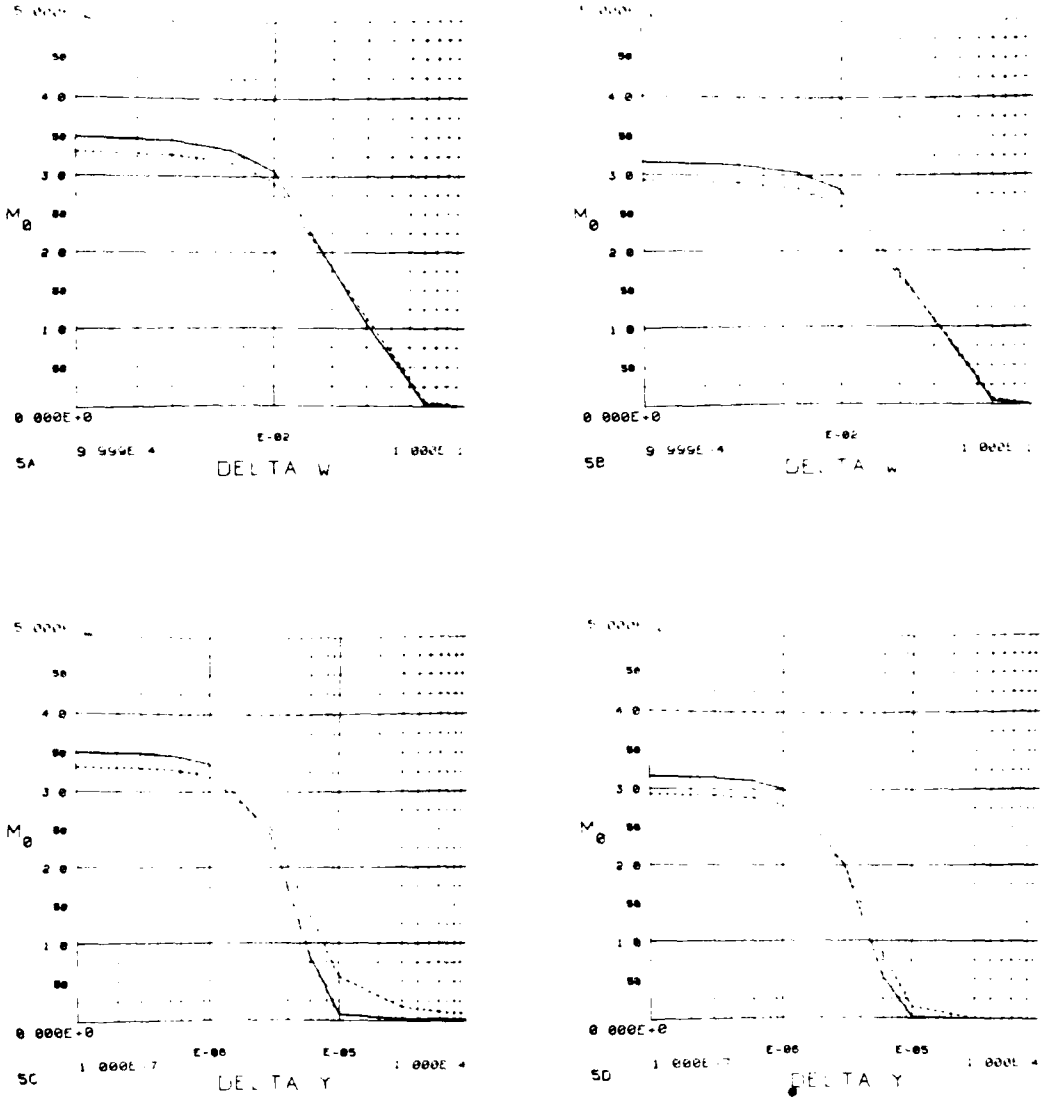

Fig. 5. A comparison of (E2) with the numerical integration of (34) for the 25 percent $C_n^2(h)$ profile (solid line - (E2); dashed line - numerical integration.

(a) $\bar{\omega} = 0.2$, $\Delta y = 10^{-7}$
(b) $\bar{\omega} = 1$, $\Delta y = 10^{-7}$
(c) $\bar{\omega} = 0.2$, $\Delta\omega = 10^{-3}$
(d) $\bar{\omega} = 1$, $\Delta\omega = 10^{-3}$

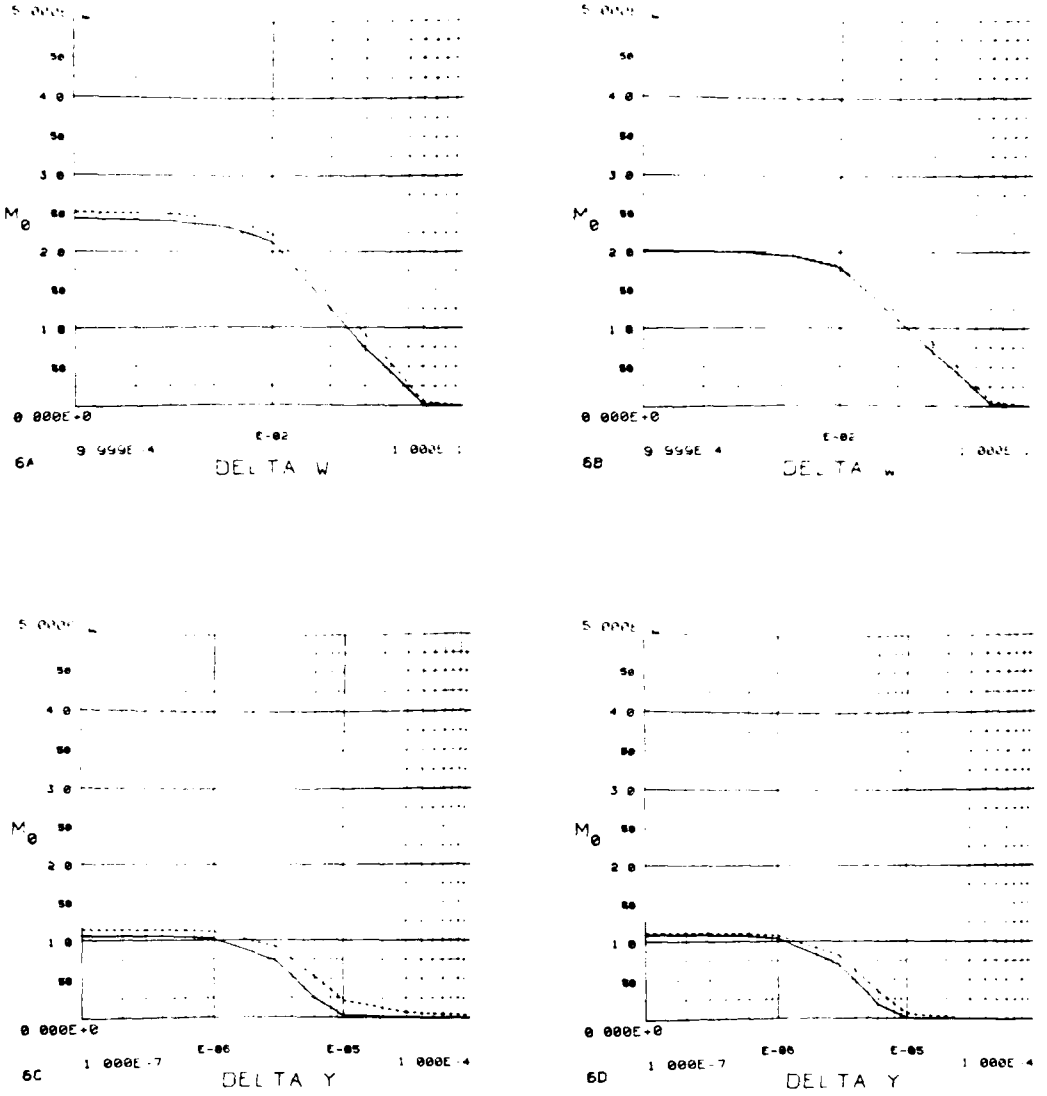

Fig. 6. A comparison of (E2) with the numerical integration of (34) for the 25 percent $C_n^2(h)$ profile (solid line - (E2); dashed line - numerical integration.

(a) $\bar{\omega} = 0.2$, $\Delta y = 3 \cdot 10^{-6}$
(b) $\bar{\omega} = 1$, $\Delta y = 3 \cdot 10^{-6}$
(c) $\bar{\omega} = 0.2$, $\Delta\omega = 3 \cdot 10^{-2}$
(d) $\bar{\omega} = 1$, $\Delta\omega = 3 \cdot 10^{-2}$

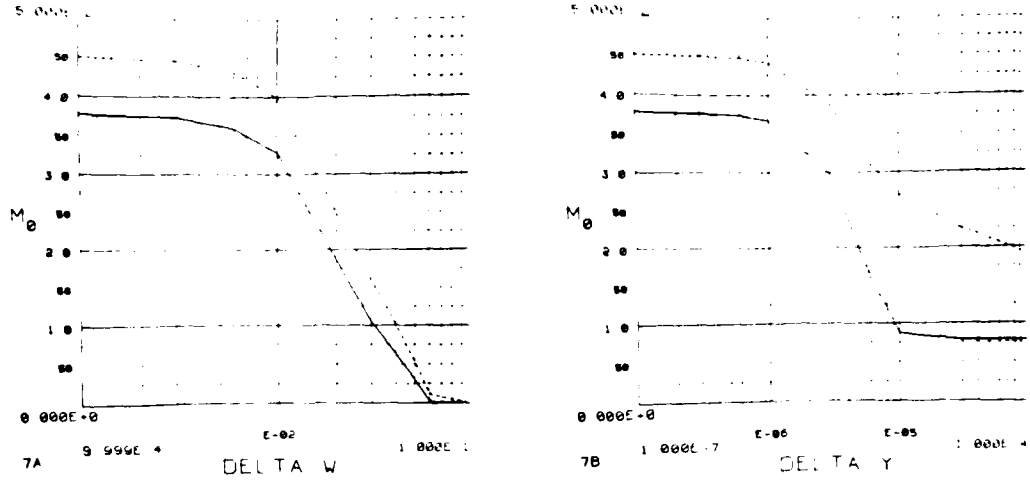

Fig. 7. A comparison of (E2) with the numerical integration of (34) for the 25 percent $C_n^2(h)$ profile with $\bar{\omega} < \bar{\omega}_{c1}$ (solid line - (E2); dashed line - numerical integration).

(a) $\bar{\omega} = 0.1$, $\Delta y = 10^{-7}$
(b) $\bar{\omega} = 0.1$, $\Delta\omega = 10^{-3}$

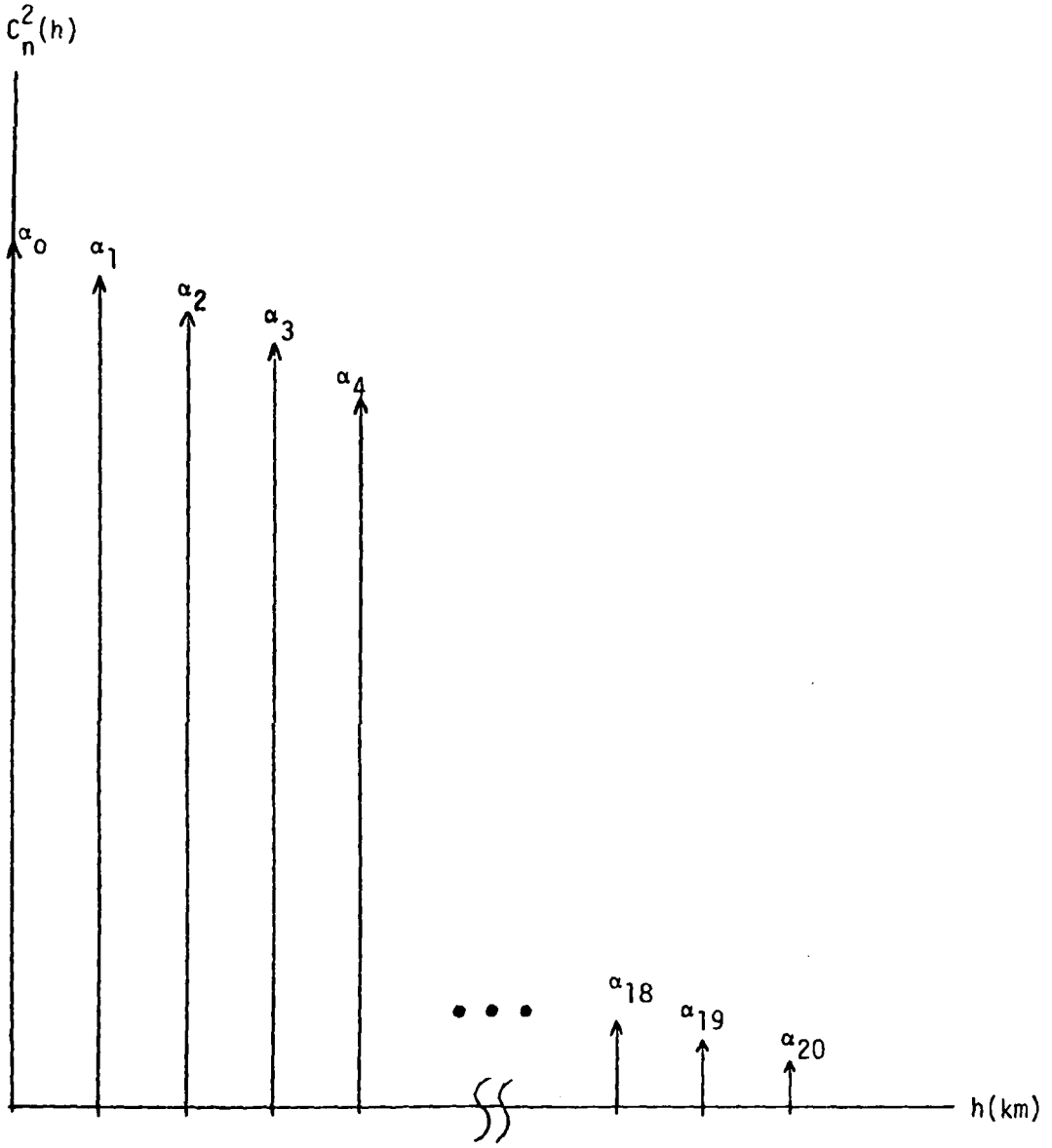

Fig. 8. The sampled Hufnagel profile for $C_n^2(h)$.

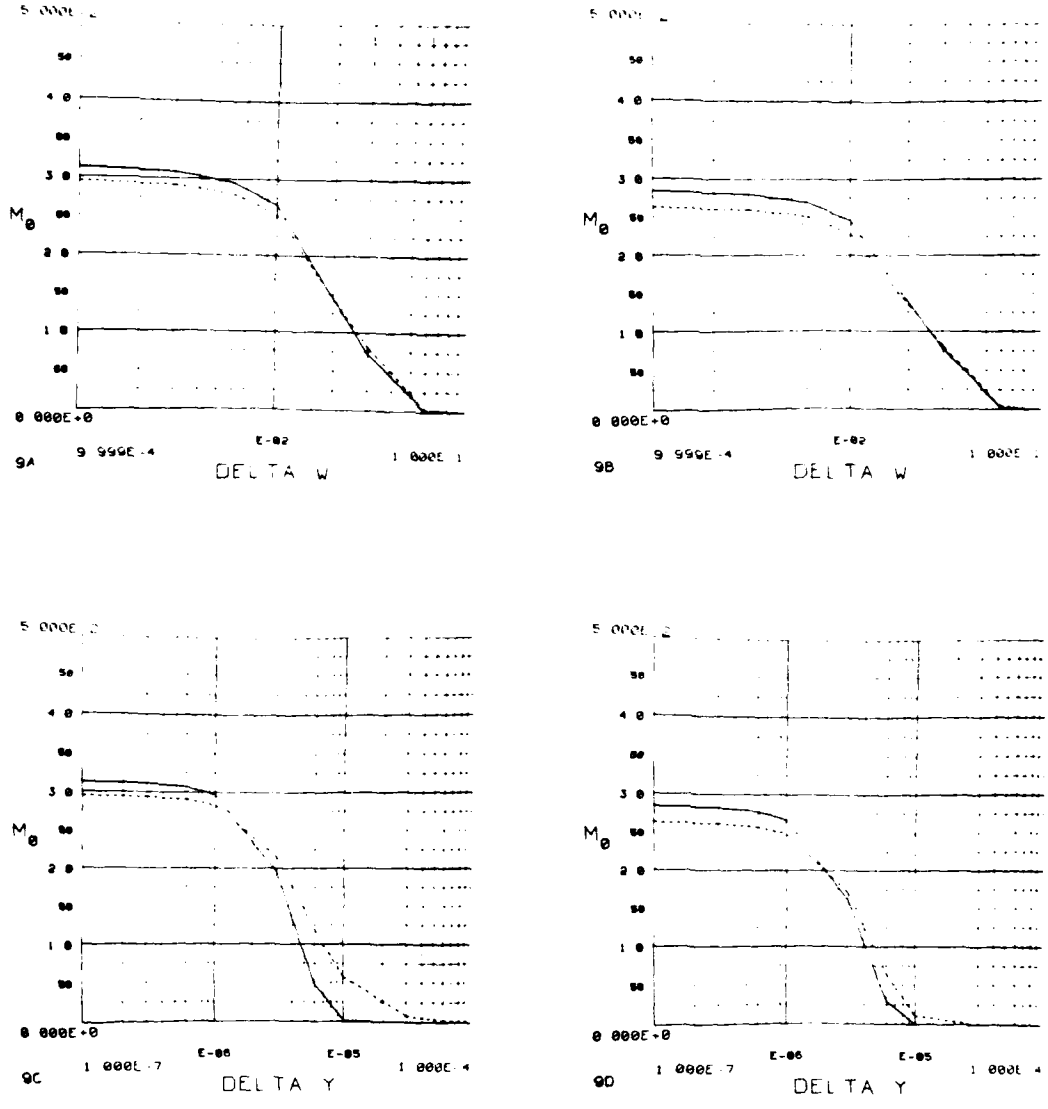

Fig. 9. A comparison of (E1) with the numerical integration of (34) for the sampled Hufnagel model $C_n^2(h)$ profile (solid line - (E1); dashed line - numerical integration.

(a) $\bar{\omega} = 0.2$, $\Delta y = 10^{-7}$
(b) $\bar{\omega} = 1$, $\Delta y = 10^{-7}$
(c) $\bar{\omega} = 0.2$, $\Delta\omega = 10^{-3}$
(d) $\bar{\omega} = 1$, $\Delta\omega = 10^{-3}$

our model.

In conclusion, we have shown the closed form expression (E2) for $M_o(\bar{\omega}, \Delta\omega, \Delta y)$ to be a reasonable approximation by comparing (E2) to data obtained by numerical integration of (34). In particular, our numerical experiments verified the following phenomena:

1. The behavior of $M_o(\bar{\omega}, \Delta\omega, \Delta y)$ in the $\Delta\omega$ direction is modeled well for all $\bar{\omega} > \bar{\omega}_{c1}$ by a Gaussian curve.
2. The behavior of $M_o(\bar{\omega}, \Delta\omega, \Delta y)$ in the Δy direction is modeled well for $\bar{\omega}_{c1} < \bar{\omega} < \bar{\omega}_{c2}$ by a Gaussian curve plus a constant. For $\bar{\omega} > \bar{\omega}_{c2}$, the behavior of $M_o(\bar{\omega}, \Delta\omega, \Delta y)$ may be modeled by a Gaussian curve in Δy. The approximation improves for increasing $\bar{\omega}$.
3. For $C_n^2(h)$ profiles with significant upper-atmospheric turbulence, $\bar{\omega}_{c2} < \bar{\omega}_{c1}$ and we may neglect the phenomenon described in (2).
4. For $\bar{\omega} < \bar{\omega}_{c1}$, the model ceases to be valid. The breakdown of the model in this region is rapid and severe.

7. Comparison with Fried

In this section of the report, we will compare some of the implications of our model for $M_o(\bar{\omega}, \Delta\omega, \Delta y)$ with similar conclusions made by Fried, et al. [10, 11]. We can associate the parameter Δy_c of the model with the size of the isoplanatic patch. Fried has proposed the following expression for Δy_c:

$$\Delta y_c' = \left\{ 2.91\, k^2 \int_0^H h^{5/3}\, C_n^2(h)\, dh \right\}^{-3/5} . \qquad (100)$$

We have compared the isoplanatic patch sizes predicted by Fried (100) and by our model (81) for the $C_n^2(h)$ profiles discussed in the previous section.

$$\Delta y_c = \left\{k^2 \gamma_1 \left(\mu_2 - \mu_1^2/\mu_o\right)\right\}^{-1/2} \tag{81}$$

with

$$\gamma_1 = 12 \left(k^2 \mu_o\right)^{1/5} - 9.73 \left(1 - \frac{1}{3} \cos^2 \theta\right) (\bar{\omega} \cdot \bar{\omega})^{-1/6}. \tag{78}$$

Since our model includes some weak dependence on $|\bar{\omega}|$ and the angle between $\bar{\omega}$ and $\Delta\omega$, we will set $|\bar{\omega}| = 1$ and $\theta = 0$ for the purpose of comparison. The results are tabulated in Table 4.

Table 4. A comparison of the isoplanatic patch size predicted by (81) and by Fried.

$C_n^2(h)$ Profile	Eq. 81	Fried
1% model	$\Delta y_c = 2.06 \cdot 10^{-5}$	$\Delta y_c' = 5.27 \cdot 10^{-5}$
10% model	$6.74 \cdot 10^{-6}$	$1.32 \cdot 10^{-5}$
25% model	$4.47 \cdot 10^{-6}$	$7.64 \cdot 10^{-6}$
Sampled Hufnagel model	$3.98 \cdot 10^{-6}$	$7.03 \cdot 10^{-6}$

We find very reasonable correlation with differences on the order of a factor of two.

8. Effects on Imaging Equations

We will now consider the effects of $\tilde{M}_o(\bar{\omega}, \Delta\omega, \Delta\omega')$ on the imaging statistics. We assume $\tilde{M}_o(\bar{\omega}, \Delta\omega, \Delta\omega')$ to be of the form given in (77):

$$\tilde{M}_o(\bar{\omega}, \Delta\omega, \Delta\omega') \approx V \exp\left\{-\Delta\omega' \cdot \Delta\omega'/(\Delta\omega_c')^2\right\} \tag{101}$$

where

$$V \equiv 2\pi^2 \sqrt{\frac{\Delta y_c^2}{k^2 \gamma_1 \mu_o}} \exp\left\{-\Delta\omega \cdot \Delta\omega/(\Delta\omega_c)^2\right\} . \tag{102}$$

Substituting this expression for $\tilde{M}_o(\bar{\omega}, \Delta\omega, \Delta\omega')$ into (39), we deduce the following expression for the Fourier transform of the second-order statistics:

$$W(\omega_1, \omega_2) = 4|A|^4 \frac{(2\pi)^4}{(k)^2} V F_4(\bar{\omega}, \Delta\omega) \iint_{-\infty}^{\infty} \tilde{O}\left(\omega_1 - \frac{\Delta\omega'}{2}\right) \tilde{O}\left(\omega_2 + \frac{\Delta\omega'}{2}\right)$$

$$\cdot \exp\left\{-\Delta\omega' \cdot \Delta\omega'/(\Delta\omega_c')^2\right\} d^2\Delta\omega' . \tag{103}$$

In the following analysis we shall neglect the factor preceding the integral in (103). This factor includes scaling constants and gain-attenuation factors in both the $\bar{\omega}$ and $\Delta\omega$ planes. Our primary interest here is in the distortion of the second-order statistics in the $\Delta\omega'$ plane. We define

$$W'(\omega_1, \omega_2) \equiv \iint_{-\infty}^{\infty} \tilde{O}\left(\omega_1 - \frac{\Delta\omega'}{2}\right) \tilde{O}\left(\omega_2 + \frac{\Delta\omega'}{2}\right)$$

$$\cdot \exp\left\{-\Delta\omega' \cdot \Delta\omega'/(\Delta\omega_c')^2\right\} d^2\Delta\omega'. \qquad (104)$$

To provide more insight into the smoothing effects of $\tilde{M}_o(\bar{\omega}, \Delta\omega, \Delta\omega')$, we shall assume the image to be Gaussian. The Fourier transform of a Gaussian is still a Gaussian so we may assume that

$$\tilde{O}(\omega) = \exp\left\{-\omega \cdot \omega/\Omega^2\right\}. \qquad (105)$$

Substituting (105) into (104), we obtain

$$W'(\omega_1, \omega_2) = \iint_{-\infty}^{\infty} \exp\left\{-\frac{(\omega_1 - \Delta\omega'/2)}{\Omega^2}\right\} \exp\left\{-\frac{(\omega_2 + \Delta\omega'/2)}{\Omega^2}\right\}$$

$$\cdot \exp\left\{-\Delta\omega' \cdot \Delta\omega'/(\Delta\omega_c')^2\right\} d^2\Delta\omega' \qquad (106)$$

The integral may be computed by expanding the exponent and completing the square in $\Delta\omega'$. Neglecting an unimportant scale factor, the integral is

$$J(\omega_1, \omega_2) = \exp\left\{\frac{2(\Delta\omega_c')^2\bar{\omega} \cdot \bar{\omega}}{\Omega^2[(\Delta\omega_c')^2 + 2\Omega^2]}\right\} \exp\left\{-\frac{\omega_1 \cdot \omega_1}{\Omega^2}\right\}$$

$$\cdot \exp\left\{-\frac{\omega_2 \cdot \omega_2}{\Omega^2}\right\}. \qquad (107)$$

We observe that the second and third exponential factors in (107)

are just $\tilde{O}(\omega_1)$ and $\tilde{O}(\omega_2)$. We can express the integral $J(\omega_1, \omega_2)$ in terms of $\bar{\omega}$ and $\Delta\omega$ by observing that

$$\omega_1 \cdot \omega_1 + \omega_2 \cdot \omega_2 = \frac{(\omega_1 - \omega_2) \cdot (\omega_1 - \omega_2) + (\omega_1 + \omega_2) \cdot (\omega_1 + \omega_2)}{2}$$

$$= 2\bar{\omega} \cdot \bar{\omega} + 2\Delta\omega \cdot \Delta\omega. \tag{108}$$

Substituting (108) into (107), we obtain

$$J(\bar{\omega}, \Delta\omega) = \exp\left\{\frac{2(\Delta\omega_c')^2\, \bar{\omega} \cdot \bar{\omega}}{\Omega^2[(\Delta\omega_c')^2 + 2\Omega^2]}\right\} \exp\left\{-\frac{2\bar{\omega} \cdot \bar{\omega}}{\Omega^2}\right\}$$

$$\cdot \exp\left\{-\frac{2\Delta\omega \cdot \Delta\omega}{\Omega^2}\right\}. \tag{109}$$

Collecting terms in $\bar{\omega}$,

$$J(\bar{\omega}, \Delta\omega) = \exp\left\{-\frac{2\bar{\omega} \cdot \bar{\omega}}{\Omega^2}\left[\frac{2\Omega^2}{(\Delta\omega_c')^2 + 2\Omega^2}\right]\right\} \exp\left\{-\frac{2\Delta\omega \cdot \Delta\omega}{\Omega^2}\right\}. \tag{110}$$

From (110) it is apparent that the imaging process has not altered the statistics in the $\Delta\omega$ plane. However, the imaging process broadens the statistcs in the $\bar{\omega}$ plane. Specifically, the width of the function in the $\bar{\omega}$ plane is increased by the factor $1 + (\Delta\omega_c')^2/2\Omega^2$.

9. Summary and Conclusions

This report deals with the problem of astronomical imaging through a turbulent atmosphere under conditions that force us to abandon the usual assumption of isoplanicity. Integral equations are developed which relate the object to the first and second moments of a series of short-exposure images. These equations involve the structure function of the atmosphere, which is shown here to be reasonably well approximated by a 5/3-law model for all values of its argument.

A detailed analysis of the effects of nonisoplanatic imaging potentially involves a considerable amount of numerical computation. Much of this computation can be avoided, and at the same time our insight into the process can be enhanced by making certain approximations to some key functions which describe the effects of the atmosphere. Several such approximations are studied in this report, and their validity is checked against results obtained by numerically integrating the original functions. We have obtained some useful models which are accurate under a wide range of reasonable conditions and whose use greatly simplifies the analysis of nonisoplanatic imaging.

APPENDIX A

In this appendix we consider the derivation of the first- and second-order statistics of a set of speckle images in greater detail. The uncertainty in the images is due to variations in the point-spread function $s(x, y)$. To obtain expressions for the first- and second-order statistics, it is necessary to compute $E\{s(x, y)\}$ and $E\{s(x_1, y_1)\, s(x_2, y_2)\}$. From (5) we find:

$$E\{s(x, y)\} = |A|^2 \int_{-\infty}^{\infty}\int \int_{-\infty}^{\infty}\int a(\beta + \omega)a(\beta) \exp[j\theta(\beta + \omega) - j\theta(\beta)]$$

$$\cdot \exp[-jk\omega \cdot (x - y)]\, E\{\exp[\psi(\beta + \omega, y) + \psi^*(\beta, y)]\} d^2\beta d^2\omega \tag{A1}$$

where

$$\psi(\cdot, \cdot) = \chi(\cdot, \cdot) + j\phi(\cdot, \cdot). \tag{A2}$$

We assume that $\chi(\cdot, \cdot)$ and $\phi(\cdot, \cdot)$ are uncorrelated, jointly Gaussian random processes. Furthermore, we assume that

$$E\{\chi(\cdot, y)\} = \bar{\chi} \tag{A3}$$

and

$$E\{\phi(\cdot, y)\} = 0. \tag{A4}$$

For notational simplicity we define

$$g(\beta, \omega; y) \equiv \psi(\beta + \omega, y) + \psi^*(\beta, y). \tag{A5}$$

We note that $g(\beta, \omega; y)$ is a Gaussian random process. To compute $E\{\exp[g]\}$ we use the fact that for a Gaussian random variable x with mean μ and variance σ^2

$$E\{\exp[x]\} = \exp\left[\mu + \frac{1}{2}\sigma^2\right]. \tag{A6}$$

Applying (A6), we find that

$$E\{\exp[\psi(\beta + \omega, y) + \psi^*(\beta, y)]\} = \exp\{E[g(\beta, \omega; y)] + \frac{1}{2} E[(g(\beta, \omega; y) - E(g(\beta, \omega; y)))^2]\}. \tag{A7}$$

From (A2-A5) we infer that

$$E\{g(\beta, \omega; y)\} = 2\bar{\psi} \tag{A8}$$

and

$$E\{[g(\beta, \omega; y) - E(g(\beta, \omega; y))]^2\} = E\{[\chi(\beta + \omega; y) + \chi(\beta, y) + j\phi(\beta + \omega; y) - j\phi(\beta, y) - 2\bar{\chi}]^2\}. \tag{A9}$$

Since $\chi(\cdot, \cdot)$ and $\phi(\cdot, \cdot)$ are uncorrelated and $\bar{\phi} = 0$, we can elimi-

nate the cross-product terms involving both $\chi(\cdot, \cdot)$ and $\phi(\cdot, \cdot)$. Hence

$$E\{[g(\beta, \omega; y) - E(g(\beta, \omega; y))]^2\} = E\{[\chi(\beta + \omega, y) + \chi(\beta, y) - 2\bar{\chi}]^2\} - E\{[\phi(\beta + \omega, y) - \phi(\beta, y)]^2\} . \quad (A10)$$

For convenience, we introduce the notation

$$D(\Delta, \delta) \equiv E\{|\psi(z + \Delta, y + \delta) - \psi(z, y)|^2\} , \quad (A11)$$

$$D_\chi(\Delta, \delta) \equiv E\{[\chi(z + \Delta, y + \delta) - \chi(z, y)]^2\} , \quad (A12)$$

$$D_\phi(\Delta, \delta) \equiv E\{[\phi(z + \Delta, y + \delta) - \phi(z, y)]^2\} , \quad (A13)$$

$$B_\chi(\Delta, \delta) \equiv E\{[\chi(z + \Delta, y + \delta)\chi(z, y) - E\{\chi(z + \Delta, y + \delta)\} \cdot E\{\chi(z, y)\}]\} , \quad (A14)$$

$$D_{\chi\phi}(\Delta, \delta) \equiv E\{[\chi(z + \Delta, y + \delta) - \chi(z, y)][\phi(z + \Delta, y + \delta) - \phi(z, y)]\}. \quad (A15)$$

With this notation and some algebraic manipulation, (A10) becomes

$$E\{[g(\beta, \omega; y) - E(g(\beta, \omega; y))]^2\} = -D_\phi(\omega, 0) - D_\chi(\omega, 0) + 4\sigma_\chi^2 \quad (A16)$$

where

$$\sigma_\chi^2 \equiv E\{[\chi(\beta, y) - \bar{\chi}]^2\}. \tag{A17}$$

It has been shown [6, 12] that from conservation of energy considerations, $\sigma_\chi^2 = -\bar{\chi}$. We also observe that

$$D(\Delta, \delta) = D_\phi(\Delta, \delta) + D_\chi(\Delta, \delta). \tag{A18}$$

With these substitutions, we have

$$E\{[g(\beta, \omega; y) - E\{g(\beta, \omega; y)\}]^2\} = -D(\omega, 0) - 4\bar{\chi}. \tag{A19}$$

Finally, from (A7, A8, and A19),

$$E\{\exp[\psi(\beta + \omega, y) + \psi^*(\beta, y)]\} = \exp\left[-\frac{1}{2} D(\omega, 0)\right]. \tag{A20}$$

Hence

$$E\{s(x, y)\} = |A|^2 \int_{-\infty}^{\infty} \int \exp\left[-\frac{1}{2} D(\omega, 0)\right] \exp[-jk\omega \cdot (x - y)]$$

$$\cdot \int_{-\infty}^{\infty} \int a(\beta + \omega)\, a(\beta) \exp[j\theta(\beta + \omega) - j\theta(\beta)]\, d^2\beta\, d^2\omega. \tag{A21}$$

To compute the second order statistics, we must develop an expression for $E\{s(x_1, y_1)\, s(x_2, y_2)\}$. From (9),

$$E\{s(x_1, y_1)s(x_2, y_2)\} = |A|^4 \int\int_{-\infty}^{\infty} \int\int_{-\infty}^{\infty} \int\int_{-\infty}^{\infty} \int\int_{-\infty}^{\infty} P(\beta_1, \omega_1, \beta_2, \omega_2)$$

$$\cdot M(\beta_1, \omega_1, y_1, \beta_2, \omega_2, y_2)\, d^2\beta_1\, d^2\beta_2\, \exp[-jk\omega_1 \cdot (x_1 - y_1)$$

$$- jk\omega_2 \cdot (x_2 - y_2)]\, d^2\omega_1\, d^2\omega_2 \qquad (9)$$

where

$$P(\beta_1, \omega_1, \beta_2, \omega_2) = a(\beta_1 + \omega_1)\, a(\beta_1)\, a(\beta_2)\, a(\beta_2 - \omega_2)$$

$$\cdot \exp[j\theta(\beta_1 + \omega_1) - j\theta(\beta_1) + j\theta(\beta_2) - j\theta(\beta_2 - \omega_2)] \qquad (10)$$

and

$$M(\beta_1, \omega_1, y_1, \beta_2, \omega_2, y_2) = E\{\exp[\psi(\beta_1 + \omega_1, y_1) + \psi^*(\beta_1, y_1)$$

$$+ \psi(\beta_2, y_2) + \psi^*(\beta_2 - \omega_2, y_2)]\}. \qquad (11)$$

The expectation in (11) can be computed by methods analogous to those used to compute the expectation in (A7). The calculations are very tedious, however, and will not be included here. Rather, we refer the reader to Fante [3] who argued that

$$E\{\exp[\psi(\beta_1 + \omega_1, y_1) + \psi^*(\beta_1, y_1) + \psi(\beta_2, y_2) + \psi^*(\beta_2 - \omega_2, y_2)]\}$$

$$= \exp[-\tfrac{1}{2} D(\omega_1, 0) - \tfrac{1}{2} D(\omega_2, 0)$$

$$- \tfrac{1}{2} D(\beta_1 - \beta_2 + \omega_1 + \omega_2, y_1 - y_2) - \tfrac{1}{2} D(\beta_1 - \beta_2, y_1 - y_2)$$

$$+ \tfrac{1}{2} D(\beta_1 - \beta_2 + \omega_1, y_1 - y_2) + \tfrac{1}{2} D(\beta_1 - \beta_2 + \omega_2, y_1 - y_2)$$

$$+ 2B_\chi(\beta_1 - \beta_2 + \omega_1, y_1 - y_2) + 2B_\chi(\beta_1 - \beta_2 + \omega_2, y_1 - y_2)$$

$$+ jD_{\chi\phi}(\beta_1 - \beta_2 + \omega_1, y_1 - y_2) - jD_{\chi\phi}(\beta_1 - \beta_2 + \omega_2, y_1 - y_2)]. \tag{A22}$$

Fante [3] has shown that the B_χ and $D_{\chi\phi}$ terms may be neglected. We conclude that

$$M(B_1, \omega_1, y_1, B_2, \omega_2, y_2) = \exp\{-\tfrac{1}{2}[D(\omega_1, 0) + D(\omega_2, 0)$$

$$+ D(\beta_1 - \beta_2 + \omega_1 + \omega_2, y_1 - y_2)$$

$$+ D(\beta_1 - \beta_2, y_1 - y_2)$$

$$- D(\beta_1 - \beta_2 + \omega_1, y_1 - y_2)$$

$$- D(\beta_1 - \beta_2 + \omega_2, y_1 - y_2)]\} . \tag{A23}$$

APPENDIX B

In this appendix we compare Kummer's function with the quadratic and 5/3-power approximations. We recall that Kummer's function is the confluent hypergeometric series

$$ {}_1F_1(a,\ b,\ z) = 1 + \frac{az}{b} + \frac{(a)(a+1)\ z^2}{(b)(b+1)\ 2!} + \ldots \qquad (17) $$

We are particularly interested in the Kummer's function that appears in (16)

$$ {}_1F_1\left(-\frac{5}{6},\ 1,\ \frac{-K_m^2\rho^2}{4}\right) $$

where $K_m \approx 5.91/l_o$ and l_o is the inner scale size of the turbulence (typically 1 mm).

The quadratic approximation of Kummer's function minus one is

$$ {}_1F_1\left(-\frac{5}{6},\ 1,\ \frac{-K_m^2\rho^2}{4}\right) - 1 \approx \left(-\frac{5}{6}\right)\left(\frac{-K_m^2\rho^2}{4}\right), \quad |\rho| << \frac{2}{K_m} \qquad (B1) $$

The term "quadratic" approximation is derived from the ρ^2 term. Similarly, the 5/3-power approximation is given by

$$ {}_1F_1\left(-\frac{5}{6},\ 1,\ \frac{-K_m^2\rho^2}{4}\right) - 1 \approx \frac{1}{\Gamma(11/6)}\left(\frac{K_m^2\rho^2}{4}\right)^{5/6} $$

$$ = \frac{1}{\Gamma(11/6)}\left(\frac{K_m^2}{4}\right)^{5/6}\rho^{5/3}, \quad |\rho| >> \frac{2}{K_m} \qquad (B2) $$

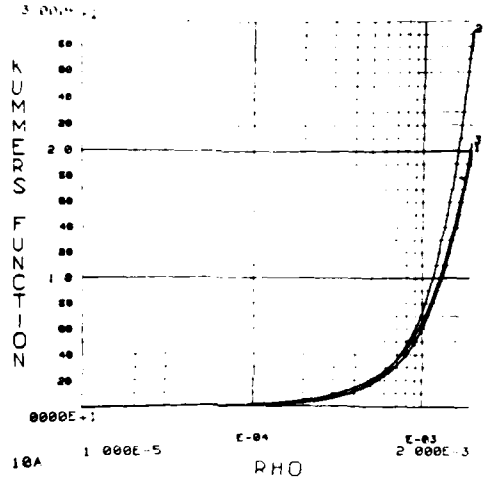

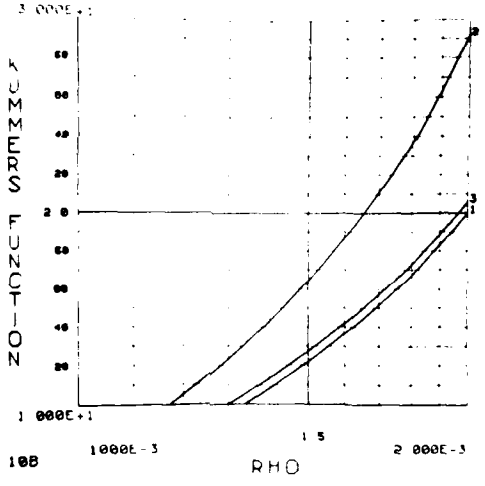

Fig. 10. A comparison of Kummer's function with the quadratic and 5/3-power approximations. Curve 1 is Kummer's function, curve 2 is the quadratic approximation, and curve 3 is the 5/3-power approximation.

Kummer's function was computed numerically by summing the first one hundred terms of the series. This partial sum was observed to converge over the range of ρ considered. The value of Kummer's function is plotted in Fig. 10 along with the quadratic and 5/3-power approximations. The quadratic approximation is observed to diverge rapidly from Kummer's function for $\rho > 8/K_m$. However, the 5/3-power approximation appears to be a reasonable approximation to Kummer's function for all ρ. Hence, we have modeled ${}_1F_1(-5/6, 1, -(K_m^2\rho^2)/4)$ by (23) throughout this paper.

APPENDIX C

In this appendix we consider the problem of selecting the coefficients c_1 and c_o in (51) so that

$$d(\rho) \approx c_1\rho \cdot \rho + c_o, \qquad |\rho| \approx \omega_c. \tag{51}$$

For convenience we define

$$g(\rho) \equiv c_1\rho \cdot \rho + c_o \tag{C1}$$

We would like the approximating function $g(\rho)$ to be optimal in some sense. In particular, we have considered four criteria for selecting the coefficients c_1 and c_o:

1. Set

$$\exp\{-d(\rho)\}\big|_{\rho=\omega_c} = \exp\{-g(\rho)\}\big|_{\rho=\omega_c}$$

and $c_o = 0$.

2. Set

$$\exp\{-d(\rho)\}\big|_{\rho=\omega_c} = \exp\{-g(\rho)\}\big|_{\rho=\omega_c}$$

and

$$\frac{d}{d\rho}\left[\exp\{-d(\rho)\}\right]\Big|_{\rho=\omega_c} = \frac{d}{d\rho}\left[\exp\{-g(\rho)\}\right]\Big|_{\rho=\omega_c}.$$

3. Minimize the functional

$$J_1 = \left[\int_0^\infty \exp\{-\alpha d(\rho)\}\, d\rho - \int_0^\infty \exp\{-\alpha g(\rho)\}\, d\rho \right]^2$$

where α is some positive constant ($\alpha > 0$).

4. Minimize the functional

$$J_2 = \int_0^{\omega_c} [d(\rho) - g(\rho)]^2\, d\rho$$

The constants c_1 and c_o can easily be solved for in each criteria listed above. The results are summarized in Table 5.

Table 5. Equations for c_o and c_1 resulting from each of the four criteria.

Criterion	Equations for c_o and c_1
1	$c_o = 0$ $c_1 = 3.15\,(k^2 \mu_o)^{1/5}$
2	$c_o = 0.33/(k^2\mu_o)$ $c_1 = 2.63\,(k^2\mu_o)^{1/5}$
3	$c_o = 0$ $c_1 = 3.093\,(k^2\mu_o)^{1/5}$
4	$c_o = 0.0822/(k^2\mu_o)$ $c_1 = 3.15\,(k^2\mu_o)^{1/5}$

From the table we observe the expressions for c_o and c_1 to be reasonably consistent for the four criteria we have considered. We have selected the following expressions for c_1 and c_o:

$$c_1 \approx 3\left(k^2\mu_o\right)^{1/5}, \tag{74}$$

$$c_o \approx 0. \tag{75}$$

APPENDIX D

In this appendix we will describe in more detail the numerical integration routine used to integrate (34). The integrand of (34) is $M'(\bar{\omega}, \Delta\omega, \Delta\beta, \Delta y)$. This function can be loosely regarded as approximating a Gaussian surface with peak near $\Delta\beta = -\Delta\omega/2$. The function rapidly approaches zero for $\Delta\beta$ such that $|\Delta\beta + \Delta\omega/2| > \omega_c$. Hence, we should concentrate the numerical effort in this region.

The numerical analysis was performed only for one-dimensional problems. It was desirable to use an algorithm that would find the peak described above and automatically concentrate the number of function evaluations in the vicinity of the peak. Since $|\Delta\omega| < \omega_c$ and the width of $M'(\bar{\omega}, \Delta\omega, \Delta\beta, \Delta y)$ in the $\Delta\beta$ direction is about ω_c, we truncated the integration over the $\Delta\beta$ line to the inverval $[-1, +1]$. Since $\omega_c \sim 0.01$ to 0.1, these bounds on $\Delta\beta$ are very loose. To guarantee that the narrow peak of $M'(\bar{\omega}, \Delta\omega, \Delta\beta, \Delta y)$ will not be missed by the routine, the interval $[-1, +1]$ was divided into twenty subintervals. An adaptive Romberg [13] integration algorithm was applied to each subinterval and the results were summed to yield the solution. In this manner the algorithm wastes little time calculating function values of $M'(\bar{\omega}, \Delta\omega, \Delta\beta, \Delta y)$ at values of $\Delta\beta$ for which the function is small and not rapidly changing. The computational effort is concentrated near the peak of $M'(\bar{\omega}, \Delta\omega, \Delta\beta, \Delta y)$.

The routine was found to be robust but rather inefficient. The emphasis here was placed on reliable results and not computational efficiency.

APPENDIX E

In the one-dimensional or slit aperture case, all vectors are colinear so $\cos^2 \theta = 1$, and the model for $M_o(\bar{\omega}, \Delta\omega, \Delta y)$ can be simplified to:

$$M_o(\bar{\omega}, \Delta\omega, \Delta y) \approx \sqrt{\frac{\pi}{k^2 \xi_1 \mu_o}} \exp\left\{-\Delta y^2/\Delta y_c^2\right\} \left\{\exp\ -\Delta\omega^2/\Delta\omega_c^2\right\} \quad \text{(E1)}$$

where

$$\xi_1 = 12\left(k^2\mu_o\right)^{1/5} - 6.49(\bar{\omega})^{-1/3}$$

$$\xi_2 = 3\left(k^2\mu_o\right)^{1/5} + 1.62(\bar{\omega})^{-1/3}$$

$$\Delta\omega_c = \sqrt{\frac{1}{k^2 \xi_2 \mu_o}}$$

$$\Delta y_c = \sqrt{\frac{1}{k^2 \xi_1 \left(\mu_2 - \mu_1^2/\mu_o\right)}}$$

For the double impulse model, we can extend the one-dimensional model (E1) into region (c) (section 5) by modeling the Δy dependence by the sum of a constant and a Gaussian. In this case, it is readily shown that

$$\lim_{|h_1 \Delta y| \to \infty} M_o(\bar{\omega}, 0, \Delta y) = \sqrt{\frac{\pi}{k^2 \xi_1 \alpha_o}} \exp\left\{-2.92\ k^2 \alpha_1 |\bar{\omega}|^{5/3}\right\}$$

If we assume that $\mu_o \approx \alpha_o$, we obtain the model

$$M_o(\bar{\omega}, \Delta\omega, \Delta y) \approx \sqrt{\frac{\pi}{k^2 \xi_1 \mu_o}} \left[\lambda + (1 - \lambda) \exp\left\{-\Delta y^2/\Delta y_c^2\right\}\right]$$

$$\cdot \exp\left\{-\Delta\omega^2/\Delta\omega_c^2\right\} \qquad \text{(E2)}$$

where

$$\lambda = \exp\left\{-2.92\ k^2\ \alpha_1\ |\bar{\omega}|^{5/3}\right\} .$$

REFERENCES

1. J. W. Sherman, "Speckle Imaging Under Nonisoplanatic Conditions", SPIE Proceedings, Vol. 24.

2. J. W. Goodman, Introduction to Fourier Optics (McGraw-Hill, New York, 1968).

3. R. L. Fante, "Some Results on the Imaging of Incoherent Sources through Turbulence", J. Opt. Soc. Am., 66, 574 (1976).

4. A. I. Kon and V. I. Feizulin, "Fluctuations in the Parameters of Spherical Waves Propagating in a Turbulent Atmosphere", Radiophysics and Quantum Electronics, 13, 51 (1970).

5. M. Abramowitz and I. A. Stegun, Ed., Handbook of Mathematical Functions (Dover, New York, 1964).

6. V. I. Tatarskii, "The Effects of the Turbulent Atmosphere on Wave Propagation" (U. S. Department of Commerce, NTIS, Springfield, Virginia, 1971).

7. D. L. Walters, D. L. Favier, and J. R. Hines, "Vertical Path Atmospheric MTF Measurements", J. Opt. Soc. Am., 69, 828 (1979).

8. R. Barletti, et al., "Mean Verticle Profile of Atmospheric Turbulence Relevant for Astronomical Seeing", J. Opt. Soc. Am., 66, 1380 (1976).

9. R. E. Hufnagel, "Propagation through Atmospheric Turbulence", in The Infrared Handbook (U. S. Government Printing Office, Washington, D. C.) 1978, Chapter 6, pp. 6-14.

10. D. L. Fried, "Angular Dependence of the Atmospheric Turbulence Effect in Speckle Interferometry", Optica Acta, 26, 597 (1979).

11. G. C. Loos and C. B. Hogge, "Turbulence of the Upper Atmosphere and Isoplanatism", Applied Optics, 18, 2654 (1979).

12. D. L. Fried, "Optical Resolution through a Randomly Inhomogeneous Medium for Very Long and Very Short Exposures", J. Opt. Soc. Am., 56, 1372 (1966).

13. H. Engles, Numerical Quadrature and Cubature (Academic Press, New York, 1980).

RESTORATION OF NON-ISOPLANATIC SPECKLE IMAGERY

Hanoch Ur
James W. Sherman

Analytic Information Processing, Inc.

November 30, 1981

Restoration of Non-isoplanatic
Speckle Imagery

1. Introduction

The efforts reported here are a continuation of the Speckle Imaging efforts previously reported [1]. Our goal was to develop a Speckle Imaging algorithm for non-isoplanatic conditions. In particular, we wanted a general framework based on linear algebra in which to examine the many various alternatives.

The remainder of this report is divided into nine sections. Section Two briefly reviews the non-isoplanatic speckle imaging problem under simplified conditions. The Third Section develops both a linear algebra representation of the discretized speckle imaging equations and a corresponding graphic representation. The decomposition of rectangular matrices is reviewed briefly in Section Four. Section Five develops the relationship that allows two-dimensional images to be treated by the linear algebraic methods being developed. Section Six develops and examines algorithms for non-isoplanatic imaging based on the factorization of the second order statistics. The joint estimation of the object and the non-isoplanation characteristics are discussed in Section Seven. Sections Eight and Nine discuss the effects of the simplifying assumptions which made the linear algebraic development tractable. Finally, a class of restoration algorithms for non-isoplanatic Speckle Imaging is given in Section Ten.

2. Statement of the Problem

Our aim in this work is to restore telescopic images, namely to find the original image, the object, from images corrupted by the turbulent atmosphere. The work is based on an analysis by Sherman [1]. In particular we wish to consider the removal of what is called the non-isoplanatic effect through use of second order statistics namely the average of many identical images (save atmospheric effects) of some celestial object. The above paper provides the analyses and we take as a starting point its equation 38 which we want to solve for the original object. It behooves us here to try to give some intuitive interpretation to this equation or rather to the corresponding relationships of the Fourier transformed variables. Thus, if we denote by a tilda ($\sim$) a Fourier transformed variable, the corresponding equation which we call ($\widetilde{38}$) is obtained from (38) by eliminating the integrals with the inverse Fourier kernel. Thus ($\widetilde{38}$) is

$$E\left\{\tilde{I}(\omega_1)\tilde{I}(\omega_2)\right\} = M_1(\bar{\omega},\Delta\omega)\,F_q(\bar{\omega},\Delta\omega)\iint_{-\infty}^{\infty}\tilde{O}(\omega_1-\tfrac{u}{2})\,M_2(u;\bar{\omega},\Delta\omega)\,\tilde{O}(\omega_2+\tfrac{u}{2})\,du \qquad (\widetilde{38})$$

In ($\widetilde{38}$), $\tilde{O}$ is the transform of the object, while $\tilde{I}$ is the transform of the image. To understand the mechanism let us substitute for the expectation of ($\widetilde{38}$)

$$E\left\{\tilde{I}(\omega_1)\,\tilde{I}(\omega_2)\right\} = \frac{1}{Q}\sum_{q=1}^{Q}\tilde{I}_q(\omega_1)\,\tilde{I}_q(\omega_2) \qquad (1)$$

namely the left hand side of ($\widetilde{38}$) is approximated by the sample, second order moment of Q images. Because the effect of the turbulence could be considered as adding a random phase component in the Fourier plane, (1) would generally represent summation of complex numbers with an added random phase which would cause partial to full cancellation except in the case where

$$\tilde{I}_q(\omega_1) = \tilde{I}_q^{*}(\omega_2) \qquad \text{,for all q.} \qquad (2)$$

Then the product is always positive with the sum adding up because

$$\tilde{I}_g^{*}(\omega_2) = \tilde{I}_g(-\omega_2) \tag{3}$$

holds for an original real (physical) image. We thus could say (proof in [1]) that the atmospheric effect on the expection of (1) for $|\omega_1|$ and $|\omega_2| > \omega_c$ is to multiply what would have been otherwise obtained by $M_1(\bar{\omega}, \Delta\omega)$, where $\bar{\omega}$ and $\Delta\omega$ are given (as defined in [1]) by:

$$\Delta\omega = \frac{\omega_1 + \omega_2}{2} \quad ; \quad \bar{\omega} = \frac{\omega_1 - \omega_2}{2} \tag{4}$$

The $\bar{\omega}, \Delta\omega$ plane (taking for illustration pusposes only one dimension of each of ω_1 and ω_2) is rotated with respect to the ω_1, ω_2 plane by 45° (and actually also reduced by a factor of $\sqrt{2}$). We show M_1 in Figure 1. M_1 is, except near the origin, a function mainly of $\Delta\omega$ and only weakly of $\bar{\omega}$. Thus, on the line $\omega_1 = -\omega_2$ M_1 is maximum and it tapers off as we move away from this line. It can be approximated by a Gaussian curve. We also have a factor, F_4, which measures overlap of the aperture with four shifts. What it signifies is that the Fourier plane is truncated by the aperture of the telescope and that the overlap of it appears in the correlation. F_4 is given by

$$F_4(\bar{\omega}, \Delta\omega) = \iint_{-\infty}^{\infty} a(\beta + \bar{\omega} + \Delta\omega)\, a(\beta)\, a(\beta + \Delta\omega)\, a(\beta + \bar{\omega})\, d\beta^2 \tag{5}$$

where $a(\cdot)$ is one inside the aperture and zero outside. We may note that, because we are interested only in the region around $\omega_1 = -\omega_2$ where $M_1 \neq 0$ and that $a(\cdot) = a^2(\cdot)$, (5) reduces to the two shift overlap function for the region of interest.

M_3 represents in ($\tilde{38}$) the non-isoplanatic effect. This is the effect we want to remove, or more precisely, the effect despite which we want to achieve reconstruction of the object from Fourier plane data. The impluse response of the imaging system and atmosphere combined is, in

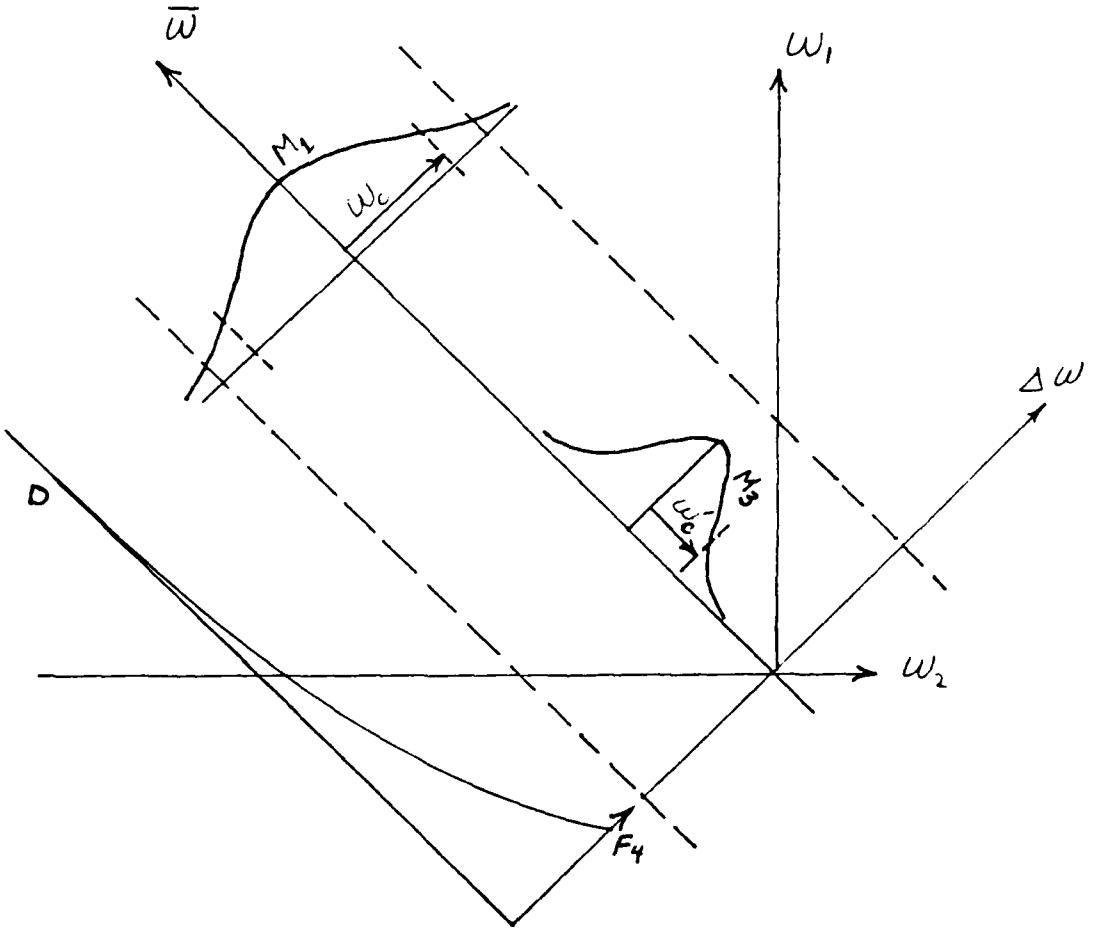

Figure 1: Region of interest of $\mathcal{D}$ in ω_1, ω_2 space.

system theory terminology, shift variant under non-isoplanatic conditions. The interpretation of $\widetilde{(38)}$ means that the effect of M_3 is that the value of the expected cross correlation at a point (ω_1, ω_2) is given apart from the M_1F_4 effect by smoothing along a segment of $\Delta\omega$= constant with M_3 as a weighting function. Figure 1 illustrates this smoothing graphically. The weighting function, M_3, is approximately a Gaussian function with a width of ω_c'.

3. Algebraic Formulation of Discretized Equations

We rewrite (38) here as

$$\mathcal{I}(\omega_1,\omega_2) = \iint O(\omega_1-\tfrac{\omega'}{2})\,O(\omega_2+\tfrac{\omega'}{2})\,M_3(\omega')\,d^2\omega' \qquad (6)$$

where the $(\tilde{\ })$ notation has been dropped and $\mathcal{I}$ is taken only in the range of support of M_1 and F_4. Let us assume for awhile that ω_1 and ω_2 are one dimensional (rather than two). Let us assume also that we digitize (6) on a uniform grid. Then we have a discrete version of (6),

$$\mathcal{I}(m_1,m_2) \triangleq \sum_{k=-R}^{R} O(m_1-k)\,O(m_2+k)\,M(k) \qquad (7)$$

O(m) is a (column) vector and thus we can consider O(m-k) to be another vector generated from the first by a shift of elements. Thus all possible values of O(m-k) for L<m<H, -R<k<R could be represented by a Toeplitz matrix whose elements are O(m-k).

$$ {}_T O \triangleq \begin{array}{c} \overset{k}{\longrightarrow} \\ m \downarrow \end{array} \begin{bmatrix} O(L+R) & \cdots & O(L-R) \\ \vdots & O(m-k) & \vdots \\ O(H+R) & \cdots & O(H-R) \end{bmatrix} \qquad (8)$$

where the left subscript T means that the Toeplitz matrix ${}_T O$ is obtained from the vector O by appropriately shifting the elements.

Because M_3 is similar to the Gaussian function, we select R according to the precision required. Similarly we can define ${}_H O$ as the generation of a Hunkel matrix whose elements are O(m+k) from the vector O. Note that while the elements of the Toeplitz matrix are the same as diagonals, they are the same on antidiagonals in Hunkel

matrices. Thus (7) can be written as

$$\left[\mathcal{A}(m_1, m_2)\right] = {}_T O M_H O^T \tag{9}$$

where superscript T indicates the transpose and M is a diagonal square matrix whose elements are

$$M_{ij} = M_i \delta(i-j). \tag{10}$$

Figure 2 graphically represents (9). Any element of $\mathcal{A}$, located say at m,n is obtained by a scalar or inner product of row m from ${}_T O$ times column n of ${}_H O^T$ (or row n of ${}_H O$), weighted by the diagonal elements of M.

We should also note that a Hunkel matrix could be obtained from a Toeplitz matrix and visa versa by multiplication by an "antidiagonal" unit matrix

$$J = J^T = \begin{bmatrix} 0 & \cdots & 0 & 1 \\ \vdots & & 1 & 0 \\ 0 & 1 & \cdots & \vdots \\ 1 & 0 & \cdots & 0 \end{bmatrix}. \tag{11}$$

so that (9) would become

$$\left[\mathcal{A}(m_1, m_2)\right] = {}_T O M J_T O^T \tag{12}$$

We note also that in (9) or (12), M could be absorbed into ${}_T O$ and being diagonal M multiplies each column of ${}_T O$ by a constant m_{kk}. It of course could be also absorbed into the right as $M=M^T$, or we could split M, say symmetrically, into $M=\sqrt{M}\sqrt{M}$. Also M commutes with J to produce for example,

$$\left[\mathcal{A}(m_1, m_2)\right] = {}_T O \sqrt{M}\, J \sqrt{M}^T_T O^T \tag{13}$$

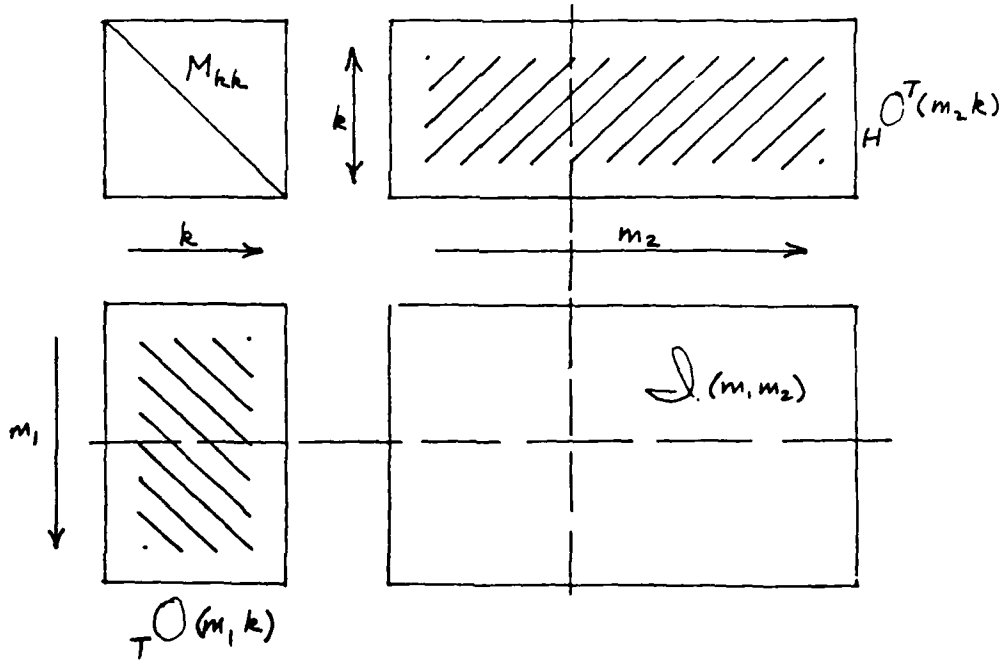

Figure 2. Illustrating equation 9

4. Decomposition of Rectangular Matrices

We wish first to review and present in a form to be used later some results from linear algebra. Consider any pxq rectangular matrix A=[a(i,j)] of rank r. This implies that we can find r independent columns of this matrix and express all other columns as linear combinations of these columns. Thus we can write

$$A = A_R A_L^T . \tag{14}$$

where A_R is the pxr matrix generated by the above columns and A_L is a qxr matrix whose columns are the coefficient of the linear combination that generate the columns of A. We could alternatively start by saying that any row of A is expressed as a linear combination of r rows. Thus, it is said that A_R and A_L are respectively composed of vectors which span and are a basis of the columns space of A and A^T. This decomposition is called "full rank decomposition or "full rank factorization". The name implies the full column rank of A_R and row rank of A_L^T. This is shown graphically in Figure 3. We should note that the decomposition is not unique, because all possible A_R span the same column space of A and all A_L span the row same space of A. One A_R is related to another by a non-singular transformation, and we actually can also write a more general decomposition

$$A = B_R C B_L^T , \tag{15}$$

where C is a non-singular rxr matrix (Figure 3c). We may note that we could use a decomposition with a number of columns in B_R and rows in B_L^T that is larger than the rank. This is more general, but we will lose some properties.

While it may seem trivial, it is worthwhile to examine Figure 3 in detail. Considering Figure 3b, we see that each element of $\mathcal{A}$, say $\mathcal{A}_{ij}$, is obtained by a scalar or inner product of the corresponding row

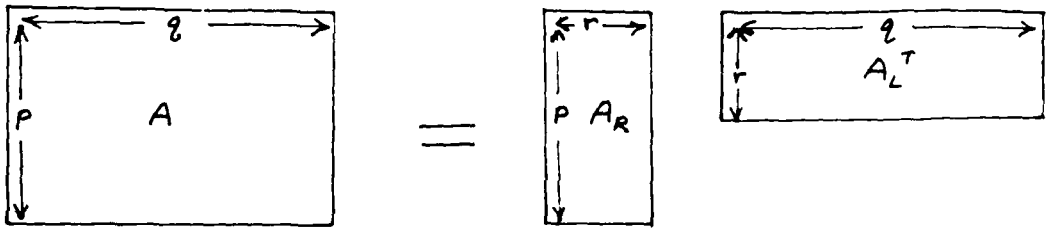

(a)

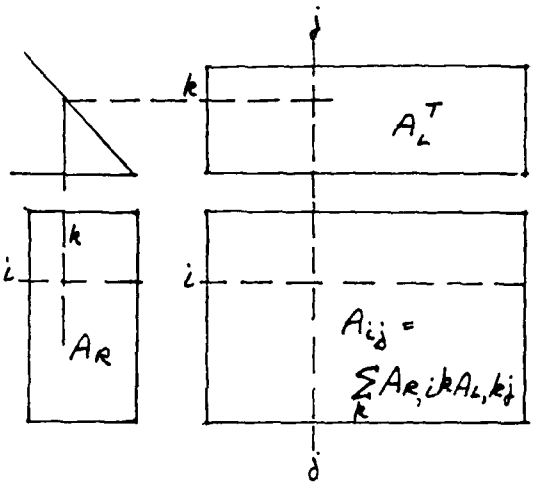

(b)

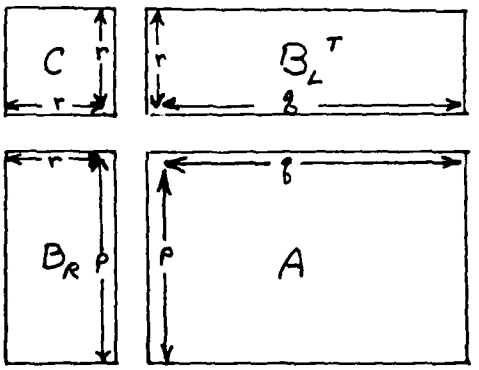

(c)

Figure 3. Illustration of matrix decomposition.

from A_R and of the corresponding column of A_L^T. Looking at Figure 3C, we see that we can absorb C into B_R. This generates a new B_R in which each column is a linear combination of those of the old B_R. One could of course absorb it in B_L^T and then the operation would be on the rows. C could also be split into a product $C_1 C_2$ and then C_1 would operate on the columns of B_R and C_2 on rows of B_L^T. In the particularly useful case when C is diagonal, what happens is that each column of A_R is multiplied by the corresponding diagonal element which is a constant.

We should also note that the matrix A can be really only a submatrix of some larger matrix that has been partitioned. If we consider Figure 4 or the corresponding equations

$$\mathcal{A}_{ij} = \sum_k A_{ik} C_{kk} B_{kj} \tag{16}$$

We note that we cannot take all i or j but only some of them. Each element in $\mathcal{A}$ is obtained from a row B_R and a column of B_L^T. Thus an independent subset of equations can be obtained if we select a set of rows and columns from B_R, B_L^T as shown in Figure 4. In fact the selected rows or columns need not be contiguous. One should be careful to note that this selection may change the nature of the equations represented by the matrix product. For example, B_R and B_L may contain the same variable which would make the equations quadratic. Proper selection may change this nature. This possibility of selection is important in particular cases both because it allows reduction in the number of equations (at the cost of redundancy or noise reduction) and change in nature of relationship.

A particular form of full rank decomposition that has become very popular in recent literature is the singular value decomposition (SVD). The SVD is a full rank decomposition with two additional requirements. First, the diagonal matrix C in (15) of positive elements (usally called Σ) is arranged by magnitude with the largest one first. Second, B_R and B_L (usually called U and V respectively)

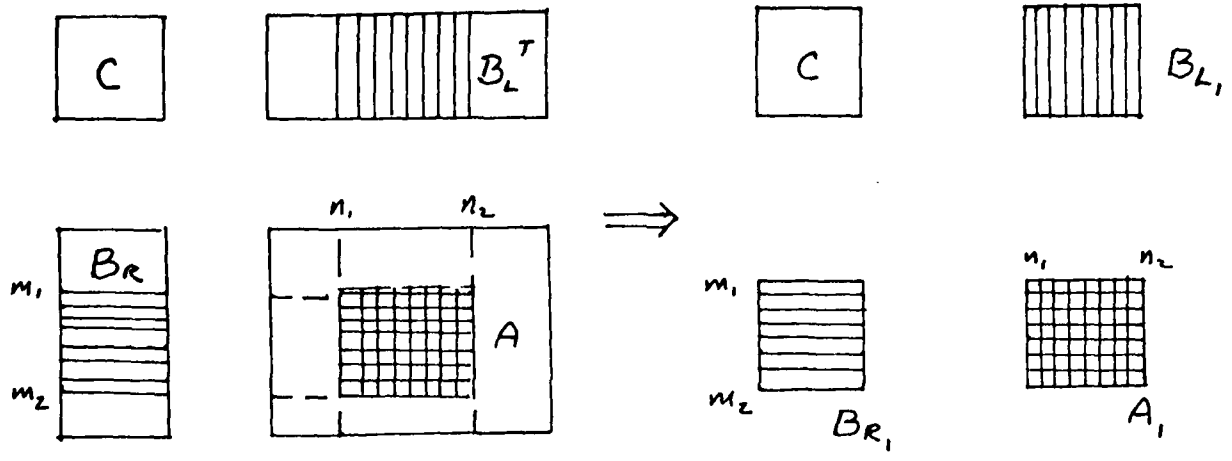

Figure 4. Selection of a consistent subset of equations.

are composed of orthogonal vectors of unit length. The SVD is usually written with the notation

$$A = U \Sigma V^T \qquad \text{or} \quad A = \sum_{i=1}^{r} u_i \sigma_i v_i^T \tag{17}$$

if A is square and Hermitian then U is the conjugate of V.

In some presentations in the literature U and V are taken to be square rather than of a number of columns equal to r, the rank of A. This is done to be able to make U,V conform to the definitions of orthogonal matrices. Because the u_i, v_i for i such that $\sigma_i = 0$ do not affect A, the two definitions coincide. Because the SVD is a full rank decomposition (factorization), we may conclude that one can represent that matrix A by either the SVD representation or the full rank decomposition of (15) and that the transformation from U to B_R (or V to B_L) is a nonsingular transformation which is recoverable if we know an r row section of U and B_R.

5.0 Representation of Two-Dimensional Data

We previously developed the analysis on the simplified assumption that our object and image were one dimensional and this led us to a matrix representation for the basic non-isoplanatic relation for second order statistics. Because our objects are two dimensional, their Fourier transforms are also two dimensional. We can write the sampled version as a function of two discrete variables, n,m or

$$O = O(m,n) \tag{19}$$

and two dimensional version of (7), the basic equation, is

$$\mathcal{I}(m_1,n_1,m_2,n_2) = \sum_{l=-K}^{K} \sum_{k=-K}^{K} O(m_1-l, n_1-k) M(l,k) O(m_2+l, n_2+k) \tag{20}$$

and our functions now have four variables rather than two.

Because, we are used to representations of functions of two variables and they are easier to represent in the plane (paper) graphically, we would like to map the four dimensional Euclidian space into a two dimensional one. This can be done in several ways. We start with the way we look at the original problem, Figures 5a and 5b. We have a 2-d plane, and each point in it is the origin of a perpendicular 2-d plane, but the axes can be selected in several ways. We deal not with continuous variables but with a finite set of discrete variables. These can be mapped from a plane to a line by taking a column at a time and cascading them. In order to be consistent with our previous representations, we will use the mapping of $\mathcal{I}$ illustrated in Figure 6. The index space will map into a column by taking a concatenation of vectors running over n for fixed m. This mapping is the common raster scan and keeps (20) in its familiar form,

$$\mathcal{I} = {}_T O M_H O^T \tag{21}$$

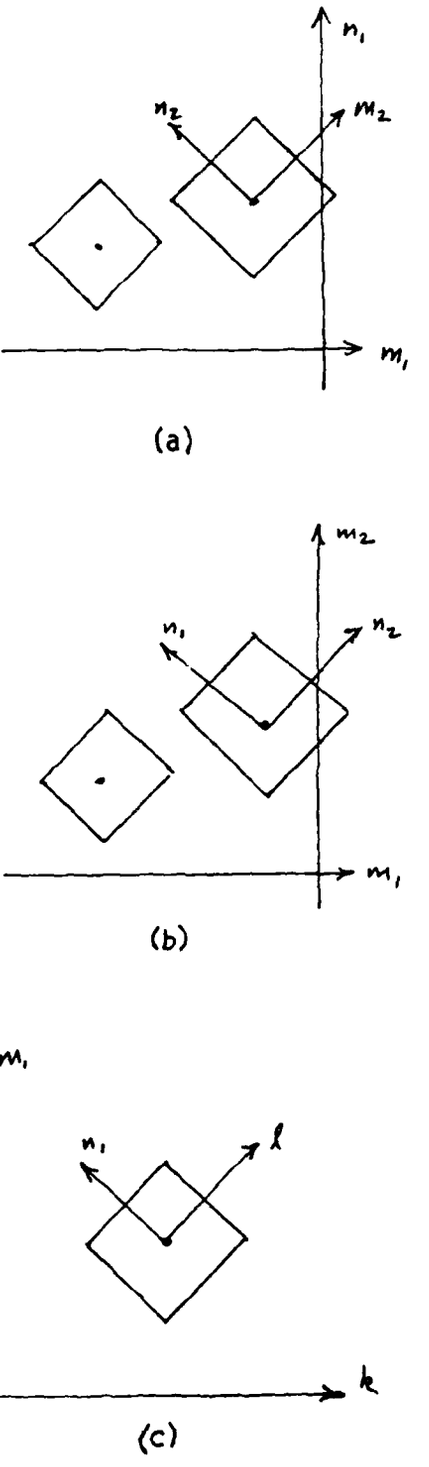

Figure 5. Possible selection of axes.

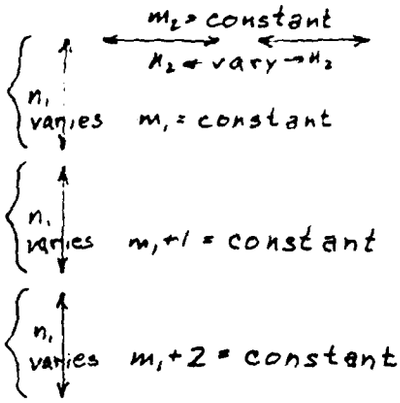

(a) $m_1 n_1$, $m_2 n_2$ mappings -axis of $\mathcal{L}$ and one axis of ${}_T O$ or ${}_H O$ - see(c).

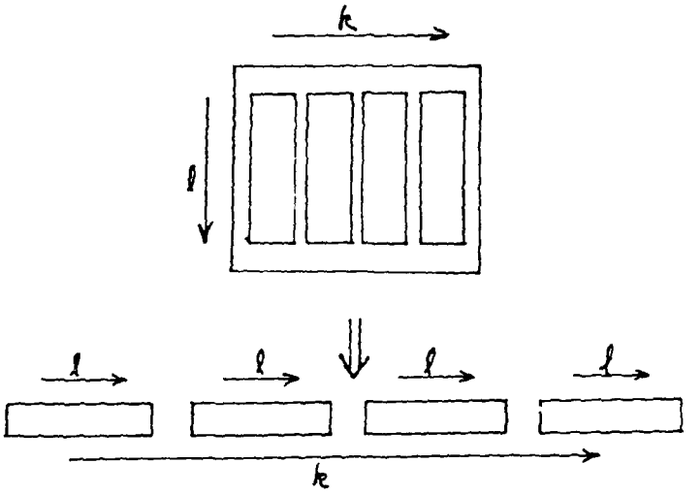

(b) k,l mapping -axis of M_3 and of ${}_T O$ or ${}_H O$.

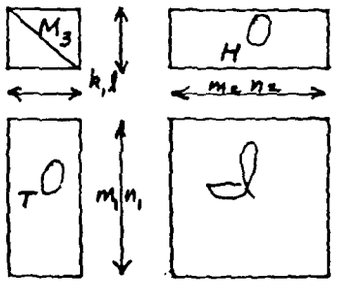

(c) combined.

Figure 6. Mappings to lower dimension.

where now the matrices $\mathcal{A}$, ${}_T0$, ${}_H0$ become block matrices. Thus, ${}_T0$ could now be considered as block-block Toeplitz. This means that in the m,k block location of matrix ${}_T0$ we have a Toeplitz block with indices n,l and the block themselves have a Toeplitz structure. Similarly, ${}_H0$ is block-block Hunkel and $\mathcal{A}$ has a corresponding block sturcture. M is now again a diagonal matrix, but the values of the elements are $M(\sqrt{k^2+l^2})$ and do not have the bell shape any more. Figure 7 shows the mapping for the ${}_T0$ matrix for an arbitrary vicinity of k,l; l ranging from -1 to + 1 (assuming R=1). This makes the width of the ${}_T0$ matrix $9=N^2$ where N=(2R+1). If the m ,n array has dimensions* uxv, then ${}_T0$ is a block matrix of uxN blocks and each block is vxN. The total matrix dimension is $uvxN^2$.

---

*Please note the different meaning of the word dimension in a matrix and in a space. The appropriate meaning will be clear from context.

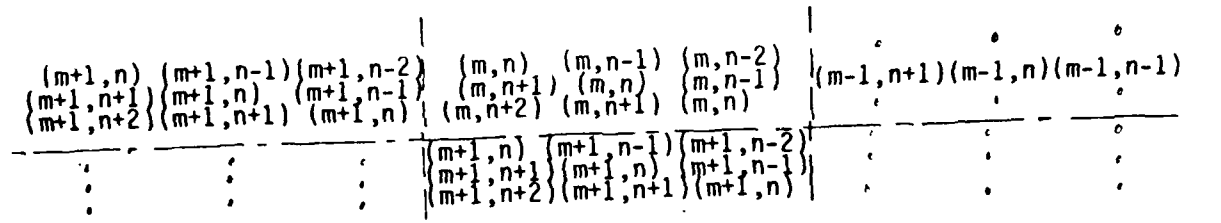

k	1	0	-1	1	0	-1	1	0	-1
ℓ	1	1	1	0	0	1	-1	-1	-1
$k^2+\ell^2$	1	2	2	1	0	2	2	1	2

(a) A detail of $_T0$ (in upper part), and M_3 (in lower part).

(b) values of $k^2 + \ell^2$.

$k^2 + \ell^2$

8	5	4	5	8	2
5	2	1	2	5	1
4	1	0	1	4	0
5	2	1	2	5	-1
8	5	4	5	8	-2
-2	-1	0	1	2	

k ℓ

Figure 7. Mappings of two-dimensional indices to one-dimension.

6. Algorithms for Factorization

We will introduce here an algorithm for finding O given $\mathcal{A}$ and M_3. We show in Section 7 that if M_3 is not known it can be found as part of the procedure. For this purpose let us consider first the Newton Raphson procedure for finding a square root or finding X given

$$X^2 = A \tag{22}$$

Let X_ℓ be the lth iterate obtained using this Newton Raphson formula

$$X_{\ell+1} = X_\ell + \frac{1}{2}\left(X_\ell^{-1}A - X_\ell\right) \tag{23}$$

or

$$X_{\ell+1} = \frac{1}{2}\left(X_\ell^{-1}A + X_\ell\right). \tag{24}$$

We purposely separated (23) and (24). While (24) seems more compact, it may be advantageous numerically to use (23).

These formulas are known to converge very strongly- namely quadratically. A simple substitution shows that

$$\frac{\delta_{\ell+1}}{X} \triangleq \frac{X_{\ell+1} - X}{X} \approx \frac{1}{2}\left(\frac{X_\ell - X}{X}\right)^2 = \frac{1}{2}\left(\frac{\delta_\ell}{X}\right)^2 \tag{25}$$

So if we have a fair approximation, say $\delta_\ell = .25X$, then after the next iteration we have $\delta_{\ell+1} = 3\%X$.

Analogously we start with

$$\mathcal{A} = {}_T O\, M_H\, O^T. \tag{26}$$

We take the left inverse of ${}_T O$ and obtain

$${}_T O^{-L}\mathcal{A} = \left({}_T O^T {}_T O\right)^{-1} O^T \mathcal{A} = M_H O^T = M J_1 O^T \tag{27}$$

where again J is the "antidiagonal unit" matrix.

We now assume that ${}_T0_\ell$ is the lth approximation to ${}_T0$ and define

$$U_{\ell+1} = \left({}_T O_\ell^T \, {}_T O_\ell\right)^{-1} {}_T O_\ell^T \mathcal{A} \tag{28}$$

We also define ${}_T{}^{-1}0$ as the (n+p-1) vector obtained from the nxp matrix ${}_T0$ by averaging all the elements on the diagonals. ${}_T0$ may not be exactly Toeplitz, or as is the case here the columns may be multiplied by the factor M_{kk}. We define ${}_H{}^{-1}0$ similarly. Now we let

$$V_{\ell+1} = \frac{1}{\sum_k M_{kk}} \left({}_H{}^{-1} U_{\ell+1}\right) \tag{29}$$

where the sum is only over the terms in M corresponding to the elements averaged. This is the complete range of k for diagonals which are not foreshortened.

Now let

$$\Delta {}_T O_{\ell+1} \triangleq \frac{1}{2} {}_T\left[V_{\ell+1} - O_\ell\right] \tag{30}$$

then

$${}_T O_{\ell+1} = {}_T O_\ell + \frac{1}{2} {}_T\left[V_{\ell+1} - O_\ell\right] \tag{31}$$

or

$${}_T O_{\ell+1} = \frac{1}{2} {}_T\left[V_{\ell+1} + O_\ell\right] \tag{32}$$

the same comments about numerical advantage apply to (31) and (32) as those of (23) or (24). Straight application of this algorithm assumes $\mathcal{A}$ (or rather the selected rows and columns of $\mathcal{A}$) is square.

A variant of this procedure which was used in [1] is to normalize

(multiply by constant) O_{l+1} in such a way that the (quadratic) norm implied from (26) will hold. This converges for the rank one case in one iteration. Consider a matrix C of rank one

$$C = XX^T \tag{33}$$

We let

$$X' = CX_0 = XX^TX_0 = X(X^TX_0) \tag{34}$$

and

$$\tilde{X} = X'\sqrt{C_0} \tag{35}$$

where the scaling constant c_0 is defined by

$$C_0 \triangleq \frac{C \bullet (X'X'^T)}{(X'X'^T) \bullet (X'X'^T)} \tag{36}$$

and the matrix dot product is defined by

$$A \bullet B \triangleq \sum_i \sum_j A_{ij} B_{ij} \tag{37}$$

Then c_0 can be reduced to

$$C_0 = (X_0^TX)^{-2} \tag{38}$$

Substituting into (35) shows that (34) and (35) converge in one iteration, when C is rank one,

$$\tilde{X} = X(X^TX_0)(X^TX_0)^{-1} = X \tag{39}$$

If there is more than one non-zero eigenvalue, then convergence will not happen in one step. The error after the lth iteration decreases as the ratio of the second largest eigenvalue to the largest

eigenvalue raised to the lth power. This method is an adaptation of the power method for computing eigenvectors.

7. Joint Estimation of M_3

We assumed that M_3 is given to a first approximation by

$$M_3(\omega') = a \exp\left(-\frac{\omega'^2}{\omega_c'^2}\right) \tag{40}$$

Actually it turns out that both ω_c' and a are weak functions of $\bar{\omega}$, as shown in Figure 8. As seen from the figure, we can divide the behavior of M_3 into three regions. In region I, low frequencies, it is essentially an impulse. Region II is a transition region in which it widens to a guassian funcion and becomes fairly independent of $\bar{\omega}$ in region III. Because the low frequency behavior of O is known, our main interest is in region III and we have modelled the behavior of M_3 in another portion of this effort.

If we do not know M_3, we can find it as part of our computation to find O. As we have seen, we obtain a Toeplitz matrix and each column of it is multipled by a sampled value of M_3 which we called M_{kk}. Thus at one of the computational stages we may obtain (noting $M_{(-k,-k)}=M_{kk}$) the matrix

$$T^{OM} = \begin{bmatrix} M_{11}O_{m-1} & M_{00}O_{m-2} & M_{11}O_{m-3} \\ M_{11}O_m & M_{00}O_{m-1} & M_{11}O_{m-2} \\ M_{11}O_{m+1} & M_{00}O_m & M_{11}O_{m-1} \\ M_{11}O_{m+2} & M_{00}O_{m+1} & M_{11}O_m \\ \vdots & \vdots & \vdots \\ M_{11}O_{m+j-1} & M_{00}O_{m+j-2} & M_{11}O_{m+j-3} \\ M_{11}O_{m+j} & M_{00}O_{m+j-1} & M_{11}O_{m+j-2} \\ M_{11}O_{m+j+1} & M_{00}O_{m+j} & M_{11}O_{m+j-1} \end{bmatrix} \tag{41}$$

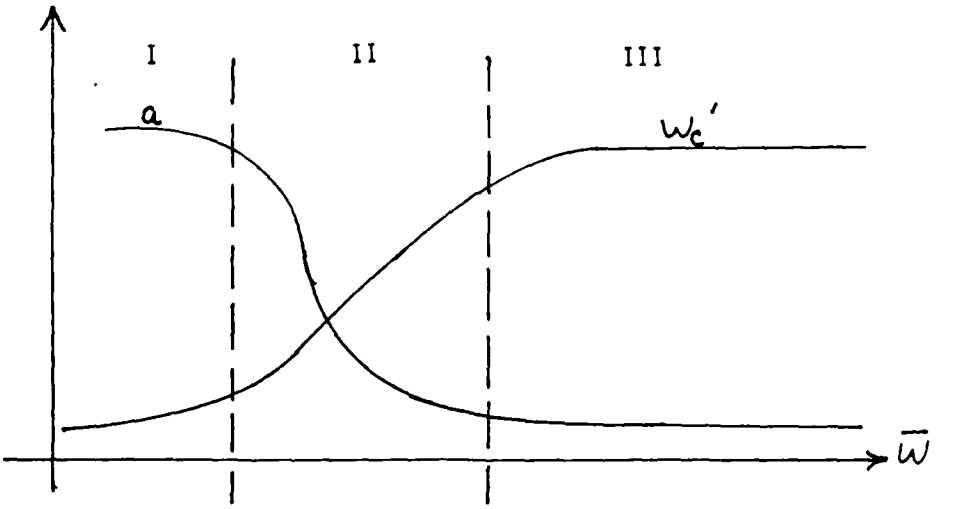

Figure 8. Behavior of M_3.

Because, apart from M_{kk}, elements on each diagonal are the same, it seems that we can take any diagonal and find M_{kk} up to a constant. (M_{kk} is a positive number). However, the entries may be corrupted by noise or numerical inaccuracy.

If we look at (41), we see that not only elements on the diagonals differ only by their M_{kk} multiplier but also the encircled elements as a group. At first glance it would seem advantagous to sum all the elements in encircled groups and normalize the results so that $M_{cc}=1$. The O_i are however complex numbers and their sum may cancel. It would behoove us thus to take the sum of the magnitudes in our example or to evaluate

$$S_k \triangleq \sum_{l=-a}^{b} |M_{kk} O_{m-l-k}| \tag{42}$$

and

$$M_{kk} = M_{cc} \frac{S_k}{S_c} \tag{43}$$

The number of elements in the summation (a+b+1) is chosen according to considerations numerical of accuracy, amount of computation, and signal-to-noise ratio.

8. Effects of Truncating of M_3

We have stated that we take R such that $M_{kk} \neq 0$. Because M_3 only goes to zero assymptotically, though very strongly, we would like to find the effect of truncating the "tails" of M_3. A smaller R is desirable, because it reduces the number of equations (proportional to R) and improves the condition number.

Figure 9 illustrates the product

$$C = A M B^T \tag{44}$$

where A is mxq, diagonal M is qxq, and B is nxq. We want to find the change in the elements of C if q is taken to be one less. We denote by

$$\Delta[C_{ij}]_q \triangleq M_{qq}[A_{iq} B_{qj}] \tag{45}$$

the change in the elements of C generated by truncating the qth element of M_3. The term in brackets is a rank one matrix or dyadic. Because A,B are respectively Toeplitz and Hunkel matrices, all their columns have about the same norm. Thus, the individuals terms are proportonal to M_{qq} and the effect of truncation of the sum at a certain q is proportional to the "area" under the tails of M which is approximately Gaussian and tapers off rapidly.

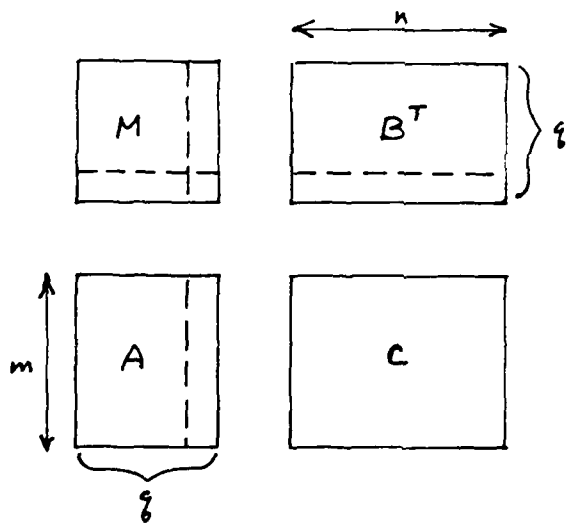

Figure 9. Illustrating the effect of truncation of M_3.

9. Effects of the $M_1 F_4$ Schur Product

As indicated before $M_1 F_4$ multiply each term of $\mathcal{I}$. This is an operation known algebraically as "Schur Product" and which does not work well together with the ordinary matrix multiplication. One could divide $\mathcal{I}$ by $M_1 F_4$, but this accentuates the noise and is not desirable. The basic non-isoplanatic equation (38) can be written as

$$\mathcal{I}_{ij} = M_{1\,ij} F_{4\,ij} \left(\sum_k {}_T O_{ik} M_{kk} {}_H O_{kj} \right) \tag{46}$$

or

$$\mathcal{I} = M_1 \circ F_4 \circ \left({}_T O \, M \, {}_H O^T \right). \tag{47}$$

One way to overcome this difficulty is to consider only one row at a time of $M_1 F_4$. Then we could take that one row of $M_1 F_4$ and write it as a diagonal matrix for one, particular ω_i. This is depicted in Figure 10 which is similar to our previous representations, with M_1 added and denoting the multiplication of each column of ${}_H O$ by the corresponding (diagonal) element of M_1,

$$\mathcal{I}(i) = {}_T O \, M \, {}_H O^T M_1(i) \tag{48}$$

We have absorbed F_4 into M_1 and we can solve for one row of ${}_T O$,

$${}_T O_i = \mathcal{I}(i) \left(M \, {}_H O^T M_1(i) \right)^{-R} \tag{49}$$

where -R indicates a right inverse.

Thus we can find one row of ${}_T O$ at a time. Because ${}_T O$ is a Toeplitz matrix, we do not need all rows to find the vector O but in order to get more redundancy we would compute one row out of about every $\omega_c'/2$ rows. The amount of work is large, because we compute every right inverse anew. Although this difficulty could be resolved if M_1 were separable, M_1 is not separable.

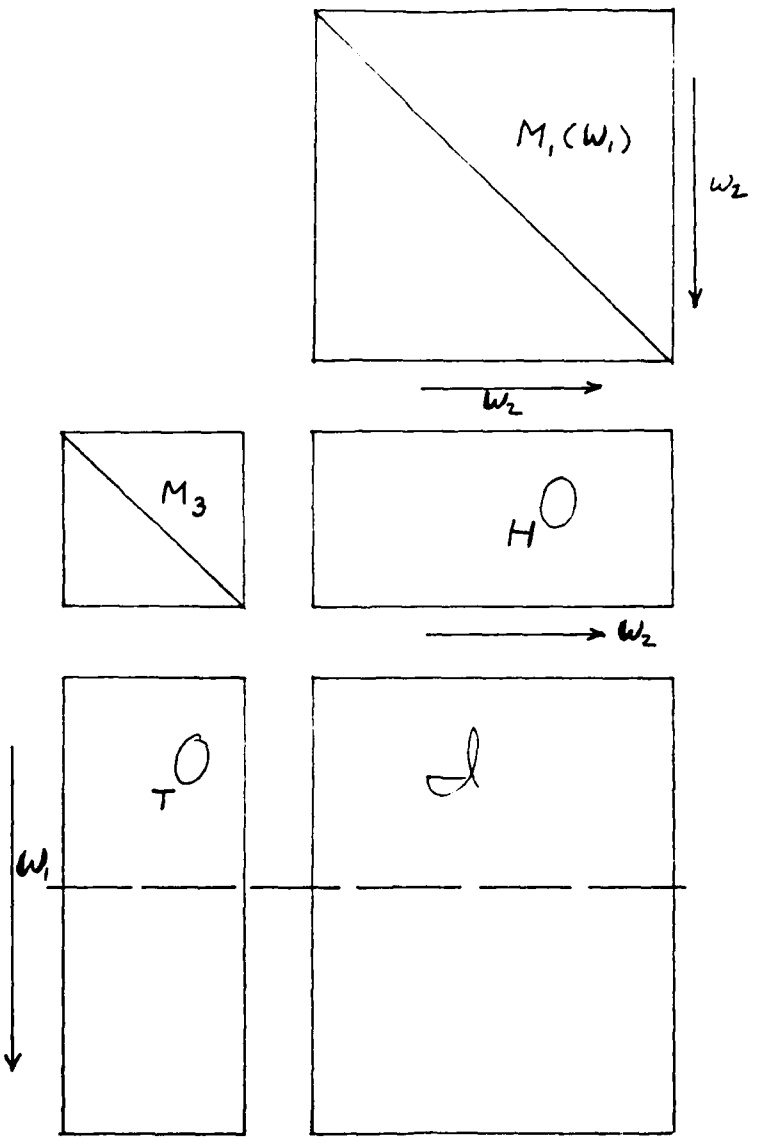

Figure 10. Representation of equation 48.

10. Restoration Algorithm

We are now ready to write a restoration algorithm for the non-isoplanatic case in simple algebraic notation. The Speckle Imaging equations for non-isoplanatic conditions can be written as functions of two dimensional variables $\underline{\omega}_1$, $\underline{\omega}_2$, and $\underline{\omega}'$,

$$\hat{\mathcal{I}}(\underline{\omega}_1, \underline{\omega}_2) = M(\underline{\omega}_1, \underline{\omega}_2) \sum_{|\underline{\omega}'| < \omega_c'} O(\underline{\omega}_1 - \underline{\omega}') O(\underline{\omega}_2 + \underline{\omega}') M_3(\underline{\omega}', \underline{\omega}_1, \underline{\omega}_2). \quad (50)$$

Again, M_1 and F_4 have been combined into M. We will assume that the sample second-order statistics denoted by $\hat{\mathcal{I}}(\underline{\omega}_1, \underline{\omega}_2)$ have been corected for the bias terms introduced by measurement noise.

Fortunately, $\hat{\mathcal{I}}(\underline{\omega}_1, \underline{\omega}_2)$ does not have to be computed for all $\underline{\omega}_1$ and $\underline{\omega}_2$. The second-order statistics have non-negligible values and hence information about the object only for $|\underline{\omega}_1 + \underline{\omega}_2| \leq \omega_c$. Thus, we only crosscorrelate those portions of the image transforms which are mutually coherent. The size of the mutually coherent area is described by the atmospheric cutoff frequency, ω_c. The non-isoplanatic effect introduces a smoothing of the second-order statistics as indicated by the summation over $\underline{\omega}'$ in (50). This allows a further reduction in the number of $\underline{\omega}_1, \underline{\omega}_2$ points at which the second-order statistics must be computed because the redundant values do not contribute substantially to the solution.

As indicated previously, we can solve for the object by solving subsets of equations from the set of equations given by (50). For example, select all equations involving a fixed $\underline{\omega}_1$ and write them as a set of "linear" equations;

$$\hat{\mathcal{I}}(\underline{\omega}_1, \underline{\omega}_2) = \sum_{|\underline{\omega}'| \leq \omega_c'} O(\underline{\omega}_1 - \underline{\omega}') \left[O(\underline{\omega}_2 + \underline{\omega}') M_3(\underline{\omega}') M(\underline{\omega}_1, \underline{\omega}_2) \right], \quad (51)$$

for $\underline{\omega}_1$ fixed and $|\underline{\omega}_2 + \underline{\omega}_1| \leq \omega_c$.

Because the isoplanatic patch is greater than the spread response, ω_c' is less than ω_c. This results in (51) having more equations than unknowns because there are more values of $|\underline{\omega}_2| \leq \omega_c$ than $|\underline{\omega}'| \leq \omega_c'$. This formulation is illustrated in Figure 10 as the selection of a particular row of $_T0$ and $\hat{\mathcal{J}}$. The remaining question of the linear independence of the equations was previously addressed in [1]. Because the subset of equations is based on a fix _ , they are independent. The equations can be written in vector form as

$$\left[\hat{\mathcal{J}}(\underline{\omega}_1, \underline{\omega}_2)\right]\Big|_{\underline{\omega}_2} = \left[O(\underline{\omega}_2 + \underline{\omega}')\, M_3(\underline{\omega}')\, M(\underline{\omega}_1, \underline{\omega}_2)\right]\Big|_{\underline{\omega}_2}\left[O(\underline{\omega}_1 - \underline{\omega}')\right]\Big|_{\forall \underline{\omega}'} \quad (52)$$

$$\underrightarrow{\omega'}$$

$$I(\underline{\omega}_1) = C(\underline{\omega}_1)\; O(\underline{\omega}_1) \quad (53)$$

or

$$C^T(\underline{\omega}_1)\, I(\underline{\omega}_1) = C^T(\underline{\omega}_1)\, C(\underline{\omega}_1)\; O(\underline{\omega}_1) \quad (54)$$

The solution can be written as

$$O(\underline{\omega}_1) = \left[C^T(\underline{\omega}_1)\, C(\underline{\omega}_1)\right] C(\underline{\omega}_1)\, O(\underline{\omega}_1) \quad (55)$$

However, the inverse would not be computed because it depends on $\underline{\omega}_1$ and the current estimate and can be used only once. Directly solving (54) using a linear equation solution method would be more computationally efficient. This yields an estimate of the object over a region of radius ω_c about $\underline{\omega}_1$.

To solve for the object over the entire Fourier transform domain, we choose a sequence of $\underline{\omega}_1$'s at which we solve (54). The sequence of $\underline{\omega}_1$'s should start at the origin and "spiral" out to the diffraction limit. The separations between the $\underline{\omega}_1$'s chosen should be less than twice ω_c to allow the regions of the estimates to overlap and cover the entire frequency domain, and should be greater than ω_c' to avoid

processing redundant information.

The steps of this restoration algorithm for non-isoplanatic Speckle Imaging can be summarized as follows:

1. Initialize the solution near $\underline{\omega}_1=0$ using the first-order statistics (average image transform).

2. Compute the coefficients of the linearized equations, $C(\underline{\omega}_1)$, from the current estimate and the models for atmospheric disturbance and measurement noise.

3. Crosscorrelate the second-order statistics with $C(\underline{\omega}_1)$ and solve (54) for the object.

4. Select a new $\underline{\omega}_1$ and repeat starting at step 2 until the diffraction limit is reached.

5. Reset $\underline{\omega}_1$ to zero and repeat starting at step 2 until a convergence criterion is satisfied or for a predetermined number of iterations.

REFERENCES

1. J. W. Sherman, "Speckle Imaging Under Nonisoplanatic Conditions", SPIE Proceedings, Vol. 243.

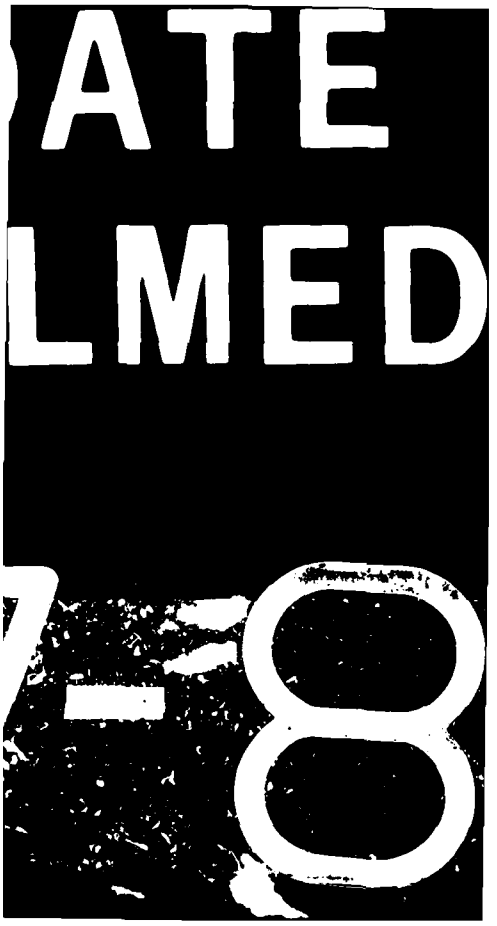
ATE
LMED
8